2002-09

Analysis of low probability of intercept (LPI) radar signals using the Wigner Distribution

Gau, Jen-Yu

Monterey California. Naval Postgraduate School

NAVAL POSTGRADUATE SCHOOL
Monterey, California

THESIS

ANALYSIS OF LOW PROBABILITY OF INTERCEPT (LPI) RADAR SIGNALS USING THE WIGNER DISTRIBUTION

by

Jen-Yu Gau

September 2002

Thesis Advisor:	Phillip E. Pace
Thesis Co-Advisor:	Herschel H. Loomis Jr.

Approved for public release; distribution is unlimited

REPORT DOCUMENTATION PAGE			Form Approved OMB No. 0704-0188
Public reporting burden for this collection of information is estimated to average 1 hour per response, including the time for reviewing instruction, searching existing data sources, gathering and maintaining the data needed, and completing and reviewing the collection of information. Send comments regarding this burden estimate or any other aspect of this collection of information, including suggestions for reducing this burden, to Washington headquarters Services, Directorate for Information Operations and Reports, 1215 Jefferson Davis Highway, Suite 1204, Arlington, VA 22202-4302, and to the Office of Management and Budget, Paperwork Reduction Project (0704-0188) Washington DC 20503.			
1. AGENCY USE ONLY *(Leave blank)*	**2. REPORT DATE** September 2002	**3. REPORT TYPE AND DATES COVERED** Master's Thesis	
4. TITLE AND SUBTITLE: Analysis of Low Probability of Intercept (LPI) Radar Signals Using The Wigner Distribution			**5. FUNDING NUMBERS**
6. AUTHOR (S) Jen-Yu Gau			
7. PERFORMING ORGANIZATION NAME (S) AND ADDRESS (ES) Naval Postgraduate School Monterey, CA 93943-5000			**8. PERFORMING ORGANIZATION REPORT NUMBER**
9. SPONSORING / MONITORING AGENCY NAME (S) AND ADDRESS (ES) Office of Naval Research			**10. SPONSORING / MONITORING AGENCY REPORT NUMBER**
11. SUPPLEMENTARY NOTES The views expressed in this thesis are those of the author and do not reflect the official policy or position of the Department of Defense or the U.S. Government.			
12a. DISTRIBUTION / AVAILABILITY STATEMENT Approved for public released, distribution is unlimited.			**12b. DISTRIBUTION CODE**

13. ABSTRACT

The parameters of Low Probability of Intercept (LPI) radar signals are hard to identify by using traditional periodogram signal processing techniques. Using the Wigner Distribution (WD), this thesis examines eight types of LPI radar signals. Signal to noise ratios of 0 dB and –6dB are also investigated.

The eight types LPI radar signals examined include Frequency Modulation Continuous Wave (FMCW), Frank code, P1 code, P2 code, P3 code, P4 code, COSTAS frequency hopping and Phase Shift Keying/Frequency Shift Keying (PSK/FSK) signals. Binary Phase Shift Keying (BPSK) signals although not LPI, are also examined to further illustrate the principal characteristics of the WD.

14. SUBJECT TERMS Low Probability of Intercept (LPI), Wigner Distribution (WD), Binary Phase Shift Keying (BPSK), Frequency Modulation Continuous Wave (FMCW), Polyphase, Frank, P1, P2, P3, P4, Costas Frequency Hopping, Phase Shift Keying/Frequency Shift Keying (PSK/FSK)			**15. NUMBER OF PAGES** 167
			16. PRICE CODE
17. SECURITY CLASSIFICATION OF REPORT Unclassified	**18. SECURITY CLASSIFICATION OF THIS PAGE** Unclassified	**19. SECURITY CLASSIFICATION OF ABSTRACT** Unclassified	**20. LIMITATION OF ABSTRACT** UL

NSN 7540-01-280-5500 Standard Form 298 (Rev. 2-89)
Prescribed by ANSI Std. 239-18

THIS PAGE INTENTIONALLY LEFT BLANK

Approved for public release; distribution is unlimited.

ANALYSIS OF LOW PROBABILITY OF INTERCEPT (LPI) RADAR SIGNALS USING THE WIGNER DISTRIBUTION

Jen-Yu Gau
Captain, Taiwan Army
BS in Electronics, Chung-Cheng Institute of Technology, Taiwan, 1992

Submitted in partial fulfillment of the
requirements for the degree of

MASTER OF SCIENCE IN SYSTEMS ENGINEERING

from the

NAVAL POSTGRADUATE SCHOOL
September 2002

Author:

Jen-Yu Gau

Approved by:

Phillip E. Pace
Thesis Advisor

Herschel H. Loomis Jr.
Thesis Co-Advisor

Dan C. Boger
Chairman, Information Sciences Department

THIS PAGE INTENTIONALLY LEFT BLANK

ABSTRACT

The parameters of Low Probability of Intercept (LPI) radar signals are hard to identify by using traditional periodogram signal processing techniques. Using the Wigner Distribution (WD), this thesis examines eight types of LPI radar signals. Signal to noise ratios of 0 dB and –6dB are also investigated.

The eight types LPI radar signals examined include Frequency Modulation Continuous Wave (FMCW), Frank code, P1 code, P2 code, P3 code, P4 code, COSTAS frequency hopping and Phase Shift Keying/Frequency Shift Keying (PSK/FSK) signals. Binary Phase Shift Keying (BPSK) signals although not used in modern LPI radars are also examined to further illustrate the principal characteristics of the WD.

THIS PAGE INTENTIONALLY LEFT BLANK

TABLE OF CONTENTS

LIST OF FIGURES

THIS PAGE INTENTIONALLY LEFT BLANK

LIST OF TABLES

THIS PAGE INTENTIONALLY LEFT BLANK

LIST OF ABBREVIATIONS

ARM	Anti-Radiation Missile
AWGN	Additive White Gaussian Noise
BPSK	Binary Phase Shift Keying
CPP	Cycles Per Phase
CW	Continuous Wave
CWD	Choi-Williams Distribution
EA	Electronic Attack
ELINT	Electronic Intelligence
ES	Electronic Support
FFT	Fast Fourier Transform
FMCW	Frequency Modulation Continuous Wave
FSK	Frequency Shift Keying
FT	Fourier Transform
LPI	Low Probability of Intercept
NPBB	Number of Periods per Barker Bit
PAF	Periodic Ambiguity Function
PSD	Power Spectral Density
PSK	Phase Shift Keying
SNR	Signal to Noise Ratio
STFT	Short Time Fourier Transform
SWD	Smoothed Wigner Distribution
TFA	Time-Frequency Analysis
WD	Wigner Distribution

THIS PAGE INTENTIONALLY LEFT BLANK

ACKNOWLEDGMENTS

I would like to thank Professor Phillip E. Pace and Professor Herschel H. Loomis Jr. for their guidance and support during this research effort. They helped me overcome numerous obstacles and made this thesis a very rewarding experience.

THIS PAGE INTENTIONALLY LEFT BLANK

I. INTRODUCTION

A. LPI RADARS

On the modern battlefield, radar systems face serious threats from EA (Electronic Attack) and ARMs (Anti Radiation Missiles). To perform the necessary target detection and tracking and simultaneously hide themselves from an enemy attack, radar systems should be Low Probability of Intercept (LPI). [Ref. 1]

Low probability of intercept radars have the property of low power, wide bandwidth, frequency variability or other design features to make them difficult to be detected or identified by passive intercept receiver devices such as Electronic Support (ES) or Electronic Intelligence (ELINT) receivers. [Ref. 2] LPI radars attempt to provide detection of targets at longer range than intercept receivers can accomplish detection of the radar. The success of LPI radars is measured by how hard it is for them to be detected.

The LPI radars typically have the following features:

(1) Very low peak power (on the order of 1W)

(2) Radiated energy spread over a wide angular region, over a long time interval, and over a wide frequency band.

(3) Continuous Wave (CW) radiation with a large time bandwidth product.

(4) Low sidelobe transmit antenna and carefully selected carrier frequency.

(5) Reduced receiver noise temperature and loss. [Ref. 1, 3, 4]

The transmitter makes use of sophisticated frequency and phase modulation to spread the signal bandwidth making the signal hard to intercept. The receiver makes use of the appropriate matched filter so that the radar performance is similar to that of traditional pulsed radar radiating the same amount of average power.

In this thesis, Binary Phase Shift Keying (BPSK), Frequency Modulation Continuous Wave (FMCW), polyphase code modulation (Frank, P1, P2, P3, P4), COSTAS frequency hopping, and PSK/FSK signals will be analyzed using the Wigner distribution in order to examine detection capability and to extract the modulation parameters.

B. TIME-FREQUENCY ANALYSIS (TFA) DETECTION TECHNIQUES

In many operation radar environments, the non-stationary nature of the received radar signal mandates the use of some form of time-frequency analysis (TFA), which can clearly bring out the non-stationary behavior of the signal. The important virtue of TFA is that it provides an indication of the specific times during which certain spectral components of the signal are observed. [Ref. 5]

Time-frequency analysis allows time and frequency resolution to be controlled independently, but when used for analysis of multi-frequency component signals this approach is vulnerable to cross-terms arising midway between frequency components. There are five techniques, which are in current use. [Ref. 6]

1. Short-Time Fourier Transform (STFT) for a discrete data $x(l)$ is defined as

$$STFT(l,k) = \sum_{n=-\infty}^{\infty} w_N(l-n) \cdot x(l) \cdot e^{-2\pi jk\frac{n}{N}} \tag{1.1}$$

Estimating of the TFA using the STFT involves computing a Fourier transform (FT) of a discrete time series $x(l)$ using a sliding window w_N. At each time index *l*, a *N* point FT is computed, giving a spectral estimate at the frequency index k. The window length *N* is chosen to optimize the time and frequency resolution; the signal is assumed to be stationary within the window. Signal energy density can be estimated from the squared modulus of the STFT. This is called the spectrogram. [Ref. 6]

$$SP(l,k) = \left|STFT(l,k)\right|^2 \tag{1.2}$$

2. Wigner Distribution of a continuous signal $x(t)$ is defined as

$$WD(t,\omega) = \int_{\tau=-\infty}^{\infty} x(t+\frac{\tau}{2}) \cdot x^*(t-\frac{\tau}{2}) \cdot e^{-j\omega\tau} d\tau \tag{1.3}$$

where ω is angular frequency $2\pi f$, the integral is from $-\infty$ to ∞, and the * indicates the complex conjugate of the signal $x(t)$. Various formulations of the WD are possible for sampled time series. One of these uses a moving window w_N with 2*N*-1 nonzero values. [Ref. 6]

3. Wigner Distribution (WD) for a discrete data $x(l)$ is defined as

$$WD(l,k) = 2\sum_{n=-N}^{N-1} w_N(n) \cdot x(l+n) \cdot x^*(l-n) \cdot e^{-2\pi jk\frac{n}{N}} \tag{1.4}$$

The WD offers very good time and frequency resolution compared with the SP, but the cross-terms generated from analysis of multi-component signals can make visual interpretation of the TFA difficult. If another window function w_M with $2M-1$ nonzero values is introduced, the cross-terms can be reduced. [Ref. 6] This gives the smoothed WD.

4. Smoothed Wigner Distribution (SWD) for a discrete data $x(l)$ is defined as:

$$SWD(l,k) = 2\sum_{n=-N}^{N-1} w_N(n)\left\{\sum_{m=-M}^{M-1} w_M(m)\cdot x(l+m+n)\cdot x^*(l+m-n)\right\}\cdot e^{-2\pi jk\frac{n}{N}} \quad (1.5)$$

The discrete time of WD (1.4) is periodic in π, but for SWD the discrete time is periodic in 2π. So unless the signal $x(l)$ has been sampled at least twice the Nyquist rate, there will be aliasing in the WD. This problem can be solved either by sampling the signal at twice the Nyquist rate or by estimating the TFA of the real valued time series $x(l)$. [Ref. 6]

5. Choi-Williams Distribution (CWD) for a discrete data $x(l)$ is defined as:

$$CWD(l,k) = 2\sum_{n=-N}^{N-1} w_N(n)\left\{\sum_{m=-M}^{M-1} w_M(m)\cdot\sqrt{\frac{\sigma}{4\pi n^2}}\cdot e^{-\frac{\sigma m^2}{4n^2}}\cdot x(l+m+n)\cdot x^*(l+m-n)\right\}\cdot e^{-2\pi jk\frac{n}{N}} \quad (1.6)$$

where the parameter σ can be adjusted to attenuate cross-terms. The CWD is a further refinement of the SWD, in which extra smoothing is achieved with an exponential weighting function. Lower values of σ attenuate cross-terms but degrade time and frequency resolution. For large values of σ, cross-terms are not suppressed at all, and the CWD becomes equivalent to the SWD. A good choice of σ is in the range 0.1 to 10. [Ref. 6]

In the following chapters, the WD and its results will be introduced and examined. The SWD and the CWD are for the further studies of the TFA techniques. They will not be examined in this thesis.

C. PRINCIPAL CONTRIBUTIONS

The objective of this thesis was to develop the Wigner distribution (in MATLAB® [Ref. 7]) and use it to analyze and extract the parameters from a variety of complex LPI radar modulations. In order to use the Fast Fourier Transform (FFT), a special kernel transformation is developed and two simple examples are worked in order to insure that the kernel transformation is calculated correctly.

The 114 signals analyzed include BPSK, FMCW, Frank code, P1 code, P2 code P3 code, P4 code, COSTAS, PSK/FSK with frequency hopping and two test signals. Using the Wigner distribution, this thesis successfully extracted all the parameters of the LPI signals except the PSK/FSK with target frequency hopping.

D. THESIS OUTLINE

Chapter II presents a complete introduction of the Wigner Distribution (WD). Two simple examples are provided in this chapter.

Chapter III presents the Binary Phase Shift Keying (BPSK) signals and the analysis of BPSK signals using the Wigner distribution.

Chapter IV presents the FMCW signals and the analysis of FMCW signals using the Wigner distribution.

Chapter V presents the polyphase signals (Frank code, P1, P2, P3 and P4) and the analysis using the Wigner distribution. This chapter also presents the comparison of polyphase signals.

Chapter VI presents the COSTAS frequency hopping signals and the analysis of COSTAS signals using the Wigner distribution.

Chapter VII presents the Phase Shift Keying/Frequency Shift Keying (PSK/FSK) combined with frequency hopping signals and the analysis of PSK/FSK signals using the Wigner distribution.

Chapter VIII presents some concluding remarks and recommendations.

The Appendix contains the MATLAB® m-files of the Wigner distribution and the LPI radar signal matrix.

II. THE WIGNER DISTRIBUTION

The Wigner Distribution (WD) introduced by Wigner in 1932 as a phase representation in quantum mechanics gives a simultaneous representation of a signal in space and spatial-frequency variables. The Wigner distribution has been noted as one of the more useful time-frequency analysis (TFA) techniques for signal processing.

A. WIGNER DISTRIBUTION EQUATION

Recall (1.3), the Wigner distribution of a continuous input signal $x(t)$ is defined as

$$W(t,\omega) = \int_{-\infty}^{\infty} x(t+\tau/2)\cdot x^*(t-\tau/2)e^{-j\omega\tau}d\tau \tag{2.1}$$

where t is the time variable and ω is the frequency variable. The Wigner distribution is a two-dimension function describing the frequency content of a signal as a function of time.

This continuous time and frequency representation can be modified for the discrete sequence $x(l)$, where l is a discrete time index, l = …,-1, 0, 1, …The discrete Wigner distribution (WD) is defined as

$$W(l,\omega) = 2\sum_{n=-\infty}^{\infty} x(l+n)x^*(l-n)e^{-j2\omega n} \tag{2.2}$$

Further modification results in the pseudo-Wigner distribution or windowed-Wigner distribution, which is defined in (2.3), the same as (1.4).

$$W(l,\omega) = 2\sum_{n=-N}^{N-1} x(l+n)x^*(l-n)w(n)w(-n)e^{-j2\omega n} \tag{2.3}$$

where $x(l)$ is a discrete input signal with l from $-\infty$ to ∞, $w(n)$ is a length $2N$ real window function with $w(0)=1$. Here N must be as large as possible within the limits of an acceptable computational cost because a large N gives more output samples, yielding a smoother result. Considering the rectangular window function with a magnitude equal to one the WD becomes [Ref. 8]

$$W(l,\omega)=2\sum_{n=-N}^{N-1}x(l+n)x^{*}(l-n)e^{-j2\omega n} \tag{2.4}$$

Using $f_l(n)$ to represent the kernel function

$$f_l(n)=x(l+n)x^{*}(l-n) \tag{2.5}$$

the WD becomes

$$W(l,\omega)=2\sum_{n=-N}^{N-1}f_l(n)e^{-j2\omega n} \tag{2.6}$$

where the continuous frequency variable ω is sampled by [Ref. 9, 10]

$$\omega=\frac{\pi k}{2N} \tag{2.7}$$

and where $k=0,1,2,...2N-1$. The kernel indexes are modified to fit the standard Discrete Fourier Transform (DFT). Since

$$f_l(n)=f_l^{*}(-n) \tag{2.8}$$

the kernel is a symmetric function, so the Discrete Fourier Transform (DFT) of the kernel is always real.

From equation (2.6) and (2.7), the WD becomes

$$W(l,\frac{\pi k}{2N}) = 2\sum_{n=-N}^{N-1} f_l(n)\exp(-\frac{j2\pi nk}{2N}) \tag{2.9}$$

Adjusting the limits of *n* in order to use the standard FFT algorithms, (2.9) becomes

$$W(l,\frac{\pi k}{2N}) = 2\sum_{n=0}^{2N-1} f_l^{'}(n)\exp(-\frac{j2\pi nk}{2N}) \tag{2.10}$$

Note that in (2.10) the kernel function has been adjusted to $f_l^{'}(n)$, where

$$f_l^{'}(n) = \begin{cases} f_l(n) & , \quad 0 \le n \le N-1 \\ 0 & , \quad n = N \\ f_l(n-2N) & , \quad N+1 \le n \le 2N-1 \end{cases} \tag{2.11}$$

The resulting WD is

$$W(l,\omega) = 2\sum_{n=0}^{2N-1} f_l^{'}(n)e^{-j2\omega n} \tag{2.12}$$

$$W(l,k) = 2\sum_{n=0}^{2N-1} f_l^{'}(n)\exp(-j\frac{\pi kn}{N}) \tag{2.13}$$

Equation (2.13) is the final WD equation, and will be used on the following paragraph to show the computational procedure of the WD values.

B. TWO SIMPLE EXAMPLES

1. Example With Real Inputs

Suppose there is an input signal

$$\begin{aligned} x(l) &= \{2,4,3,6,1,7\} \\ &= \{2(l=-3),4(l=-2),3(l=-1),6(l=0),1(l=1),7(l=2)\} \end{aligned} \tag{2.14}$$

where the length of the input signal $x(l)$ is $2N = 6$, or $N = 3$. l is a discrete time index from $-N$ to N-1. Note that $x = 0$ for $l \le -4$ or $l \ge 3$. Recall (2.11), since now $N = 3$, so

$$f_l'(n) = \begin{cases} f_l(n) & , \quad 0 \le n \le 2 \\ 0 & , \quad n = 3 \\ f_l(n-6), & 4 \le n \le 5 \end{cases} \tag{2.15}$$

For example, for l = -3, the kernel $f_{-3}'(n)$ becomes

$f_{-3}'(n) = \{f_{-3}(n=0), f_{-3}(n=1), f_{-3}(n=2), f_{-3}(n=3), f_{-3}(n=4), f_{-3}(n=5)\}$, from (2.15)

$f_{-3}'(n=3) = f_{-3}(n=3) = 0$, $f_{-3}'(n=4) = f_{-3}(n=4-6) = f_{-3}(n=-2)$ and

$f_{-3}'(n=5) = f_{-3}(n=5-6) = f_{-3}(n=-1)$

Hence,

$f_{-3}'(n) = \{f_{-3}(n=0), f_{-3}(n=1), f_{-3}(n=2), 0, f_{-3}(n=-2), f_{-3}(n=-1)\}$

Recall that $f_l(n) = x(l+n) \cdot x^*(l-n)$,

and $x(l) = \{2(l=-3), 4(l=-2), 3(l=-1), 6(l=0), 1(l=1), 7(l=2)\}$

and $x(l) = 0$ for $l \le -4$ or $l \ge 3$.

$f_{-3}(n)$ for input signal $x(l)$ is computed as follows

$f_{-3}(n=0) = x(-3+0) \cdot x^*(-3-0) = x(-3) \cdot x^*(-3) = 2 \cdot 2 = 4$

$f_{-3}(n=1) = x(-3+1) \cdot x^*(-3-1) = x(-2) \cdot x^*(-4) = 4 \cdot 0 = 0$

$f_{-3}(n=2) = x(-3+2) \cdot x^*(-3-2) = x(-1) \cdot x^*(-5) = 3 \cdot 0 = 0$

$f_{-3}(n=3) = 0$

$f_{-3}(n=4) = f_{-3}(n=-2) = x(-3-2) \cdot x^*(-3+2) = x(-5) \cdot x^*(-1) = 0 \cdot 3 = 0$

$f_{-3}(n=5) = f_{-3}(n=-1) = x(-3-1) \cdot x^*(-3+1) = x(-4) \cdot x^*(-2) = 0 \cdot 4 = 0$

So, $f_{-3}'(n) = \{4, 0, 0, 0, 0, 0\}$

And similarly for $l = 0$,

$$f_0(n=0) = x(0+0)\cdot x^*(0-0) = x(0)\cdot x^*(0) = 6\cdot 6 = 36$$

$$f_0(n=1) = x(0+1)\cdot x^*(0-1) = x(1)\cdot x^*(-1) = 1\cdot 3 = 3$$

$$f_0(n=2) = x(0+2)\cdot x^*(0-2) = x(2)\cdot x^*(-2) = 7\cdot 4 = 28$$

$$f_0(n=3) = 0$$

$$f_0(n=4) = f_0(n=-2) = x(0-2)\cdot x^*(0+2) = x(-2)\cdot x^*(2) = 4\cdot 7 = 28$$

$$f_0(n=5) = f_0(n=-1) = x(0-1)\cdot x^*(0+1) = x(-1)\cdot x^*(1) = 3\cdot 1 = 3$$

So, $f_0^{'}(n) = \{36, 3, 28, 0, 28, 3\}$

Repeating the above procedures, the kernel matrix for l = -4 to 3, and n = 0 to 5 is as shown in Figure 1.

l=3	0	0	0	0	0	0
l=2	49	0	0	0	0	0
l=1	1	42	0	0	0	42
l=0	36	3	28	0	28	3
l=-1	9	24	2	0	2	24
l=-2	16	6	0	0	0	6
l=-3	4	0	0	0	0	0
l=-4	0	0	0	0	0	0
	n =0	*n*=1	*n*=2	*n*=3	*n*=4	*n*=5

Symmetric

Figure 1. The Kernel $f_l^{'}(n)$ Matrix for the Real Six Input Example.

The second step is to use (2.13) to calculate the Wigner distribution. As an example of the calculation, one can pick any l and k to examine the values inside the WD matrix. For example, choose $l = 1$, $k = 2$ and $N = 3$. The WD is

$$\begin{aligned} W(l=1,k=2) &= 2\sum_{n=0}^{2N-1} f_l^{'}(n)\exp(-j\frac{\pi kn}{N}) \\ &= 2\sum_{n=0}^{2\cdot 3-1} f_1^{'}(n)\exp(-j\frac{\pi 2n}{3}) \\ &= 2\sum_{n=0}^{5} f_1^{'}(n)\exp(-j\frac{2\pi n}{3}) \end{aligned} \tag{2.16}$$

From the kernel matrix in Figure 1, the kernel function for $l = 1$ is

$f_1^{'}(n) = \{1, 42, 0, 0, 0, 42\}$. Which means that

$f_1^{'}(0) = 1, f_1^{'}(1) = 42, f_1^{'}(2) = 0, f_1^{'}(3) = 0, f_1^{'}(4) = 0, f_1^{'}(5) = 42$.

So from (2.16), the WD for $l = 1$, $k = 2$ is

$$\begin{aligned} W(1,2) &= 2f_1^{'}(0)\cdot\exp(-j\frac{2\cdot\pi\cdot 0}{3}) + 2f_1^{'}(1)\cdot\exp(-j\frac{2\cdot\pi\cdot 1}{3}) + 2f_1^{'}(2)\cdot\exp(-j\frac{2\cdot\pi\cdot 1}{3}) \\ &\quad + 2f_1^{'}(3)\cdot\exp(-j\frac{2\cdot\pi\cdot 3}{3}) + 2f_1^{'}(4)\cdot\exp(-j\frac{2\cdot\pi\cdot 4}{3}) + 2f_1^{'}(5)\cdot\exp(-j\frac{2\cdot\pi\cdot 5}{3}) \\ &= 2\cdot 1\cdot(0) + 2\cdot 42\cdot(\text{-0.5000 - 0.8660i}) + 2\cdot 0 + 2\cdot 0 + 2\cdot 0 + 2\cdot 42\cdot(\text{-0.5000 + 0.8660i}) \\ &= -82 \end{aligned}$$

Repeating the above procedures, gives the WD matrix at discrete time index l = -4 to 3 and discrete frequency index k = 0 to 5 as a symmetric matrix shown in Figure 2. An important feature in this Wigner distribution computation result is that all the components in WD matrix are real.

l=3	0	0	0	0	0	0
l=2	98	98	98	98	98	98
l=1	170	86	-82	-166	-82	86
l=0	196	22	10	172	10	22
l=-1	122	62	-34	-70	-34	62
l=-2	56	44	20	8	20	44
l=-3	8	8	8	8	8	8
l=-4	0	0	0	0	0	0
	k=0	k=1	k=2	k=3	k=4	k=5

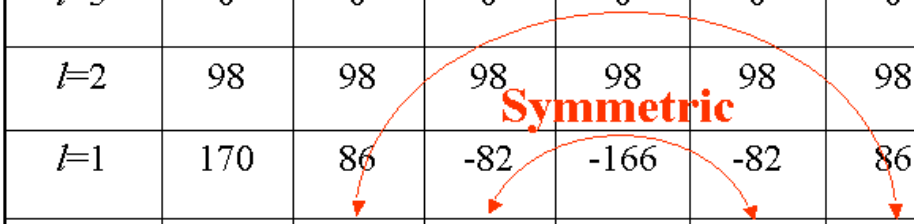

Figure 2. The WD Matrix $W(l,k)$ for the Real Six Input Example.

2. Example With Complex Inputs

Consider the input signal

$$x = I + j \cdot Q \tag{2.17}$$

where

$$I = \cos(2\pi f_c t) \tag{2.18}$$

$$Q = \sin(2\pi f_c t) \tag{2.19}$$

If carrier frequency f_c=1kHz; sampling frequency f_s= 7kHz; and $t = 0 : \frac{1}{f_s} : \frac{7}{f_s}$, then the first eight input points from discrete time index l = -4 to 3 is

$$x(l) = \{1+0i,\ 0.6235\ +\ 0.7818i,\ -0.2225\ +\ 0.9749i,\ -0.9010\ +\ 0.4339i,\\ -0.9010\ -\ 0.4339i,\ -0.2225\ -\ 0.9749i,\ 0.6235\ -\ 0.7818i,\ 1+0i\} \tag{2.20}$$

Consider the value when $l = 0$, $n = 3$.
Using (2.11) with an input length $2N = 8$ or $N = 4$. The kernel is

$$f_l^{'}(n) = \begin{cases} f_l(n) & ,0 \le n \le 3 \\ 0 & ,n = 4 \\ f_l(n-8) & ,5 \le n \le 7 \end{cases} \tag{2.21}$$

Here $f_l^{'}(n) = \{f_l(1), f_l(2), f_l(3), 0, f_l(-3), f_l(-2), f_l(-1)\}$

Since $f_l(n) = x(l+n) \cdot x^*(l-n)$, the kernel at $l = 0$, $n = 3$ is

$$\begin{aligned} f_0^{'}(3) = f_0(3) &= x(0+3) \cdot x^*(0-3) = x(3) \cdot x^*(-3) \\ &= 1 \cdot (0.6235 + 0.7818 \cdot i)^* \\ &= 0.6235 - 0.7818 \cdot i \end{aligned}$$

Repeating the same procedures as discussed in real input case, the kernel matrix for the eight inputs complex input example is shown in Figure 3.

1	0	0	0	0	0	0	0	3
1	-0.2225 + 0.9749i	0	0	0	0	0	-0.2225 - 0.9749i	2
0.9999	-0.2226 + 0.9749i	-0.9010 - 0.4339i	0	0	0	-0.9010 + 0.4339i	-0.2226 - 0.9749i	1
1.0001	-0.2225 + 0.9749i	-0.9009 - 0.4339i	0.6235 - 0.7818i	0	0.6235 + 0.7818i	-0.9009 + 0.4339i	-0.2225 - 0.9749i	0
1.0001	-0.2225 + 0.9749i	-0.9009 - 0.4339i	0.6235 - 0.7818i	0	0.6235 + 0.7818i	-0.9009 + 0.4339i	-0.2225 - 0.9749i	-1
0.9999	-0.2226 + 0.9749i	-0.9010 - 0.4339i	0	0	0	-0.9010 + 0.4339i	-0.2226 - 0.9749i	-2
1	-0.2225 + 0.9749i	0	0	0	0	0	-0.2225 - 0.9749i	-3
1	0	0	0	0	0	0	0	-4
0	1	2	3	4	5	6	7	

l=0,*n*=3

l

n

Figure 3. The Kernel Matrix for the Complex Eight Input Example.

Now the WD matrix is examined from Figure 3, when $l = -1$, the kernel is

$$f_{-1}^{'}(n) = \{1.0001,\ -0.2225 + 0.9749i,\ -0.9009 - 0.4339i,\ 0.6235 - 0.7818i,\ 0,\ 0.6235 + 0.7818i,\ -0.9009 + 0.4339i,\ -0.2225 - 0.9749i\} \tag{2.22}$$

Consider the case when $l = -1$, $k = 4$. Recall (2.13), the WD for $N = 4$ is

$$\begin{aligned} W(l=-1,k=4) &= 2\sum_{n=0}^{2N-1} f_l^{'}(n)\exp(-j\frac{\pi kn}{N}) \\ &= 2\sum_{n=0}^{2\cdot 4-1} f_{-1}^{'}(n)\frac{\pi 4n}{4}) \\ &= 2\sum_{n=0}^{7} f_{-1}^{'}(n)\exp(-jn\pi) \end{aligned} \tag{2.23}$$

From (2.22) and (2.23)

$$W(l=-1,k=4)=2\sum_{n=0}^{7} f_{-1}^{'}(n)\cdot\exp(-jn\pi)$$

$$=2\begin{bmatrix} f_{-1}^{'}(0)\cdot\exp(0)+f_{-1}^{'}(1)\cdot\exp(-j\pi)+f_{-1}^{'}(2)\cdot(-j2\pi)+f_{-1}^{'}(3)\cdot(-j3\pi) \\ +f_{-1}^{'}(4)\cdot(-j4\pi)+f_{-1}^{'}(5)\cdot(-j5\pi)+f_{-1}^{'}(6)\cdot(-j6\pi)+f_{-1}^{'}(7)\cdot(-j7\pi) \end{bmatrix}$$

$$=2\cdot\begin{bmatrix} 1.0001\cdot(1)+(-0.2225+0.9749i)\cdot(-1)+(-0.9009-0.4339i)\cdot(1) \\ +(0.6235-0.7818i)\cdot(-1)+0+(0.6235+0.7818)\cdot(-1) \\ +(-0.9009+0.4339i)\cdot(1)+(-0.2225-0.9749i)\cdot(-1) \end{bmatrix}$$

$$=-3.2073$$

Again the WD matrix of the eight input points is another real and symmetric $2N\times 2N$ matrix. Note the important feature: The WD is always real whether the input signal is real or complex. Figure 4 shows the WD matrix of the eight complex input samples.

2.0000	2.0000	2.0000	2.0000	2.0000	2.0000	2.0000	2.0000	3
1.1099	4.1280	5.8995	5.3867	2.8899	-0.1282	-1.8997	-1.3868	2
-2.4943	2.3923	9.5036	7.1225	-0.7139	-1.8638	1.7041	0.3485	1
0.0004	-1.5882	12.6307	6.6749	-3.2073	2.1112	-1.4231	0.7965	0
0.0004	-1.5882	12.6307	6.6749	-3.2073	2.1112	-1.4231	0.7965	-1
-2.4943	2.3923	9.5036	7.1225	-0.7139	-1.8638	1.7041	0.3485	-2
1.1099	4.1280	5.8995	5.3867	2.8899	-0.1282	-1.8997	-1.3868	-3
2.0000	2.0000	2.0000	2.0000	2.0000	2.0000	2.0000	2.0000	-4
0	1	2	3	k	4	5	6	7

l

l=-1,*k*=4

Figure 4. The WD Matrix for the Complex Eight Input Example.

Figure 5(a) shows the mesh plot of the eight input complex example in time domain. The time resolution $1/f_s$ is indicated on this plot. Figure 5(b) shows the mesh plot in frequency domain. The carrier frequency in this plot is about 900Hz, very close to real value 1kHz. The frequency resolution $f_s/2/\#samples$ is also indicated on this plot.

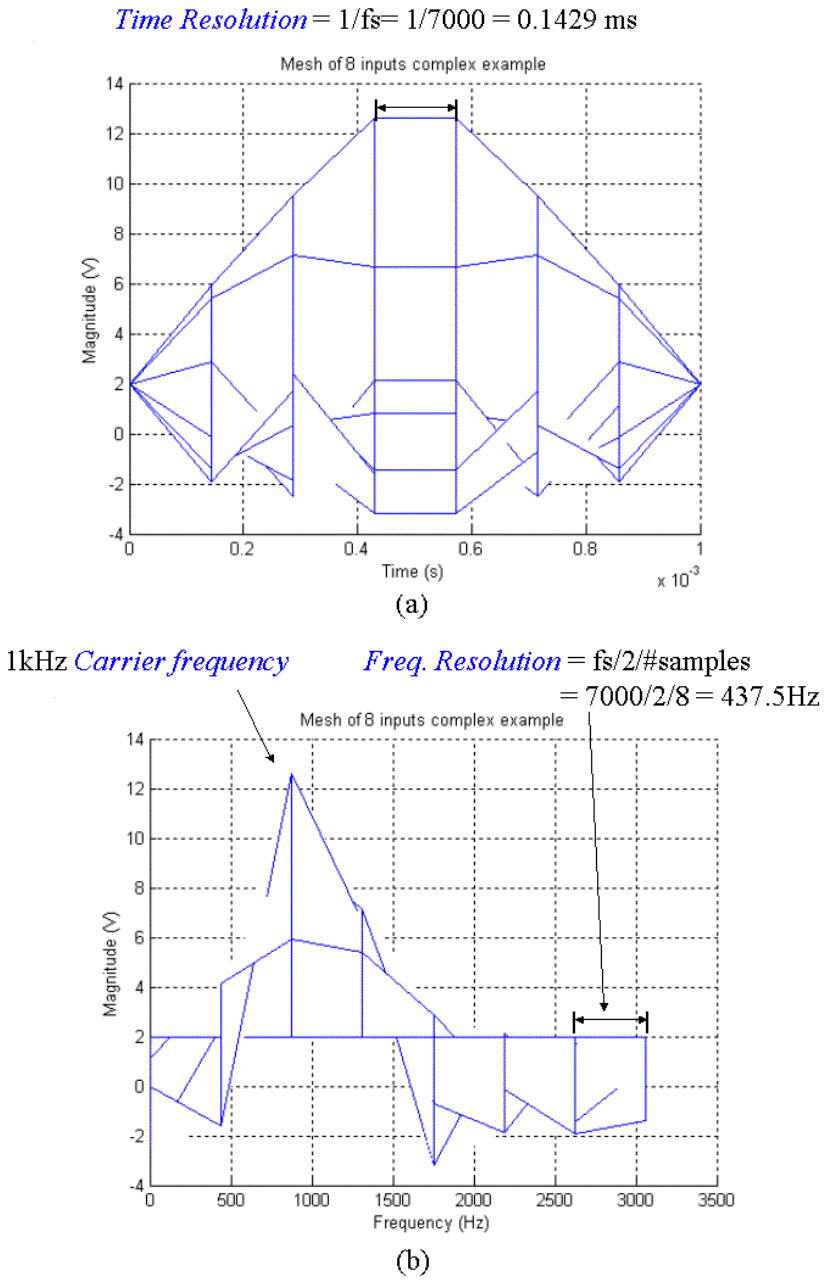

Figure 5. WD for Eight Inputs Complex Example (a) 2D Mesh in Time Domain. (b) 2D Mesh in Frequency Domain.

Figure 6(a) shows the 3D mesh plot of the eight inputs complex example. This plot shows the magnitude in both time and frequency domain. Figure 6(b) shows the contour plot. The contour plot is a 2D time- frequency domain plot. The magnitude is represented by different color as shows in the color bar.

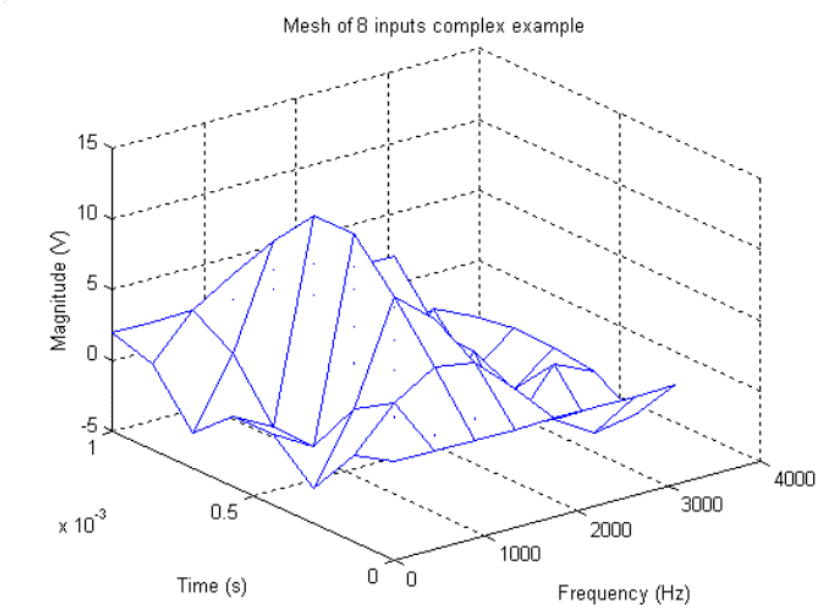

(a)

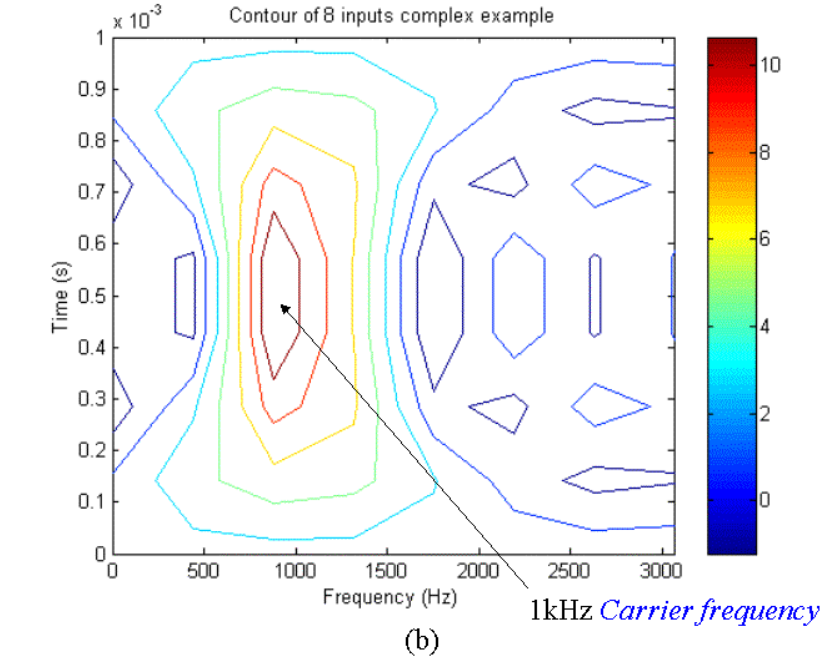

(b)

Figure 6. WD for Eight Inputs Complex Example (a) 3D Mesh. (b) Contour.

Figure 7(a)(b) shows the 2D time domain and frequency domain mesh plot of the 101 inputs complex example (Eq. (2.18), (2.19) with $t = 0 : \frac{1}{f_s} : \frac{100}{f_s}$). The 1kHz carrier frequency is more clearly shown in Figure 7(b) than that in Figure 5(b). Comparing with Figure 5 and Figure 7 one can find the more input sample points that are used the better is the WD output performance.

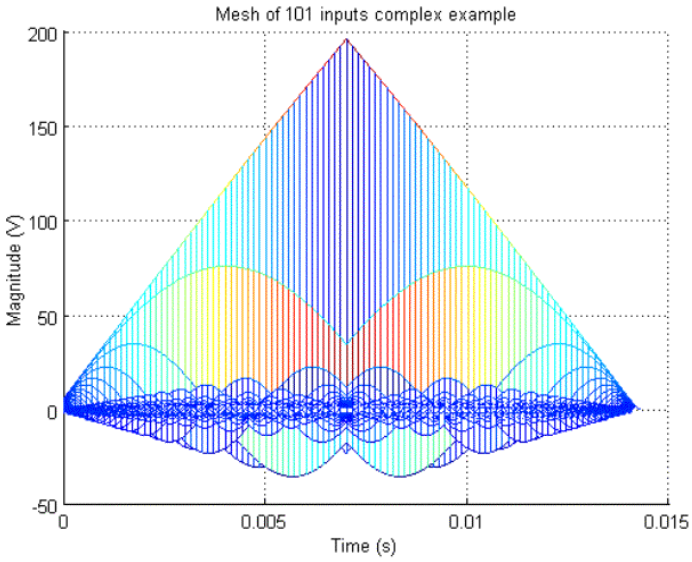

(a)

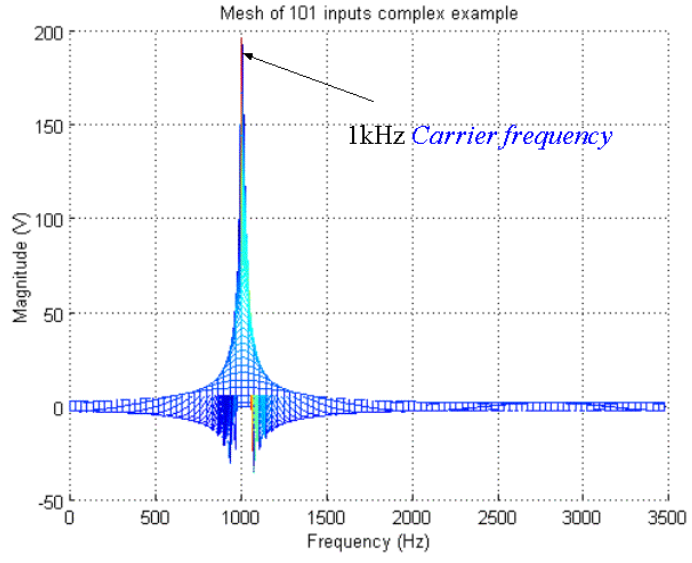

(b)

Figure 7. WD for 101 Inputs Complex Example (a) 2D Mesh in Time Domain. (b) 2D Mesh in Frequency Domain.

Figure 8(a) shows a zoom in of the mesh plot in time domain. The total time interval and time resolution $1/f_s$ are indicated on this plot. Figure 8(b) shows the zoom in mesh plot in the frequency domain and indicates the frequency interval and frequency resolution $f_s/2/\#samples$.

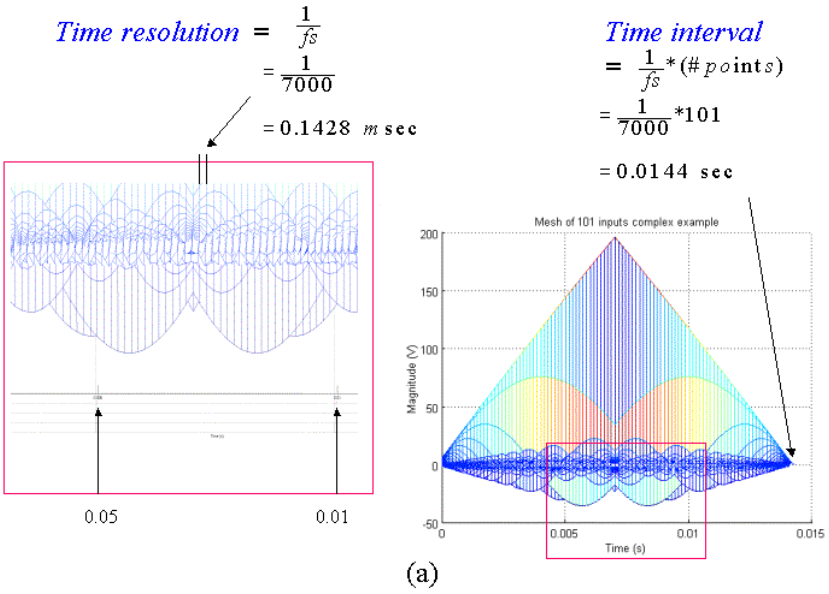

Figure 8. WD for 101 Inputs Complex Example (a) Zoom In 2D Mesh in Time Domain. (b) Zoom In 2D Mesh in Frequency Domain.

Figure 9(a) shows the three-dimension mesh plot of the 101 inputs complex example. This plot shows the magnitude in both time and frequency domain. Figure 9(b) shows the contour plot of the 101 inputs complex example. Contour plot is a 2D time-frequency domain plot. The magnitude is represented by different color as shows in the color bar. The carrier frequency is also marked on the plot.

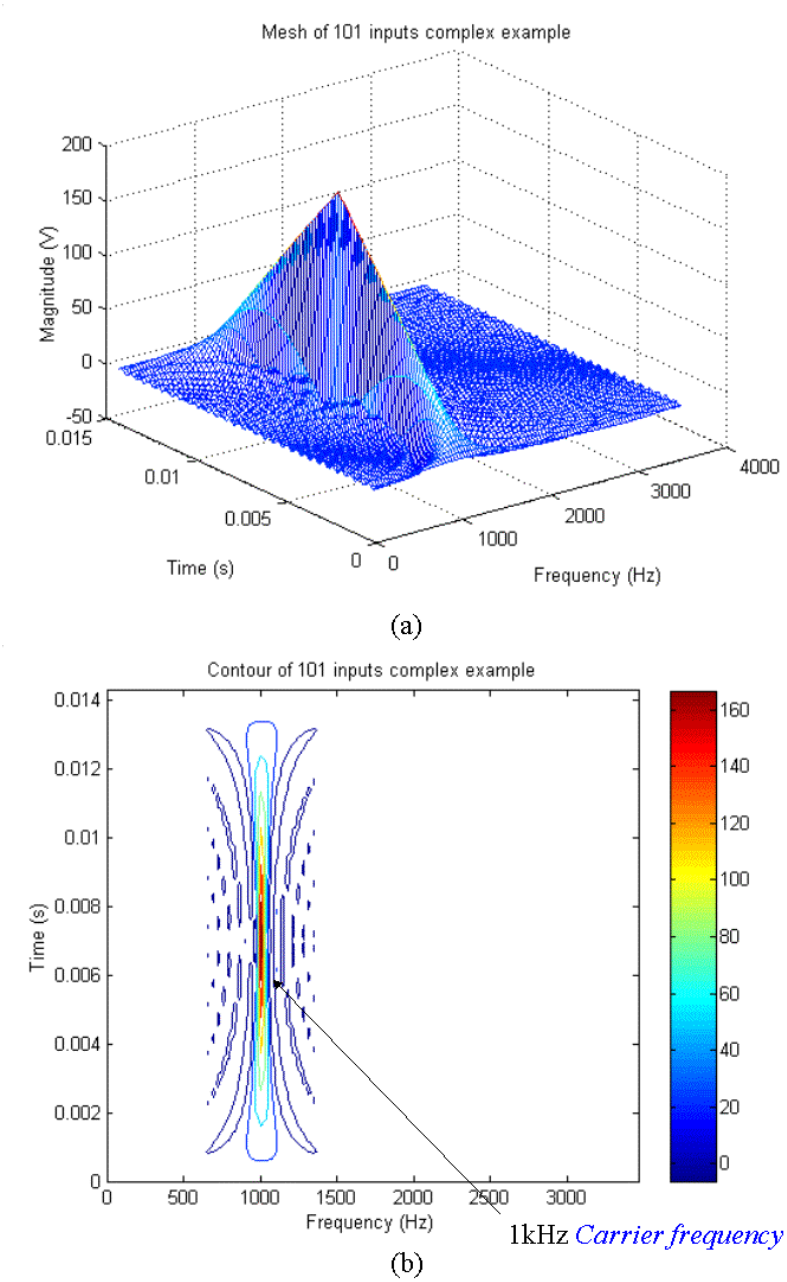

Figure 9. WD for 101 Inputs Complex Example (a) 3D Mesh. (b) Contour.

Now consider the WD for two carrier frequencies with $f_{c1} = 1kHz$, $f_{c2} = 2kHz$ as shown in Figure 10. Recall that $I = \cos(2\pi f_c t)$ and $Q = \sin(2\pi f_c t)$. Now

$I' = \cos(2\pi f_{c1} t) + \cos(2\pi f_{c2} t)$ and $Q' = \sin(2\pi f_{c1} t) + \sin(2\pi f_{c2} t)$

Figure 10 (a) is the 2D frequency domain mesh plot which shows the two carrier frequencies as well as the frequency cross term. The frequency of the cross term is $\frac{f_{c1} + f_{c2}}{2}$. Note that the magnitudes[1] are positive for the two real carrier frequencies. But for the cross term, the magnitude includes both the positive and negative parts.

Figure 10(b) shows the contour plot of these two carrier frequencies and their cross term. Note that the shape and color of the cross term is not like those of the two real carrier frequencies. The cross term contains many red and blue 'dots', but the real $f_{c1,} f_{c2}$ are yellow 'strips'.

Figure 11(a) shows the 3D mesh plot. In this plot displays the cross term is combined by many 'peaks'. The positive peaks represents the red dots, the negative peaks represents the blue dots in figure 10(b).

Figure 11(b) is the 2D mesh in the time domain. It shows the real signal and the cross term in the time domain. This plot states that the cross term is consisted of a series of positive and negative magnitude components in time domain.

---

[1] The label "Magnitude" was used for WD value in all the mesh plots. Note that is not a true magnitude.

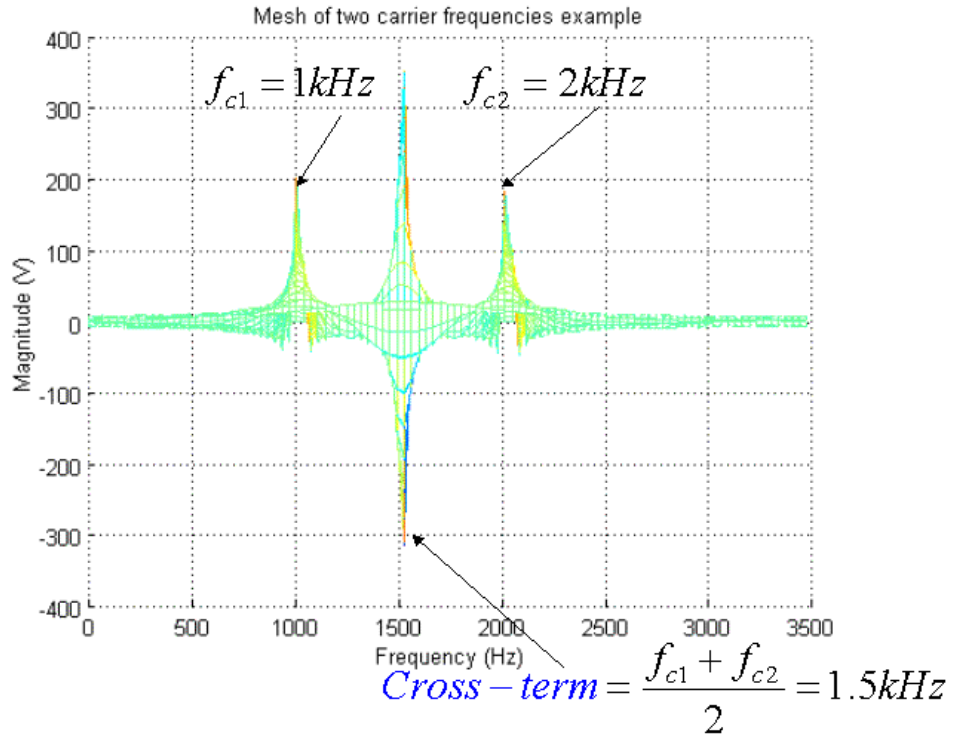

(a)

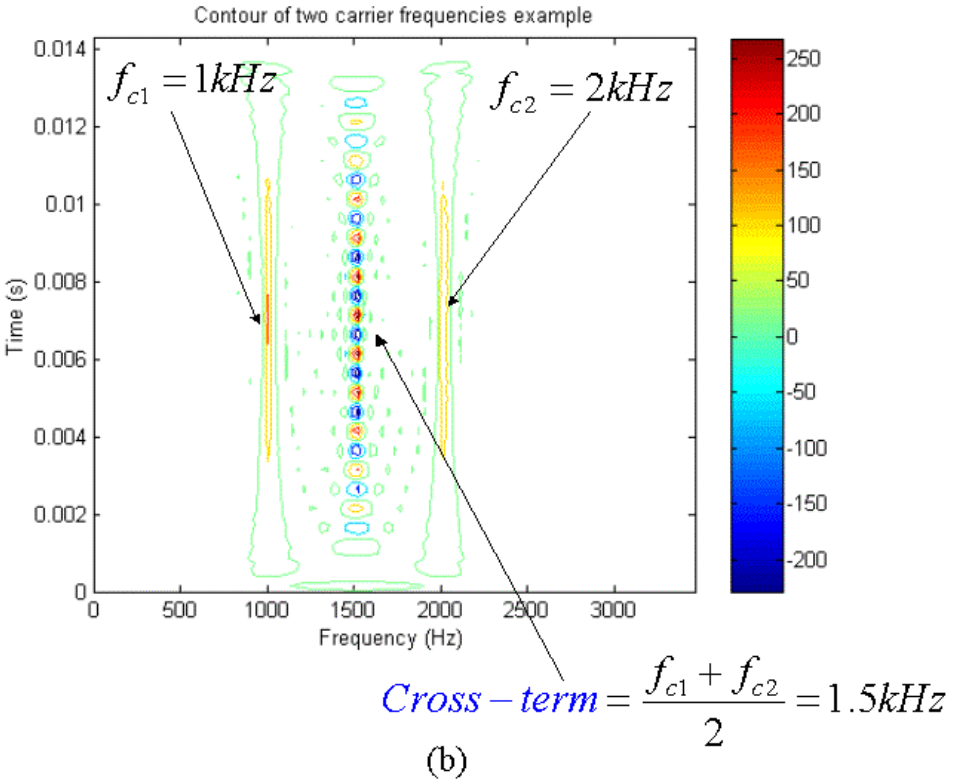

(b)

Figure 10. WD for Two Carrier Frequencies Example (a) 2D Mesh in Frequency Domain. (b) Contour.

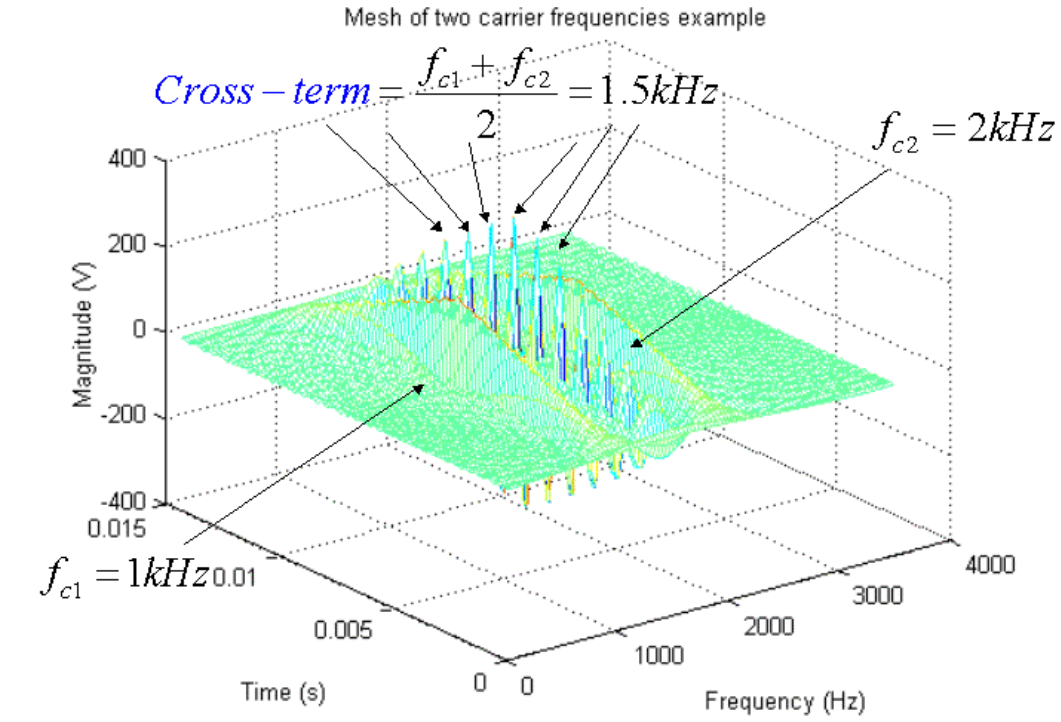

(a)

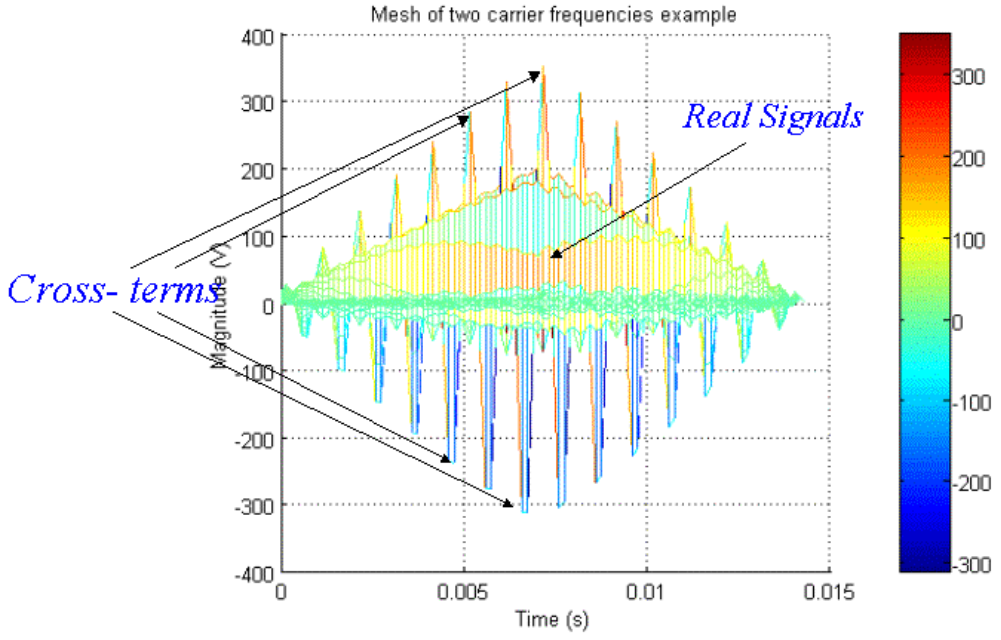

(b)

Figure 11. WD for Two Carrier Frequencies Example (a) 3D Mesh. (b) 2D Mesh in Time Domain.

C. SUMMARY

This chapter contains some simple example signals to generate the kernel function and Wigner distribution (WD). No matter whether the signals are real or complex, the kernel and WD matrix are always real and symmetric. This is a very important feature for the Wigner distribution and an important reason why the WD is a good tool to analyze signals by the mesh and contour plots.

In Figures 5 through 11, the carrier frequencies are very easy to identify in these simple examples. In the following chapters, the signals contain complex LPI modulations and are no longer that simple. The Wigner distribution's ability to determine the phase and frequency modulations for those signals will be demonstrated.

Figures 10 and 11 illustrate the frequency cross terms and how they are represented in the WD mesh and contour plots. It is shown that the cross terms sometimes make the signal analysis more difficult.

In the next chapter, the BPSK signals and its WD analysis will be examined.

THIS PAGE INTENTIONALLY LEFT BLANK

III. BINARY PHASE SHIFT KEYING (BPSK)

A. BPSK

Phase shift keying (PSK) is an angle-modulated, constant-amplitude digital modulation. PSK is similar to conventional phase modulation except that with PSK the input signal is a binary digital signal and a limited number of output phases are possible.

Binary phase shift keying (BPSK) has two phases for a single carrier frequency ("binary" meaning "2"). One output phase represents logic 1 and the other is logic 0. As the input digital signal changes state, the phase of the output carrier shifts between two angles that are 180° out of phase. BPSK is a form of suppressed-carrier, square-wave modulation of a continuous wave (CW) signal. [Ref. 11]

Figure 12 shows the BPSK modulator phase diagram. Figure 13 shows the BPSK modulator output phase vs. time relationship. Normally, there are many carrier cycles per modulation period.

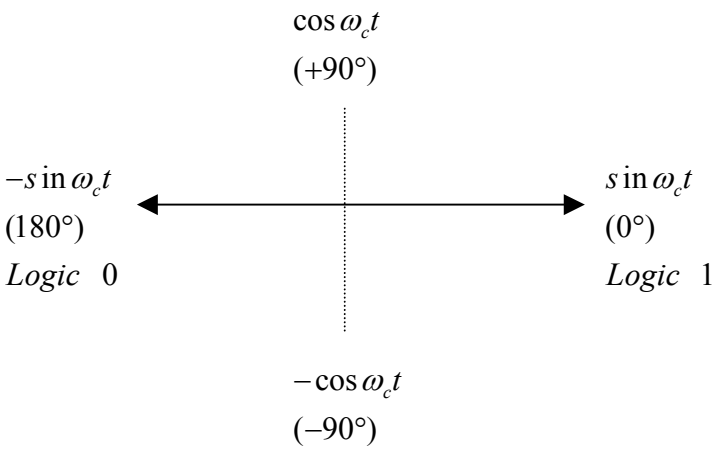

Figure 12. BPSK Modulator Phase Diagram.

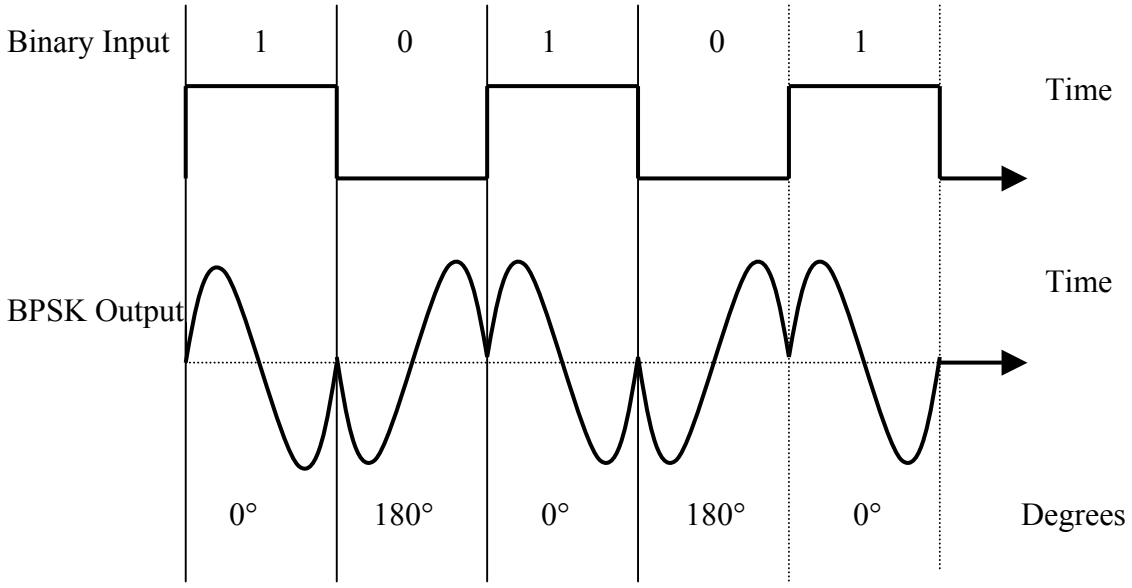

Figure 13. BPSK Modulator Output Phase vs. Time Relationship.

1. Binary Phase-Coded Pulse Compression

Phase changes can be used to increase the signal bandwidth of a long pulse for purpose of pulse compression. A long pulse of duration T is divided into N subpulses each of width t_b. An increase in bandwidth is achieved by changing the phase of each subpulse (since the rate of change of phase with time is a frequency). A common form of phase change is binary phase coding, in which the phase of each subpulse is selected to be either 0 or π radians according to some specified criterion.

The radar receiver correlates the received pulses with the known transmitted pulse, usually with a matched filter. Thus output of the matched filter will be a compressed pulse of width t_b and will have peak N times greater than that of the long pulse. The pulse compression ratio equals to the number of subpulses $N = T/t_b \sim BT$, where the bandwidth $B \sim 1/t_b$.

The matched filter output extends for a time T on either side of the peak response. The unwanted but unavoidable portions of the output waveform other than the compressed pulse are known as time sidelobes. When the selection of the phase is made at random, the expected maximum (power) sidelobe is about $2/N$ below the peak of the compressed pulse. [Ref. 4]

2. Barker Codes

One family of binary phase codes that produce compressed waveform with constant sidelobe levels equal to unity is the Barker code. Figure 14 illustrates this concept for a Barker code of length seven. There are only nine known Barker codes that share this unique property. They are listed in Table 1. [Ref. 12]

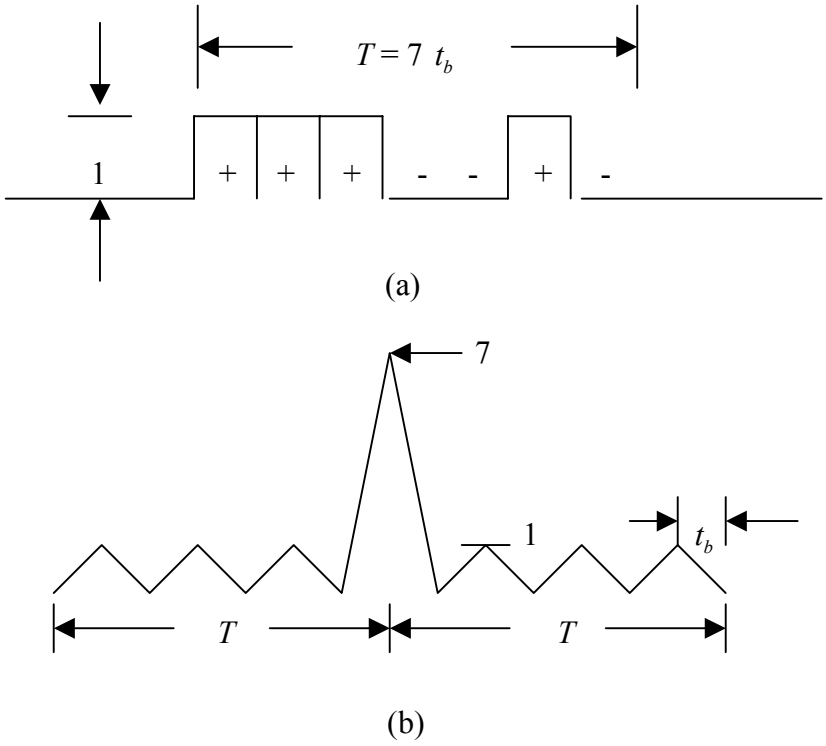

Figure 14. Barker Code of Length 7 (a) A Long Pulse with 7 Equal Subdivisions Whose Individual Phase are 0°(+) or 180°(-). (b) Autocorrelation Function for Plot (a).

In general, the autocorrelation function (which is an approximation for the matched filter output) for code length N, Barker code will be $2Nt_b$ wide. The main lobe is $2t_b$ wide. The peak value is equal to N. There are (N-1)/2 sidelobes on either side of the main lobe. Note that in Figure 14(b) the main lobe is 7 and all the other sidelobes are one. [Ref. 12]

Code Length	Code Elements	Sidelobe Level, dB
2	+ −, + +	-6.0
3	+ + −	-9.5
4	+ + − +, + + + −	-12.0
5	+ + + − +	-14.0
7	+ + + − − + −	-16.9
11	+ + + − − − + − − + −	-20.8
13	+ + + + + − − + + − + − +	-22.3

Table 1. Barker Codes.

The most sidelobe reduction offered by a Barker code is –22.3dB (13 bit code length), which may not be sufficient for the desired radar application. However, Barker codes can be combined to generate much longer codes. In the following example and Figure 15, Barker code B54 is a Barker code combines code length 5 and code length 4. But unfortunately, the sidelobes of a combined Barker code autocorrelation function are no longer equal to unity.

$$B54 = \{ 11101, 11101, 00010, 11101 \} \quad (3.1)$$

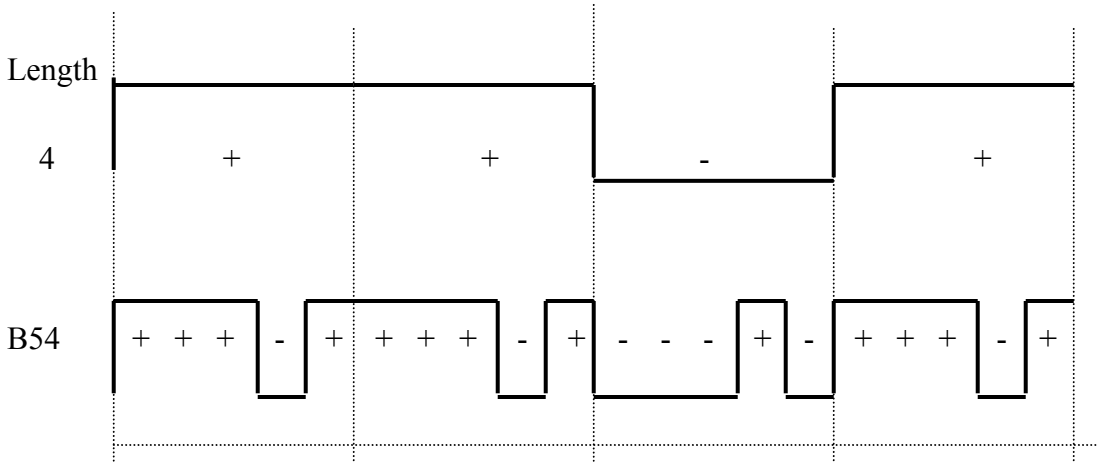

Figure 15. Combined Barker Code with Code Length 5 and 4.

Figure 16 below shows a basic block diagram of the transmitter design. The signal *x(t)* is a CW sinusoid, which for this project was set to

$$x(t) = \sin(2\pi f_c t) \tag{3.2}$$

with carrier frequency f_c. The discrete signal *xnT* is created by sampling *x(t)* with at a sample rate at least twice that of the highest frequency of the CW signal to obey the Nyquist sampling theorem and avoid aliasing. The sampling frequency, f_s, is the product of the carrier frequency f_c and the sample ratio variable

$$SAR = f_s / f_c \tag{3.3}$$

that is set by the user. To obey the Nyquist sampling theorem, *SAR* must be greater than two to avoid anomalies that may arise from floating point operations right at the Nyquist rate. Due to these limitations, the minimum useful sampling frequency is three times the signal frequency, or *SAR* >= 3. [Ref. 13]

Although there are only 13 bits in this Barker code, the actual sequence of bits in brkseq also depends on the sampling frequency and the number of complete periods of

signal *xnT* that are to occur within the same timeframe as one Barker code bit. If the number of periods per Barker bit (*NPBB*) is set to one, one full period of the carrier frequency fits within one bit of the 13-bit Barker code.

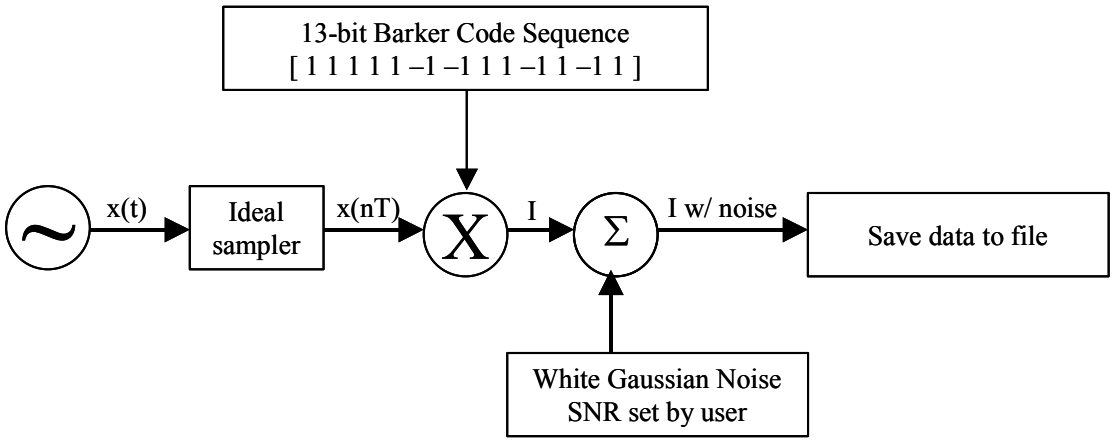

Figure 16. BPSK Transmitter Block Diagram.

In this chapter, twelve BPSK signals will be examined. They are numbered from one to twelve and listed in Table 2. A 1kHz carrier frequency and 7kHz sampling frequency are used for these signals.

No.	BPSK	Barker Code Length	NPBB	SNR
1	B_1_7_7_1_s	7	1	Signal Only
2	B_1_7_7_1_0	7	1	0 dB
3	B_1_7_7_1_-6	7	1	-6 dB
4	B_1_7_11_1_s	11	1	Signal Only
5	B_1_7_11_1_0	11	1	0 dB
6	B_1_7_11_1_-6	11	1	-6 dB
7	B_1_7_7_5_s	7	5	Signal Only
8	B_1_7_7_5_0	7	5	0 dB
9	B_1_7_7_5_-6	7	5	-6 dB
10	B_1_7_11_5_s	11	5	Signal Only
11	B_1_7_11_5_0	11	5	0 dB
12	B_1_7_11_5_-6	11	5	-6 dB

Table 2. BPSK Signals.

B. WIGNER DISTRIBUTION FOR BPSK

Consider the same twelve BPSK signals in Table 2 and use them as the inputs for Wigner distribution (WD). The WD results of these twelve signals are shown in Figure 17 through 20. The mesh plots show the frequency domain of the BPSK signals after the WD processing. The contour plots show both the frequency domain and time domain of the results.

In Figure 17, the carrier frequency f_c can be clearly identified by the location of the highest or lowest peak value in Figure 17(a), or by the center of the symmetric shapes in Figure 17(b).

Secondly, the peak magnitude in Figure 175(a) is about 600. So the 3dB bandwidths should be the frequency range between 300 on both sides, which extends from 500Hz to 1500 Hz in Figure 17(a). The 3dB bandwidth is also the value of f_c divided by *NPBB*. That is equal to 1000Hz in Figure 17, 18 (*NPBB* = 1), or 200Hz in Figure 19, 20 (*NPBB* = 5). The 3dB bandwidth is also called the chip rate.

Thirdly, in Figure 17(a), if we look closely within the 3dB bandwidth, one can find there are 15 peaks in the bandwidth range. In other words, there are 14 intervals in the range from 500Hz to 1500Hz, and 14 is two times the Barker code length. In Figure 18(a), 22 intervals are in the 3dB bandwidth range since the Barker code length is eleven.

Using the same analysis for Figures 17 to 20, we can find the carrier frequency, 3dB bandwidth and barker code length. However, for *NPBB* more than one, the analysis of Barker code length becomes difficult.

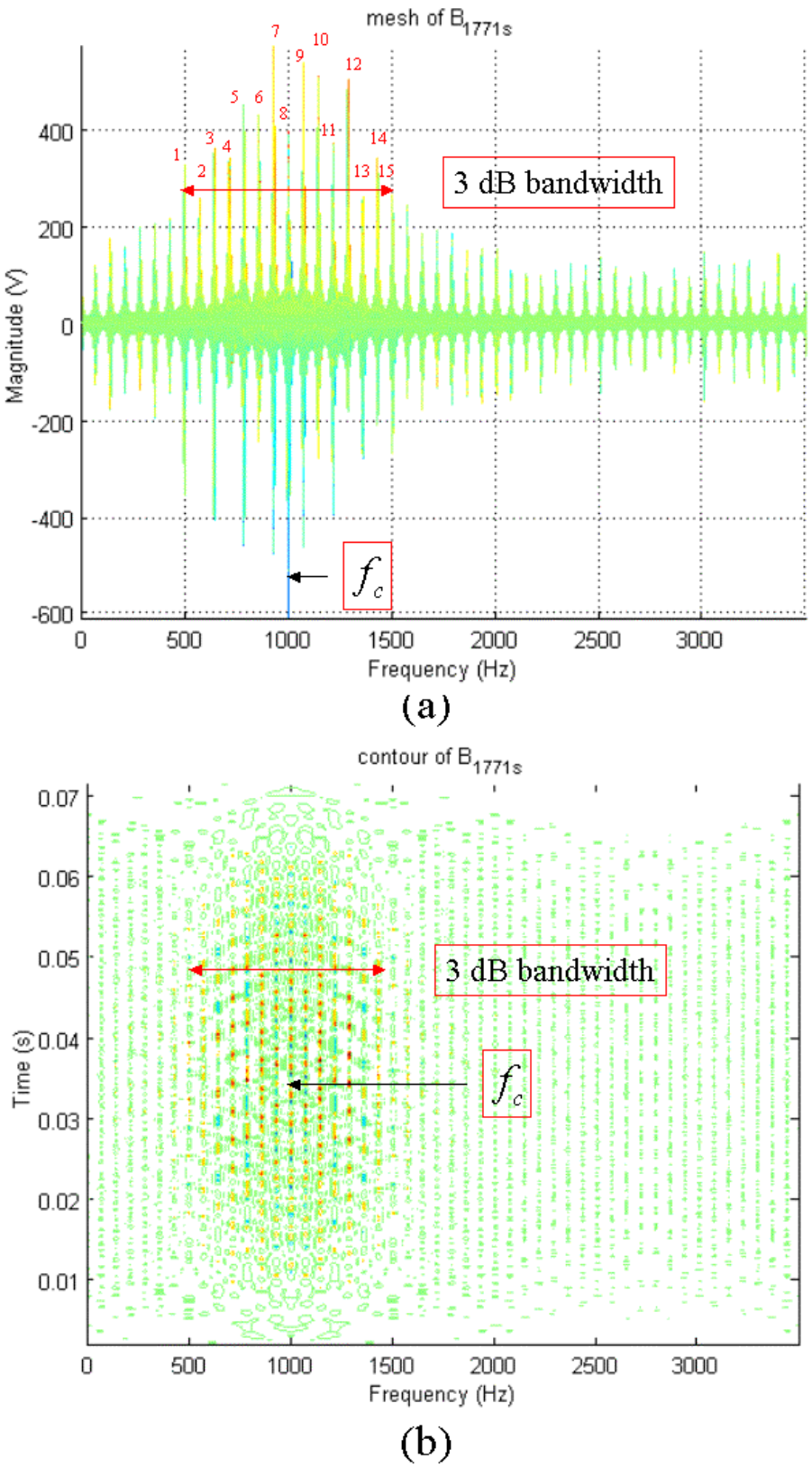

Figure 17. WD for BPSK with 7 Bit Barker Code, NPBB = 1, Signal Only, (No.1) (a) 2D Mesh in Frequency Domain. (b) Contour.

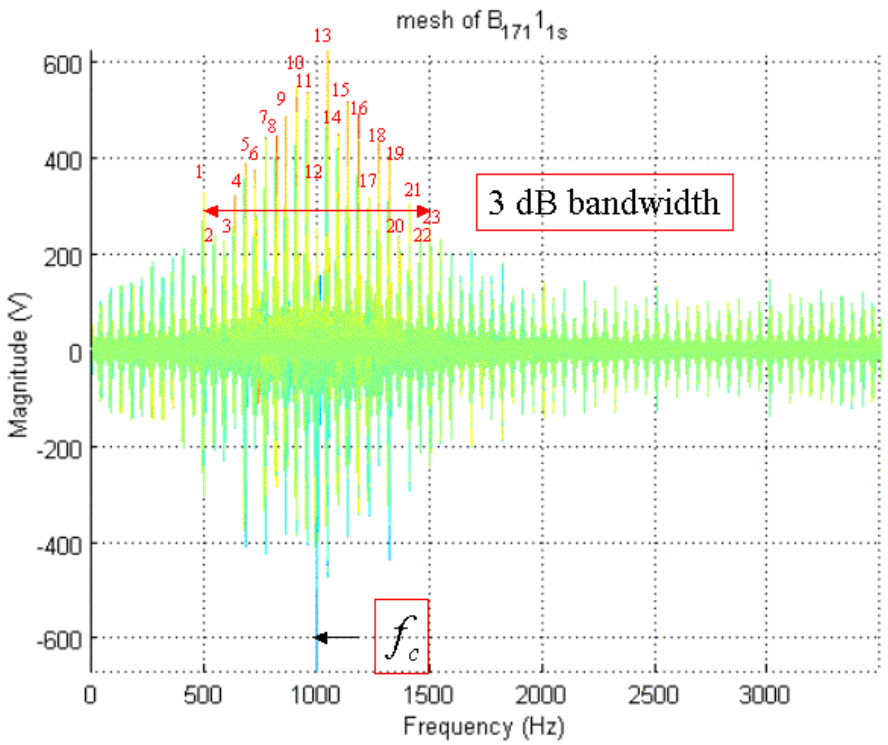

(a)

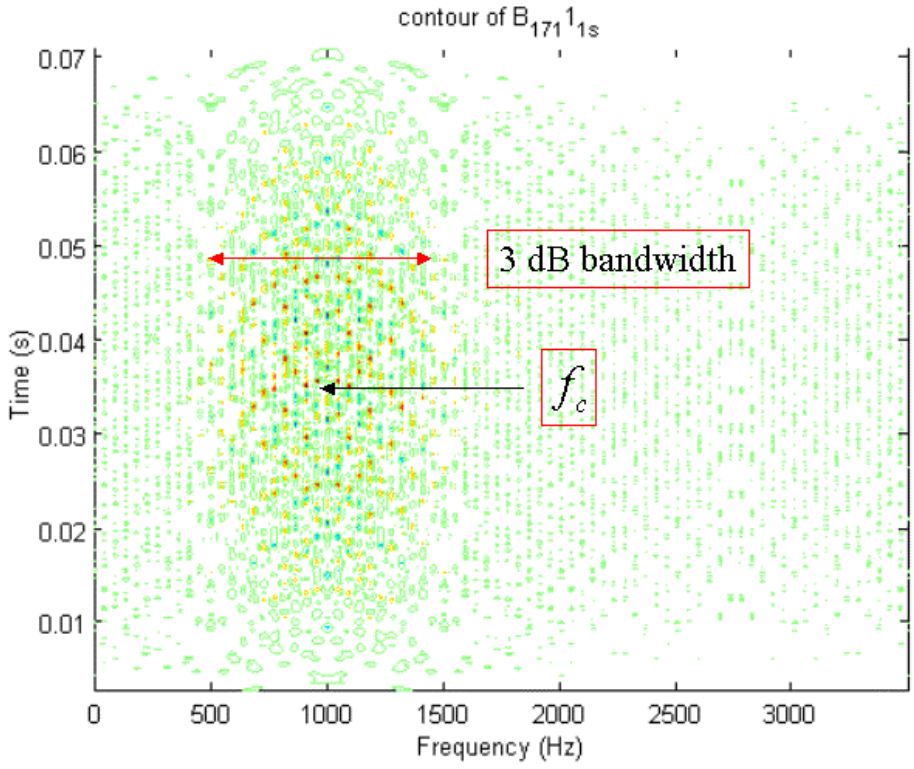

(b)

Figure 18. WD for BPSK with 11 Bit Barker Code, NPBB = 1, Signal Only, (No.4) (a) 2D Mesh in Frequency Domain. (b) Contour.

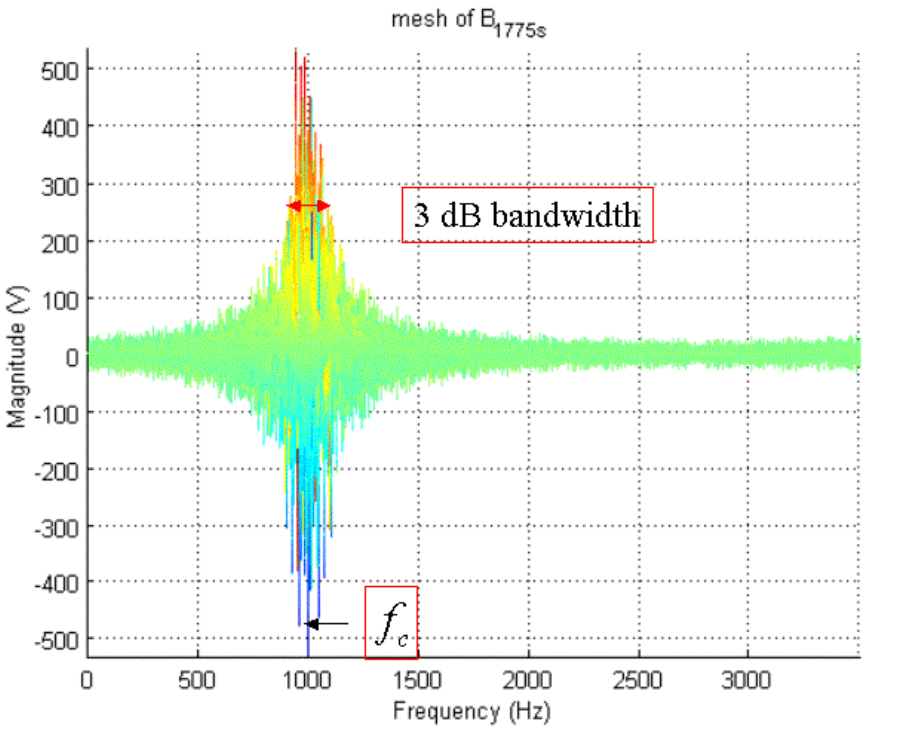

(a)

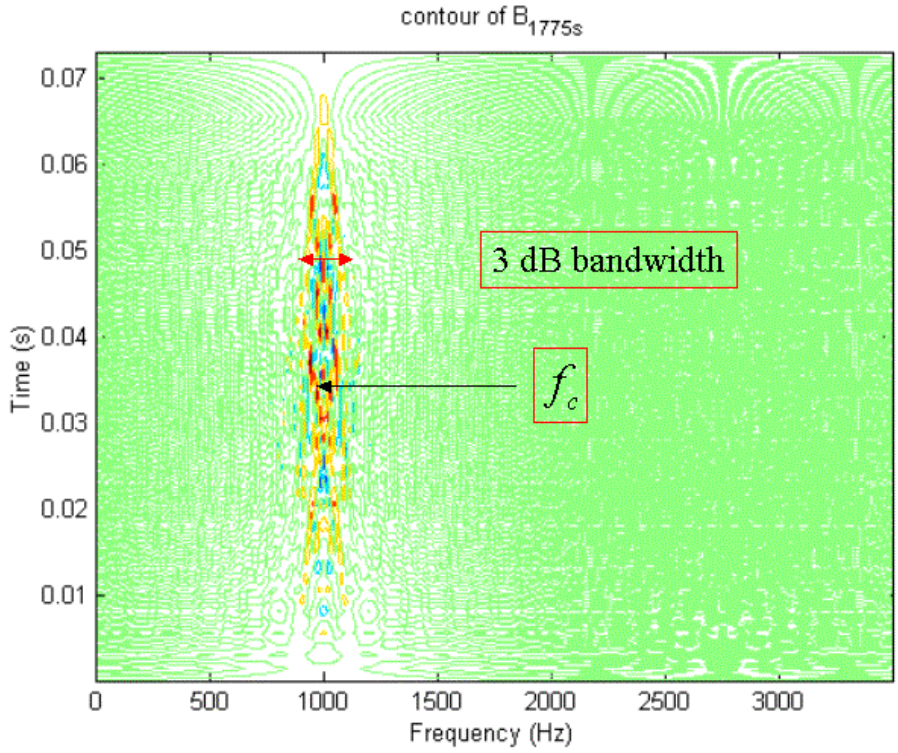

(b)

Figure 19. WD for BPSK with 7 Bit Barker Code, NPBB = 5, Signal Only, (No.7) (a) 2D Mesh in Frequency Domain. (b) Contour.

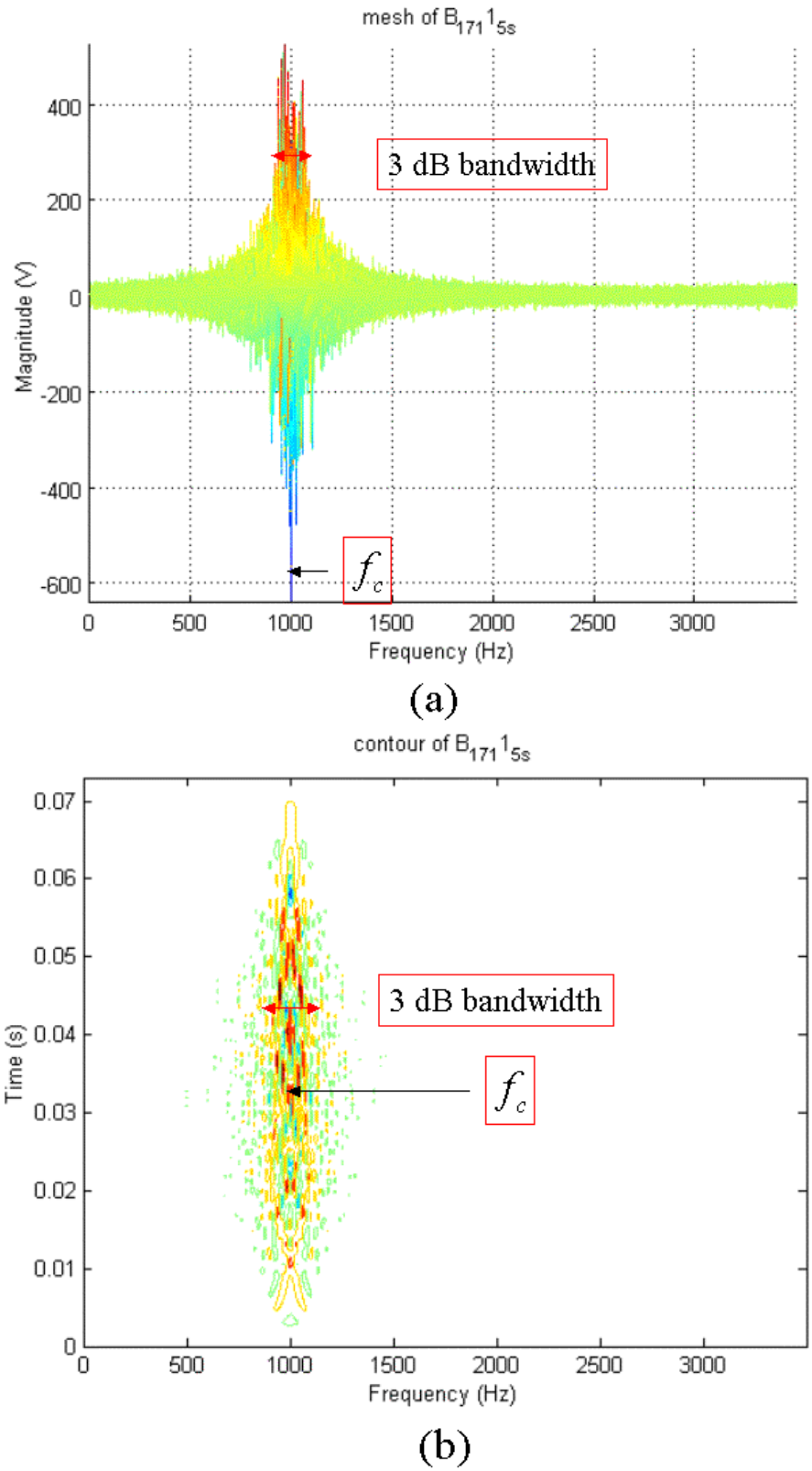

Figure 20. WD for BPSK with 11 Bit Barker Code, NPBB = 5, Signal Only, (No.10) (a) 2D Mesh in Frequency Domain. (b) Contour.

C. SUMMARY

The results of Wigner Distribution analysis for BPSK signals are discussed for two situations. When the *NPBB* (the number of cycles per barker bit) is equal to one, the Barker code length can be easily found by the Wigner Distribution. But the disadvantage is the carrier frequency information becomes more difficult to determine in low SNR (the result figures are not contained in this thesis). Second, when the *NPBB* is higher than one, the carrier frequency and 3 dB bandwidth can be easily found in low SNR, but the Barker code length becomes hard to analyze.

Table 3 below shows the detection effectiveness of the carrier frequency, 3dB bandwidth, code period and Barker code bit from Figure 17 to 20. They are done by the visible inspection of the WD results.

In the next chapter, the FMCW signals and their WD analysis will be examined.

BPSK				
N0.	Carrier Frequency	Bandwidth	Code Period	Bits/Code
1	100%	100%	100%	100%
2	100%	110%	100%	100%
3	0%	0%	0%	0%
4	100%	100%	100%	100%
5	100%	90%	100%	100%
6	0%	0%	0%	0%
7	100%	100%	0%	0%
8	100%	120%	0%	0%
9	100%	150%	0%	0%
10	100%	100%	0%	0%
11	100%	120%	0%	0%
12	100%	150%	0%	0%

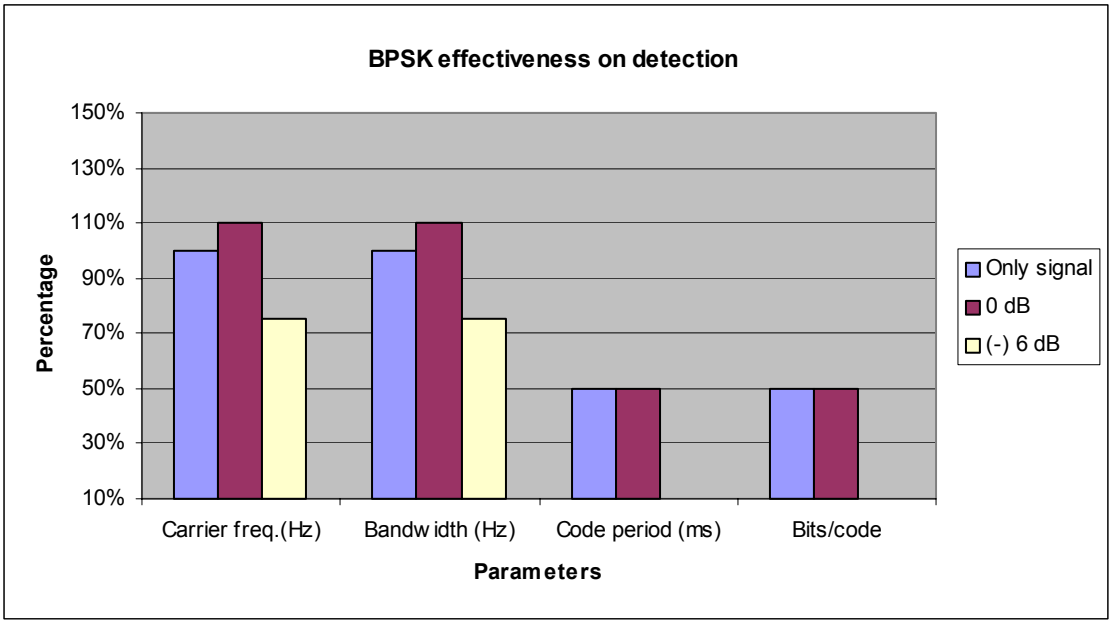

Table 3. WD Detection Effectiveness for BPSK Signals.

THIS PAGE INTENTIONALLY LEFT BLANK

IV. FREQUENCY MODULATION CONTINUOUS WAVE (FMCW)

A. FMCW

FMCW radar is a technique for obtaining refined range information from radar by frequency modulating a continuous signal. The FMCW modulation is readily compatible with a wide variety of solid-state transmitters. The frequency measurement of FMCW, which is performed to obtain range measurement, can be performed digitally using the FFT. The FMCW signals are very difficult to detect with conventional intercept receivers. [Ref. 14]

The frequency modulation used by the radar can take many forms. Linear and sinusoidal modulations have been used before. Linear frequency modulation is very suitable with the FFT processor to get the range information of targets. The linear FMCW emitter uses a continuous 100% duty cycle waveform so that both the target range and Doppler information can be measured. The FMCW waveform represents the best use of output power available from solid-state devices. Linear FMCW is also easier to implement than phase code modulation as long as there is no strict demand on linearity specifications over the modulation bandwidth. [Ref. 2]

The most basic Linear FMCW technique varies frequency in a sawtooth fashion, whereby frequency values ramp up over the course of a modulation period and then drop back down to the starting frequency to begin the ramp up for the next modulation period. Several repetitions of this sequence produce a sawtooth shape in the frequency vs. time plot. By processing the reflected waveform, one can extract range information about the target. [Ref. 15]

Figure 21 shows a functional block diagram of a Triangular FMCW transmitter. A sinusoidal carrier is frequency-modulated with a message signal that takes the triangular shape as shown in Figure 22. The modulated signal is then corrupted with channel distortion, which is assumed to be additive white Gaussian noise (AWGN) with zero mean and variance.

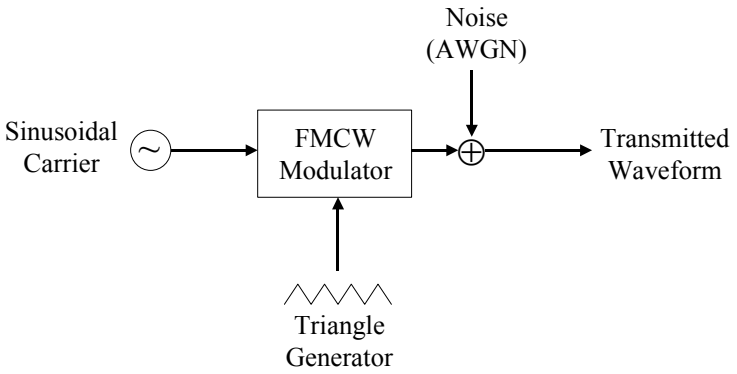

Figure 21. Triangular FMCW Block Diagram.

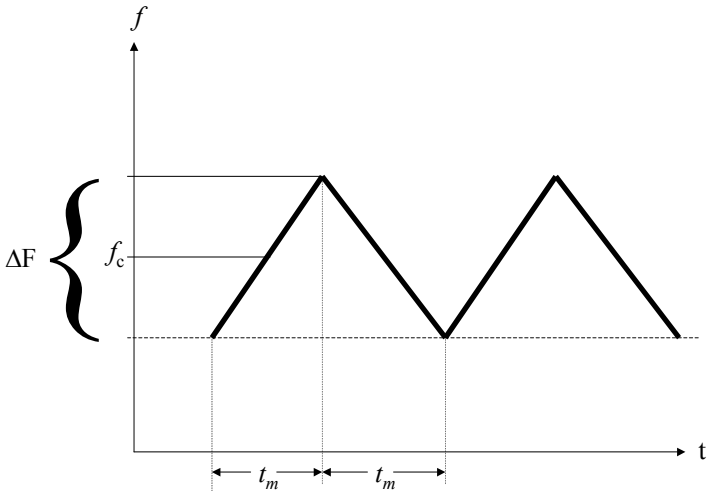

Figure 22. FMCW Modulation Signal in Time Domain.

The variables in the diagram are as follows.

f_c = Carrier frequency

ΔF = Modulation bandwidth

t_m = Modulation period

The up ramp and down ramp of each triangle must be constructed separately by the triangle generator. The modulating waveform for the up ramp can be modeled as

$$f_u(t)=\left\{\begin{array}{c} f_c-\frac{\Delta F}{2}+\frac{\Delta F}{t_m}t,\ 0<t<t_m \\ 0,\ elsewhere \end{array}\right\} \tag{4.1}$$

Similarly, the modulating waveform for the down ramp is modeled as

$$f_d(t)=\left\{\begin{array}{c} f_c+\frac{\Delta F}{2}-\frac{\Delta F}{t_m}t,\ 0<t<t_m \\ 0,\ elsewhere \end{array}\right\} \tag{4.2}$$

In FM systems, the transmit phase (instantaneous frequency) of the carrier is computed as

$$\phi(t)=2\pi\int_0^t f(x)dx \tag{4.3}$$

Now, assuming the initial conditions of $\phi_o = 0$ at $t = 0$ and substituting $f_u(t)$ and $f_d(t)$ into (4.3) yields the RF phases for the up ramp and down ramp as

$$\phi_u(t)=2\pi\left\{(f_c-\frac{\Delta F}{2})\cdot t+\frac{\Delta F}{2t_m}t^2\right\},\quad 0 < t < t_m \tag{4.4}$$

$$\phi_d(t)=2\pi\left\{(f_c+\frac{\Delta F}{2})\cdot t-\frac{\Delta F}{2t_m}t^2\right\},\quad 0 < t < t_m \tag{4.5}$$

It is then a simple substitution to arrive at the form of the transmitted signals for the up and down ramps [Ref. 14, 15]

$$s_{u1}(t) = A\cos 2\pi\left\{(f_c - \frac{\Delta F}{2})\cdot t + \frac{\Delta F}{2t_m}t^2\right\}, \quad 0 < t < t_m \tag{4.6}$$

$$s_{d1}(t) = A\cos 2\pi\left\{(f_c + \frac{\Delta F}{2})\cdot t - \frac{\Delta F}{2t_m}t^2\right\}, \quad 0 < t < t_m \tag{4.7}$$

$$s_{u2}(t) = A\sin 2\pi\left\{(f_c - \frac{\Delta F}{2})\cdot t + \frac{\Delta F}{2t_m}t^2\right\}, \quad 0 < t < t_m \tag{4.8}$$

$$s_{d2}(t) = A\sin 2\pi\left\{(f_c + \frac{\Delta F}{2})\cdot t - \frac{\Delta F}{2t_m}t^2\right\}, \quad 0 < t < t_m \tag{4.9}$$

Like those codes in BPSK, the amplitude A is equal to one. The most important three parameters in FMCW code generator are f_c, ΔF and t_m.

Twelve FMCW signals will be introduced in this chapter. They are numbered from 13 to 24 and listed in Table 4. The "Mod. BW" means the modulation bandwidth; 250Hz and 500Hz are used in this table. The "Mod. Period" means the modulation period, 20 ms and 30 ms are used here. A 1kHz carrier frequency and 7kHz sampling frequency are used for these signals

No.	FMCW	Mod. BW (Hz)	Mod. Period (ms)	SNR
13	F_1_7_250_20_s	250	20	Signal Only
14	F_1_7_250_20_0	250	20	0 dB
15	F_1_7_250_20_-6	250	20	-6 dB
16	F_1_7_250_30_s	250	30	Signal Only
17	F_1_7_250_30_0	250	30	0 dB
18	F_1_7_250_30_-6	250	30	-6 dB
19	F_1_7_500_20_s	500	20	Signal Only
20	F_1_7_500_20_0	500	20	0 dB
21	F_1_7_500_20_-6	500	20	-6 dB
22	F_1_7_500_30_s	500	30	Signal Only
23	F_1_7_500_30_0	500	30	0 dB
24	F_1_7_500_30_-6	500	30	-6 dB

Table 4. FMCW Signals.

B. WIGNER DISTRIBUTION FOR FMCW

Consider the same twelve FMCW signals in Table 4 and use them as the inputs for the Wigner distribution (WD). The WD results of these twelve signals are shown in Figure 23 to 26. The mesh plots show the frequency domain of the FMCW signals after the WD. The contour plots show both the frequency domain and time domain of the results.

Take Figure 23 as an example. First, the carrier frequency f_c can be clearly found by the location of the highest or lowest peak value in Figure 23(a). In Figure 23(b), by the location of the arc shape one can also identify the carrier frequency.

Secondly, the modulation bandwidth ΔF and modulation period t_m have scaled and marked in Figures 23(b) to 26(b)

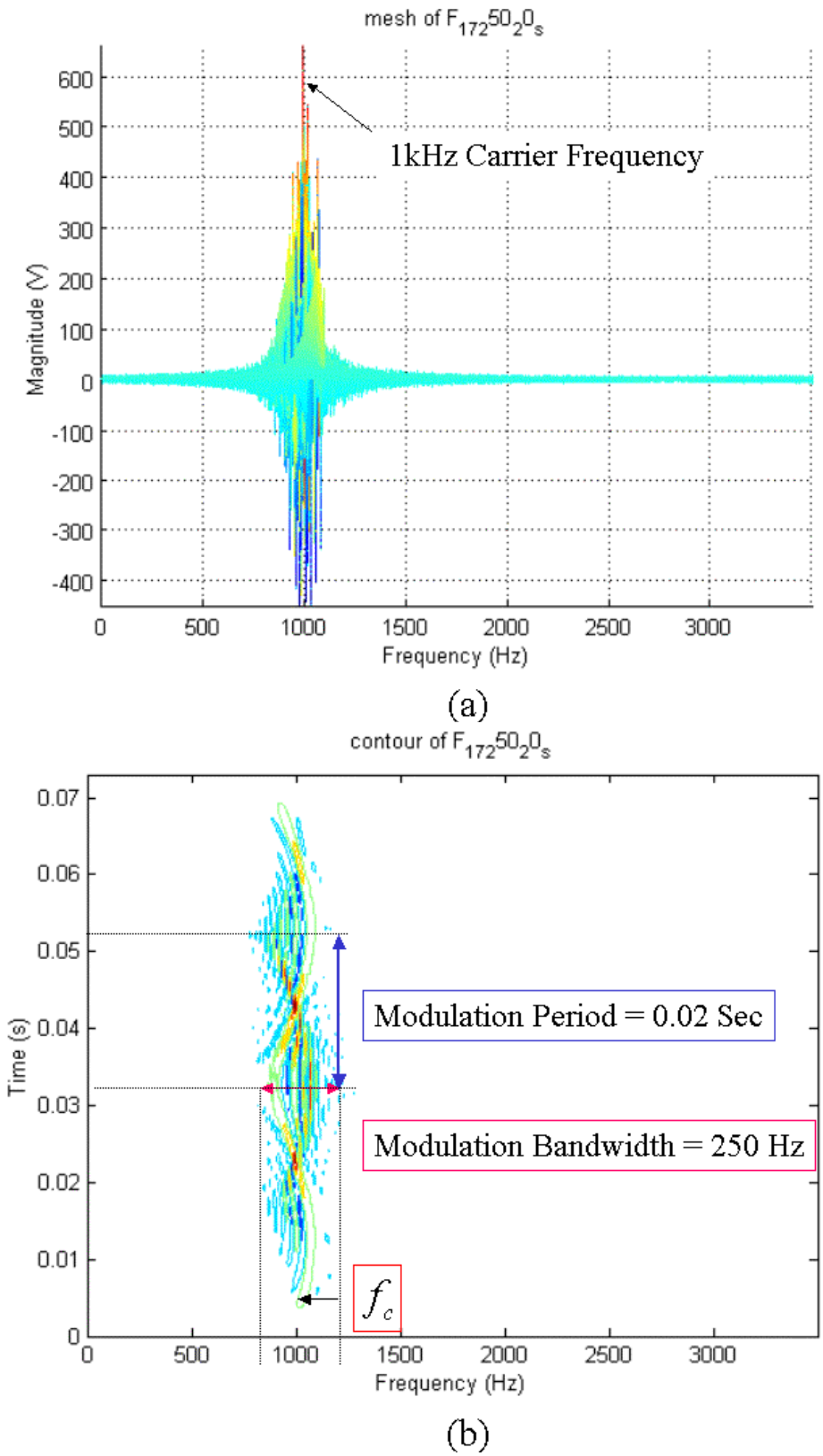

Figure 23. WD for FMCW with $\Delta F = 250Hz, t_m = 20ms$ Signal Only (a) 2D Mesh in Frequency Domain. (b) Contour.

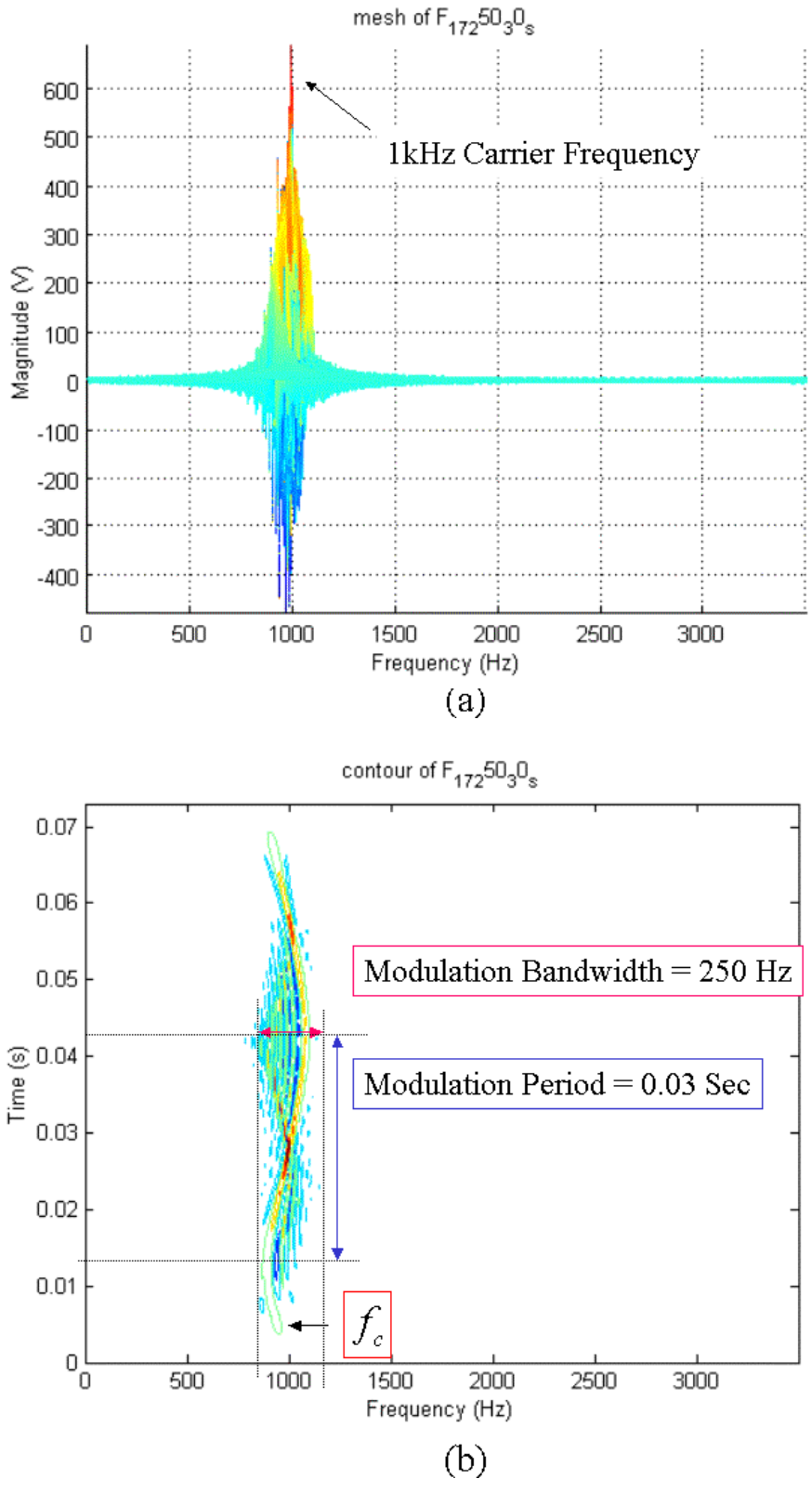

Figure 24. WD for FMCW with $\Delta F = 250Hz, t_m = 30ms$ Signal Only (a) 2D Mesh in Frequency Domain. (b) Contour.

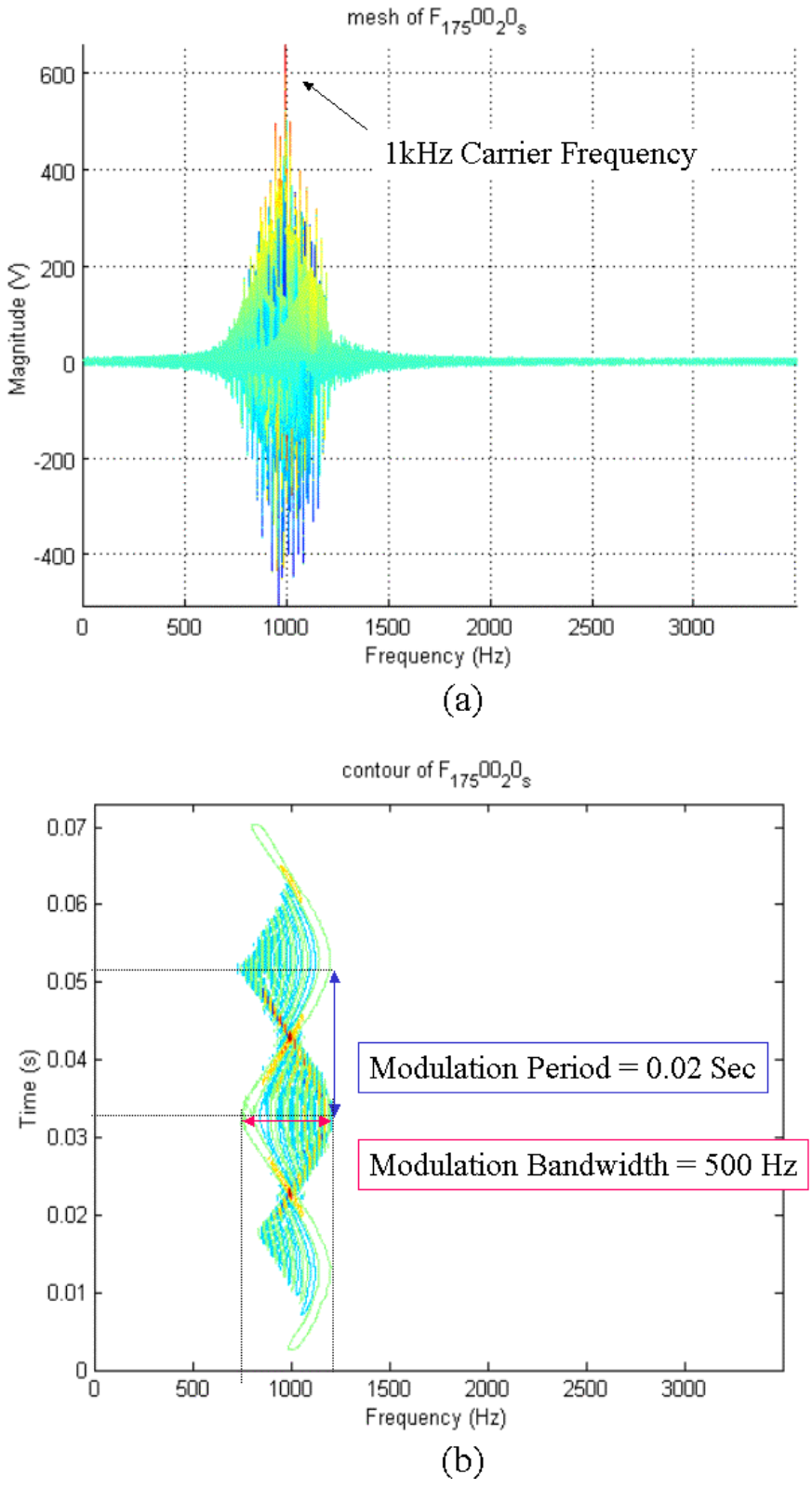

Figure 25. WD for FMCW with $\Delta F = 500Hz, t_m = 20ms$ Signal Only (a) 2D Mesh in Frequency Domain. (b) Contour.

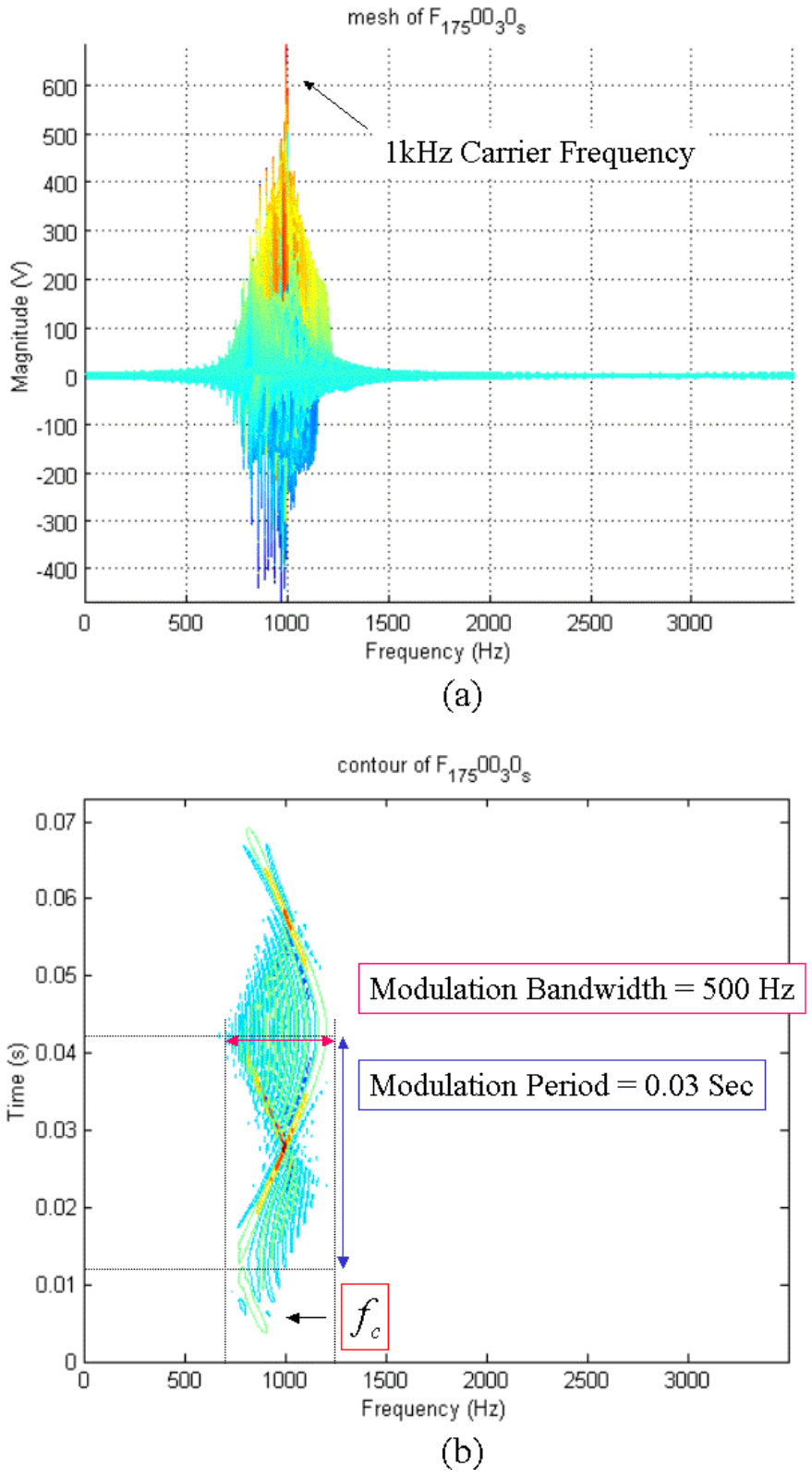

Figure 26. WD for FMCW with $\Delta F = 500Hz, t_m = 30ms$ Signal Only (a) 2D Mesh in Frequency Domain. (b) Contour.

C. SUMMARY

For all the LPI signals in this thesis, Wigner Distribution provides better parameter estimation for FMCW than the others. Without any other analysis beyond the contour plot, one can see the most two important parameters, modulation bandwidth and modulation period.

Chapter I introduced the fact that the Wigner distribution is a Time-Frequency Analysis (TFA) technique. Since the FMCW signals have the character that both the frequency and time were modulated, using the Wigner distribution can yield excellent results for FMCW signals, even at SNR equal to –6 dB. See the technical report to be published soon for more details. [Ref. 16]

Table 5 below shows the detection effectiveness of the carrier frequency, modulation bandwidth and modulation period by visible measurement from Figure 23 to 26. They are done by the visible inspection of the WD processing results.

After the BPSK and FMCW signals, the polyphase signals and their WD analysis will be examined in the next chapter.

FMCW			
No.	Carrier Frequency	Mod. BW (Hz)	Mod. Period (ms)
13	100%	100%	100%
14	100%	100%	100%
15	100%	90%	100%
16	100%	100%	100%
17	100%	100%	100%
18	100%	90%	100%
19	100%	100%	100%
20	100%	100%	100%
21	100%	90%	100%
22	100%	100%	100%
23	100%	100%	100%
24	100%	90%	100%

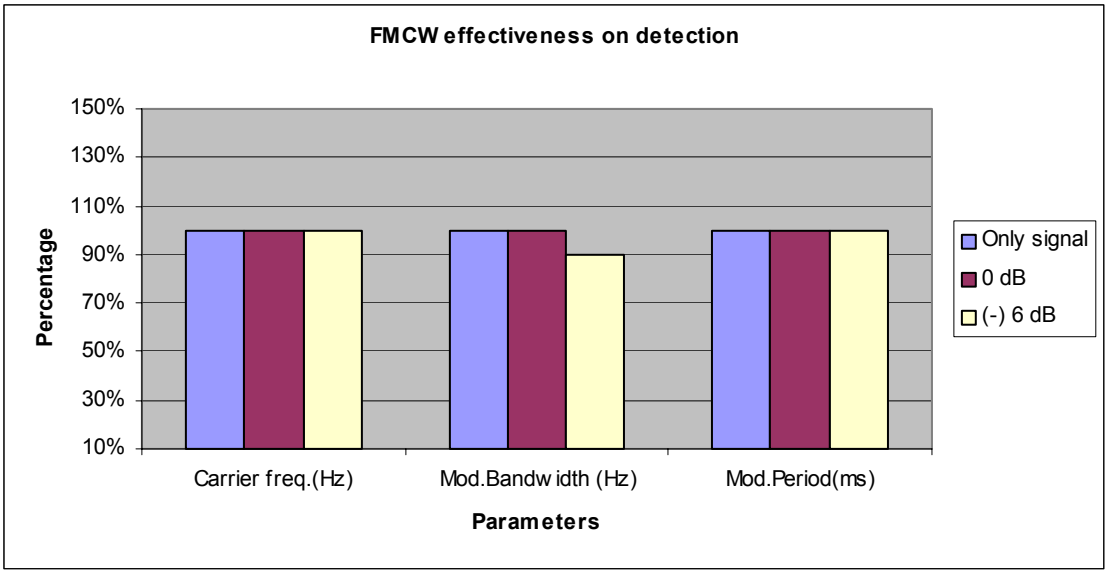

Table 5. WD Detection Effectiveness for FMCW Signals.

THIS PAGE INTENTIONALLY LEFT BLANK

V. POLYPHASE

A. POLYPHASE CODE MODULATION

Polyphase codes have many useful features such as low range-time sidelobes, ease of implementation, compatibility with digital implementation, low cross-correlation between codes, the Doppler tolerance of the frequency modulation codes and compatibility with bandpass limited receivers. The largest pulse compression ratio that can be obtained with the linear Barker codes is only 13 but the Polyphase codes are not limited to any finite pulse compression ratio. [Ref. 17]

The phase of the subpulses in Polyphase coded pulse compression need not be restricted to the two levels of 0 and π in the binary phase codes. Polyphase codes produce lower sidelobe levels than the binary phase codes and are tolerant to Doppler frequency shift if the Doppler frequencies are not too large. [Ref. 4]

The Polyphase code waveforms provide a class of frequency derived phase coded waveforms that can be sampled upon reception and processed digitally. [Ref. 18] Polyphase codes also addresses the reality of the espionage threat as well as the electronic attack threat. Programmability and variety are two code characteristics that make espionage a more difficult task; thus, Polyphase code will no doubt prove to be the LPI waveform of the following decades. [Ref. 19]

In this thesis, the polyphase codes including Frank code, P1 code, P2 code, P3 code, and P4 code are examined.

B. FRANK CODE

Frank codes are a family of polyphase codes that are closely related to the chirp and have been used successfully in LPI radars. The Frank code has a length N^2, which is also the corresponding pulse compression ratio. If *i* is the number of the sample in a given frequency and *j* is the number of the frequency, the phase of the *i*th sample of *j*th frequency is [Ref. 20]

$$\phi_{i,j} = \frac{2\pi}{N}(i-1)(j-1) \tag{5.1}$$

where $i = 1:N \quad and \quad j = 1:N$

Twelve Frank code signals are introduced in this chapter. They are numbered from 25 to 36 and listed in Table 6. In this chapter, the $N = 4$ and 8 and cycles per phase (*CPP*) = 1 and 5 are used. A 1kHz carrier frequency and 7kHz sampling frequency are used for these signals.

No.	FRANK	N (Phase)	Cycles/Phase	SNR
25	FR_1_7_4_1_s	4	1	Signal Only
26	FR_1_7_4_1_0	4	1	0 dB
27	FR_1_7_4_1_-6	4	1	-6 dB
28	FR_1_7_4_5_s	4	5	Signal Only
29	FR_1_7_4_5_0	4	5	0 dB
30	FR_1_7_4_5_-6	4	5	-6 dB
31	FR_1_7_8_1_s	8	1	Signal Only
32	FR_1_7_8_1_0	8	1	0 dB
33	FR_1_7_8_1_-6	8	1	-6 dB
34	FR_1_7_8_5_s	8	5	Signal Only
35	FR_1_7_8_5_0	8	5	0 dB
36	FR_1_7_8_5_-6	8	5	-6 dB

Table 6. Frank Code Signals.

1. Wigner Distribution for Frank Code

Consider the same twelve Frank code signals in Table 6 and use them as the inputs for Wigner Distribution (WD). The WD results of these twelve signals are shown in Figure 27 to 30. The mesh plots show the frequency domain of the Frank code signals after WD. The contour plots show both the frequency domain and time domain of the results.

Take Figure 27 as an example. First, the carrier frequency f_c can be clearly found by the location of the highest or lowest peak value in Figure 27(a). Secondly, in Figure 27(b), the 3dB bandwidth can be measured as 1000Hz. Since

$$B = \frac{1}{t_b} = \frac{f_c}{CPP} \tag{5.2}$$

so, the cycles per phase (*CPP*) can be computed by $CPP = \frac{f_c}{B} = \frac{1000}{1000} = 1$ For Frank code

$$T = N^2 t_b = \frac{N^2}{B} \tag{5.3}$$

since the code period (*T*) is measured as 0.016 in Figure 27(b), so the phase length (N^2) can be calculated from $N^2 = B \cdot T = 1000 \cdot 0.016 = 16$. The slope which measured in Figure 27(b) as 1.6×10^{-6} sec^2 can be also use to determine the N^2 and *CPP* by the following equation.

$$S = \frac{T}{B} = \frac{N^2}{B^2} = \frac{N^2 \cdot CPP^2}{f_c^2} \tag{5.4}$$

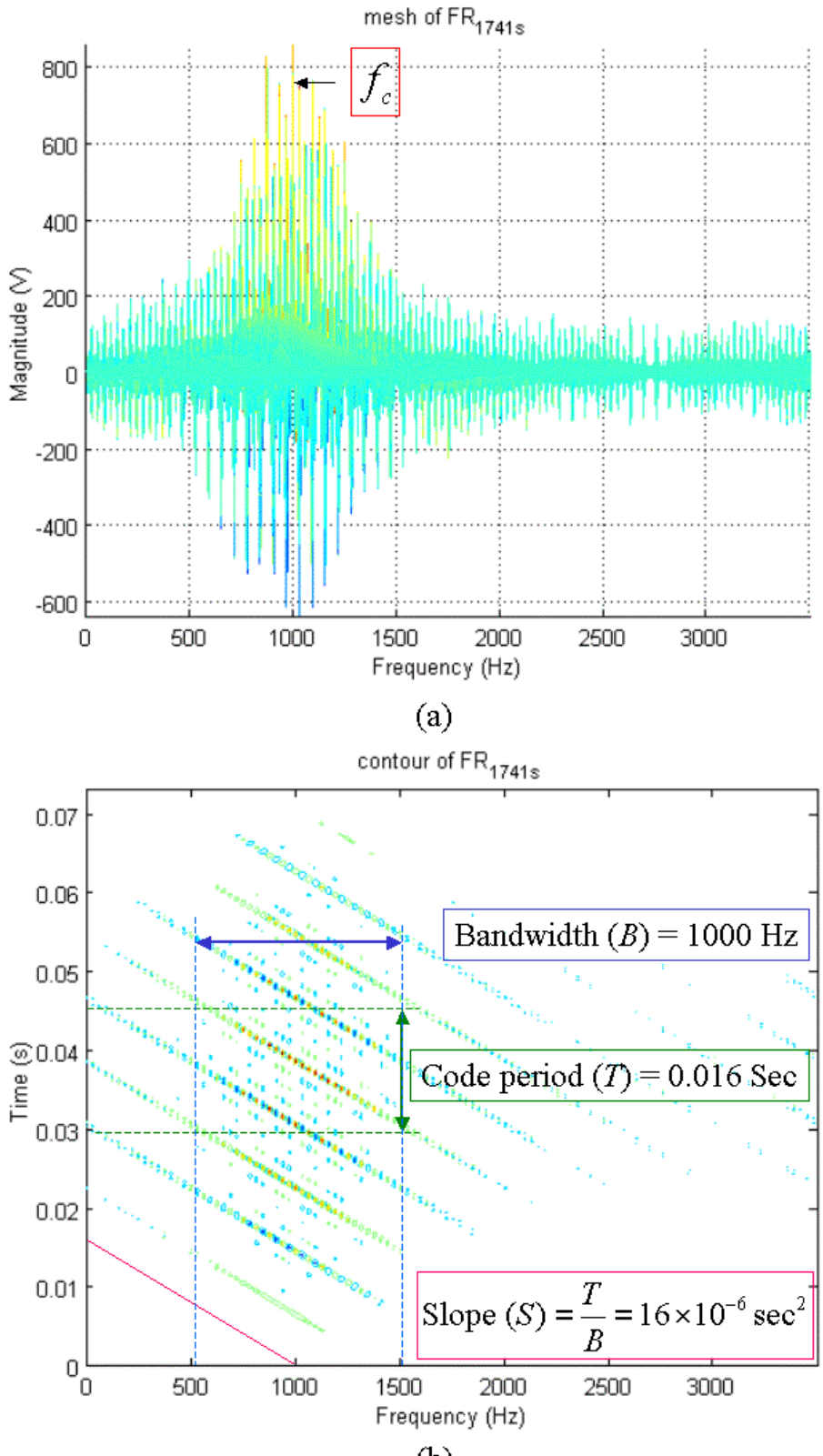

Figure 27. WD for Frank Code with Phase Length = 16, CPP = 1, Signal Only, (No.25)
(a) 2D Mesh in Frequency Domain. (b) Contour.

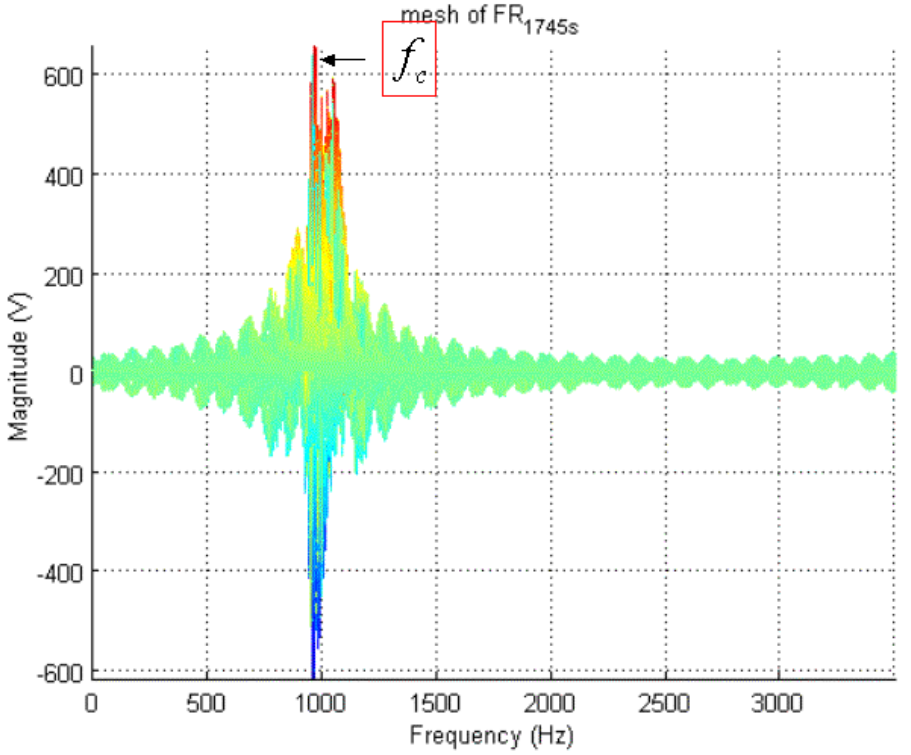

(a)

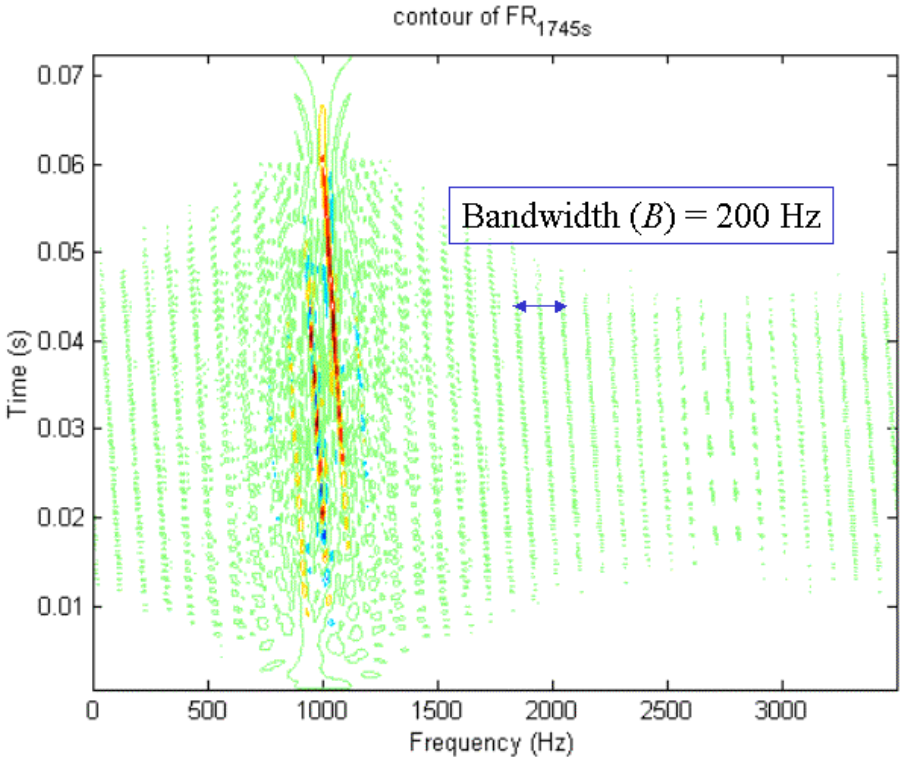

(b)

Figure 28. WD for Frank Code with Phase Length = 16, CPP = 5, Signal Only, (No.28)
(a) 2D Mesh in Frequency Domain. (b) Contour.

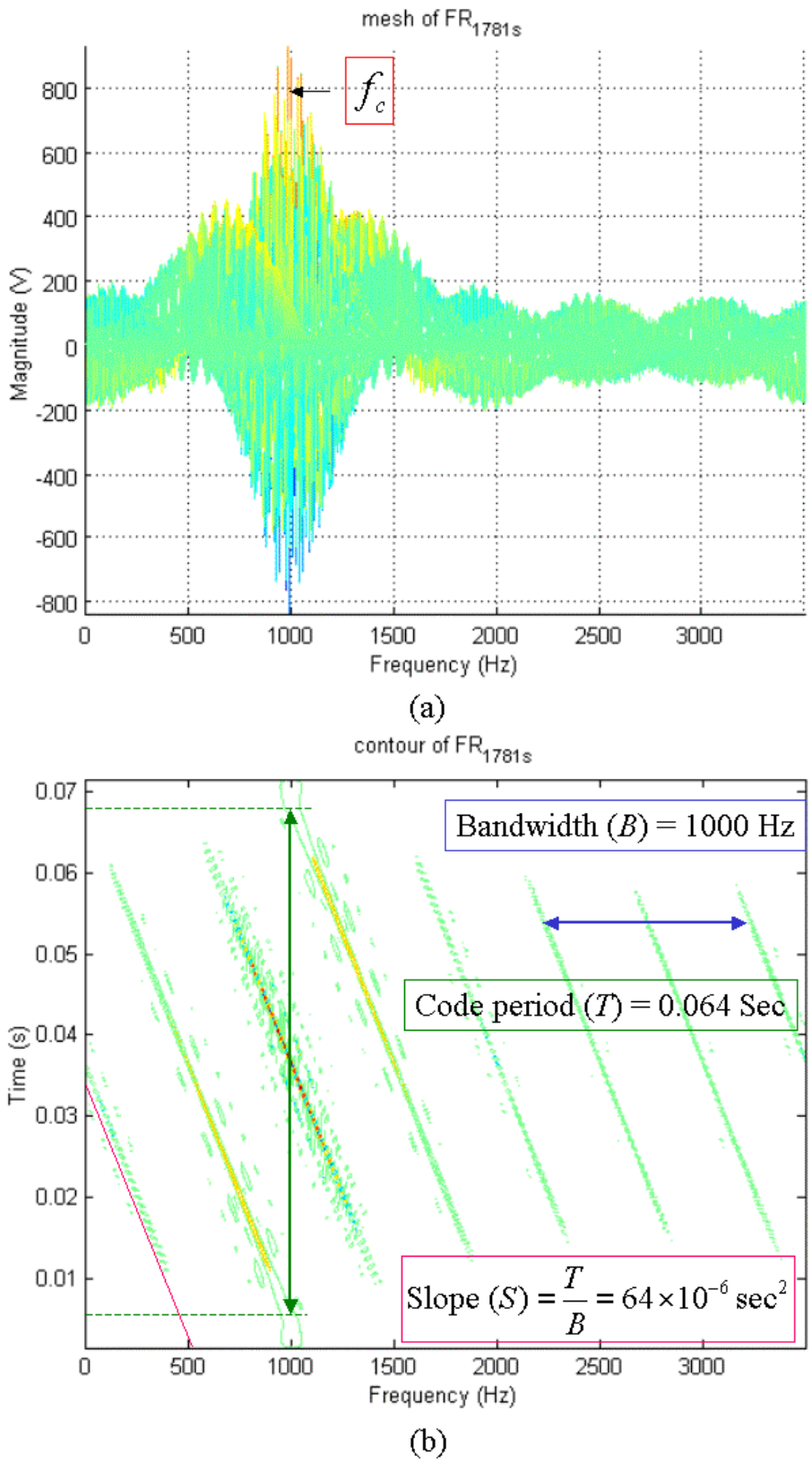

Figure 29. WD for Frank Code with Phase Length = 64, CPP = 1, Signal Only, (No.31)
(a) 2D Mesh in Frequency Domain. (b) Contour.

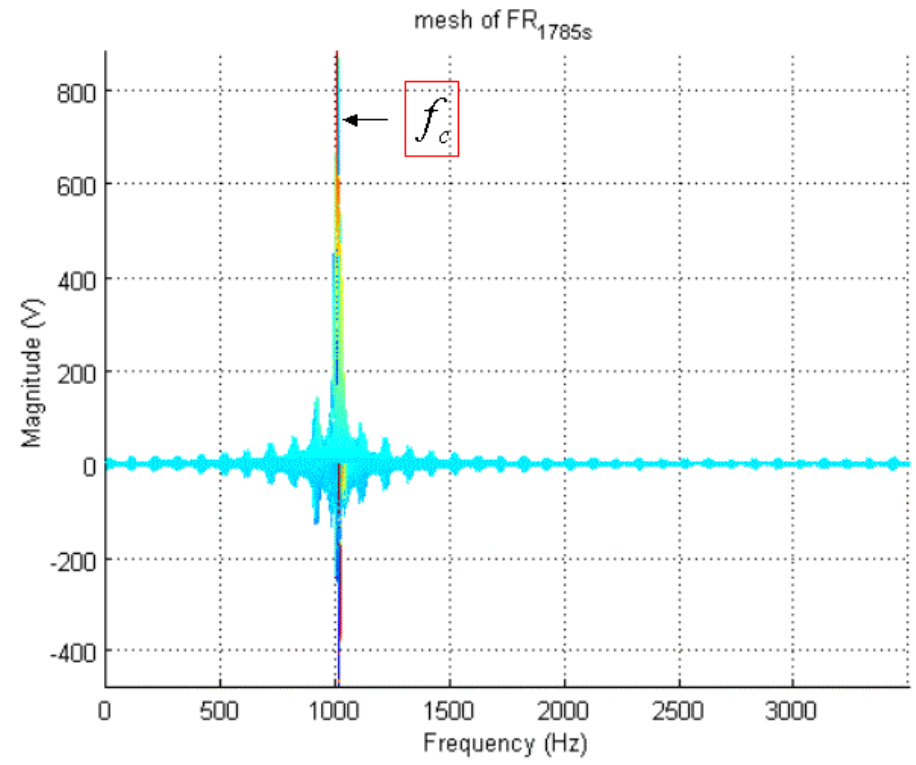

(a)

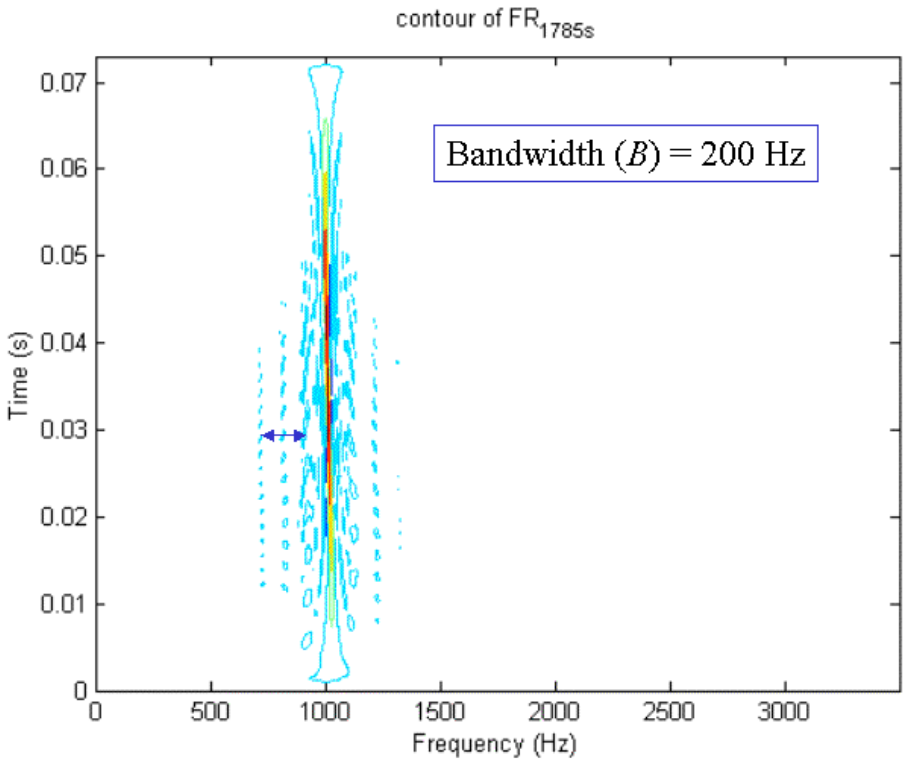

(b)

Figure 30. WD for Frank Code with Phase Length = 64, CPP = 5, Signal Only, (No.34)
(a) 2D Mesh in Frequency Domain. (b) Contour.

2. Summary

Applying the Wigner Distribution, one can quickly know the carrier frequency (f_c) of the Frank codes. The carrier frequency is always the first parameter need to be identified. Once the carrier frequency is found, by the bandwidth can determine the *CPP* ; by the code period or the slope can determine the phase length(N^2).

In Figure 28(b) (N^2 =16, *CPP*=5) only bandwidth is obtained but not the code period. The reason is that the sample number (#*sample*) is not enough. From (5.3), the code period is $T = \frac{N^2}{B} = \frac{16}{200} = 0.080\,\text{sec}$, hence only when $\frac{\#sample}{f_s} \geq T$, the code period can be shown in the figure. In this chapter, the $\frac{\#sample}{f_s} = \frac{512}{7000} = 0.073 \leq 0.080$.

Table 7 below shows the detection effectiveness of the carrier frequency, 3dB bandwidth, code period and phase length from Figure 27 to 30. They are done by the visible inspection of the WD results.

Frank				
No.	Carrier Frequency	Bandwidth	Code Period	Phase Length
25	100%	100%	100%	100%
26	90%	110%	100%	100%
27	110%	110%	100%	100%
28	95%	100%	0%	0%
29	98%	95%	0%	0%
30	0%	0%	0%	0%
31	100%	100%	100%	100%
32	95%	105%	100%	100%
33	98%	105%	100%	100%
34	100%	100%	0%	0%
35	100%	0%	0%	0%
36	100%	0%	0%	0%

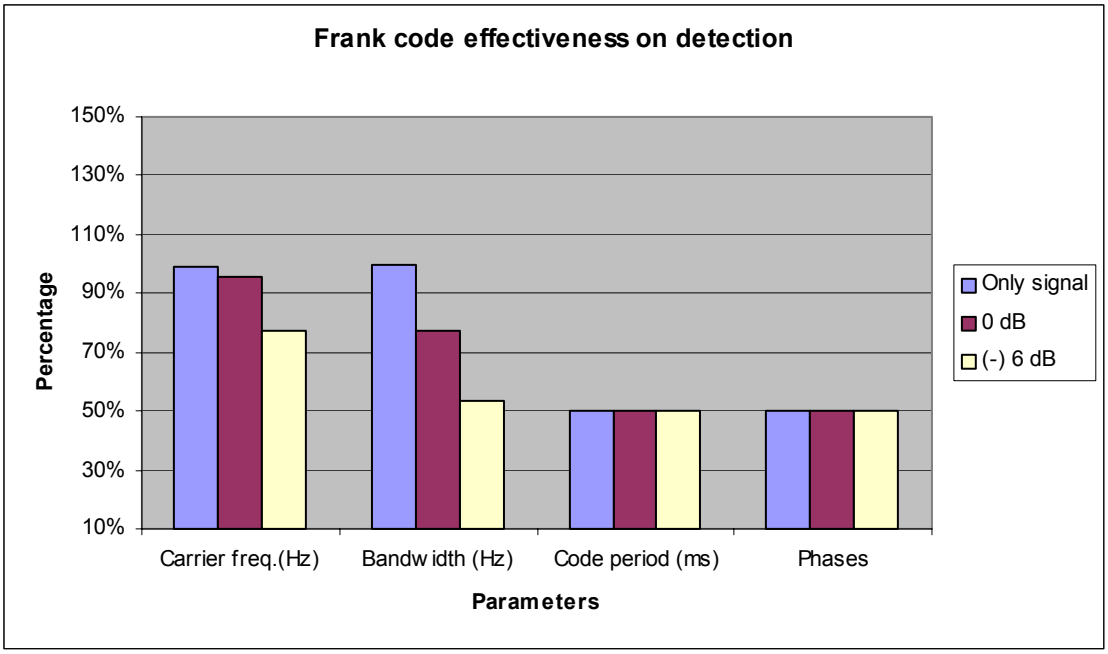

Table 7. WD Detection Effectiveness for Frank Code Signals.

C. P1 CODE

In case of a double sideband detection (local oscillator is at band center) of a step approximation of a linear frequency modulation, which is the P1 code. The P1 code also consists of N^2 elements. If i is the number of the sample in a given frequency and j is the number of the frequency, the phase of the ith sample of jth frequency is [Ref. 20]

$$\phi_{i,j} = \frac{-\pi}{N}[N-(2j-1)][(j-1)N+(i-1)] \tag{5.5}$$

where $i = 1:N \quad and \quad j = 1:N$

Twelve P1 code signals are introduced in this chapter. They are numbered from 37 to 48 and listed in Table 8. A 1kHz carrier frequency and 7kHz sampling frequency are used for these signals.

No.	P1	N (Phase)	Cycles/Phase	SNR
37	P1_1_7_4_1_s	4	1	Signal Only
38	P1_1_7_4_1_0	4	1	0 dB
39	P1_1_7_4_1_-6	4	1	-6 dB
40	P1_1_7_4_5_s	4	5	Signal Only
41	P1_1_7_4_5_0	4	5	0 dB
42	P1_1_7_4_5_-6	4	5	-6 dB
43	P1_1_7_8_1_s	8	1	Signal Only
44	P1_1_7_8_1_0	8	1	0 dB
45	P1_1_7_8_1_-6	8	1	-6 dB
46	P1_1_7_8_5_s	8	5	Signal Only
47	P1_1_7_8_5_0	8	5	0 dB
48	P1_1_7_8_5_-6	8	5	-6 dB

Table 8. P1 Code Signals.

1. Wigner Distribution for P1 Code

Consider the same twelve P1 code signals in Table 8 and use them as the inputs for Wigner Distribution (WD). The WD results of these twelve signals are showed in Figure 31 to 34. The mesh plots show the frequency domain of the P1 code signals after WD. The contour plots show both the frequency domain and time domain of the results.

Take Figure 31 as an example. First, the carrier frequency f_c can be clearly found by the location of the highest or lowest peak value in Figure 31(a). Secondly, in Figure 31(b), the 3dB bandwidth can be measured as 1000Hz. Since

$$B = \frac{1}{t_b} = \frac{f_c}{CPP} \tag{5.6}$$

so, the cycles per phase (*CPP*) can be computed by $CPP = \frac{f_c}{B} = \frac{1000}{1000} = 1$ For P1 code

$$T = N^2 t_b = \frac{N^2}{B} \tag{5.7}$$

since the code period (*T*) is measured as 0.016 in Figure 31(b), so the phase length (N^2) can be calculated from $N^2 = B \cdot T = 1000 \cdot 0.016 = 16$. The slope which measured in Figure 31(b) as 1.6×10^{-6} sec^2 can be also use to determine the N^2 and *CPP* by the following equation.

$$S = \frac{T}{B} = \frac{N^2}{B^2} = \frac{N^2 \cdot CPP^2}{f_c^2} \tag{5.8}$$

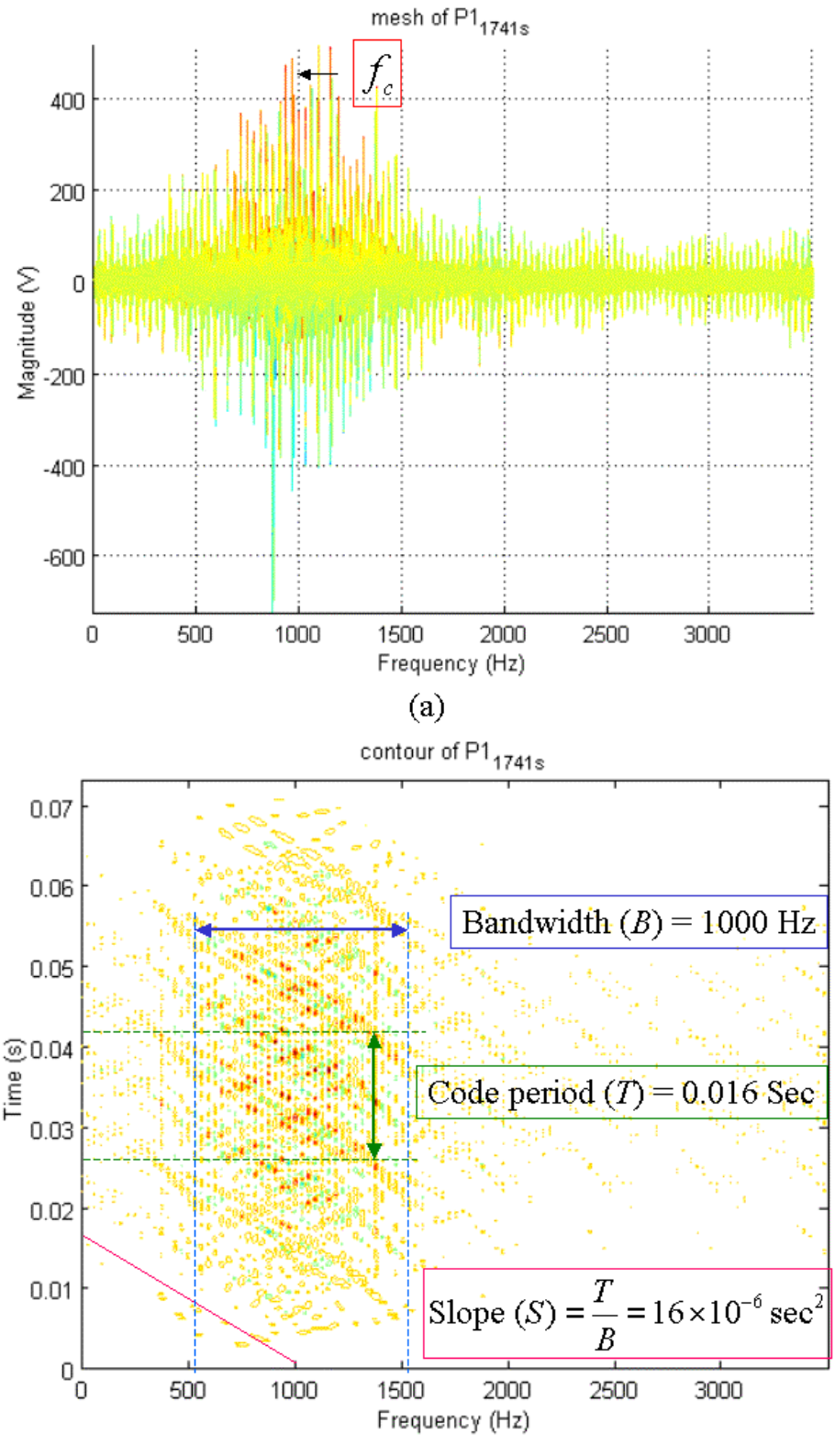

Figure 31. WD for P1 Code with Phase Length = 16, CPP = 1, Signal Only, (No.37) (a) 2D Mesh in Frequency Domain. (b) Contour.

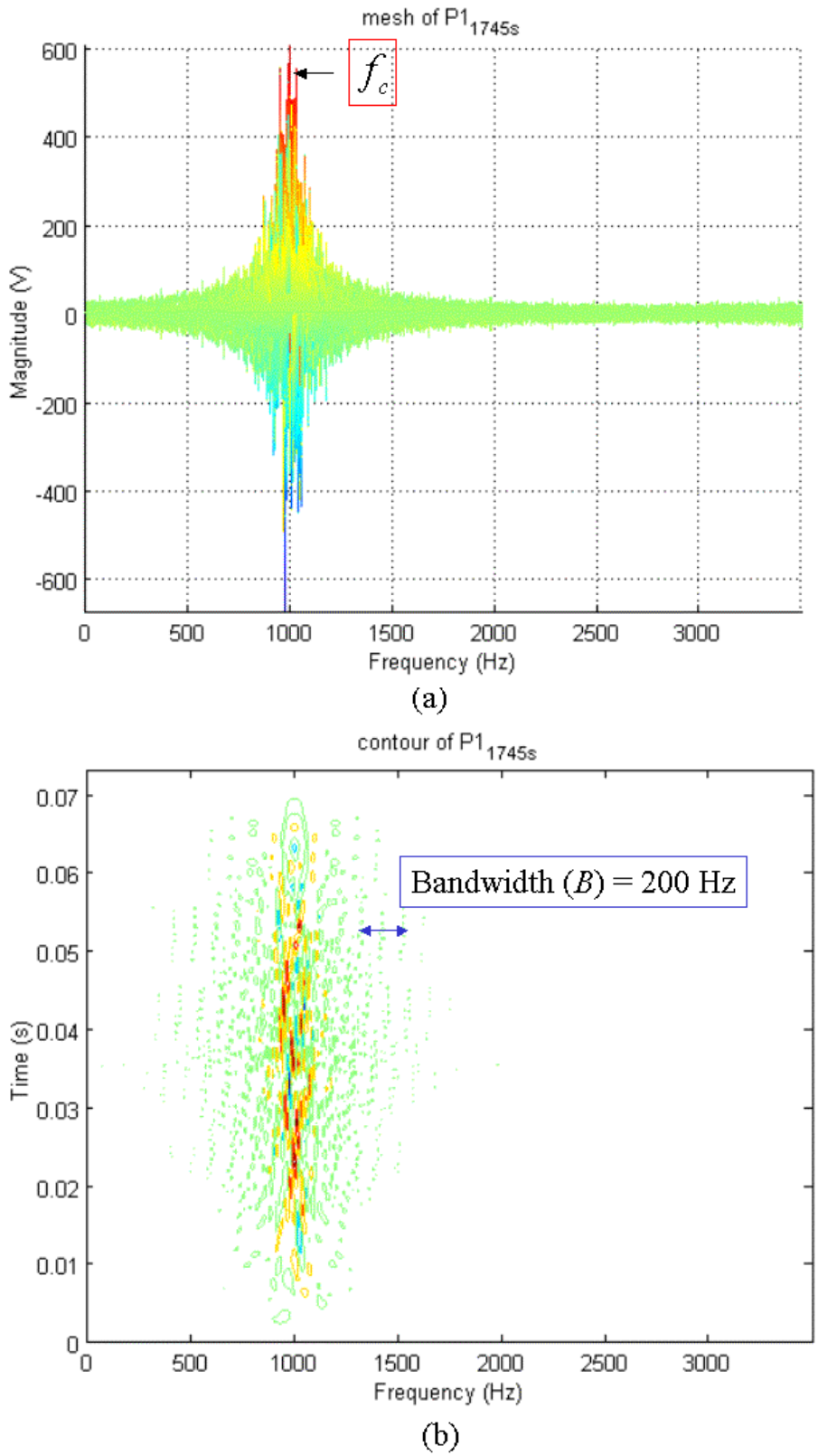

Figure 32. WD for P1 Code with Phase Length = 16, CPP = 5, Signal Only, (No.40) (a) 2D Mesh in Frequency Domain. (b) Contour.

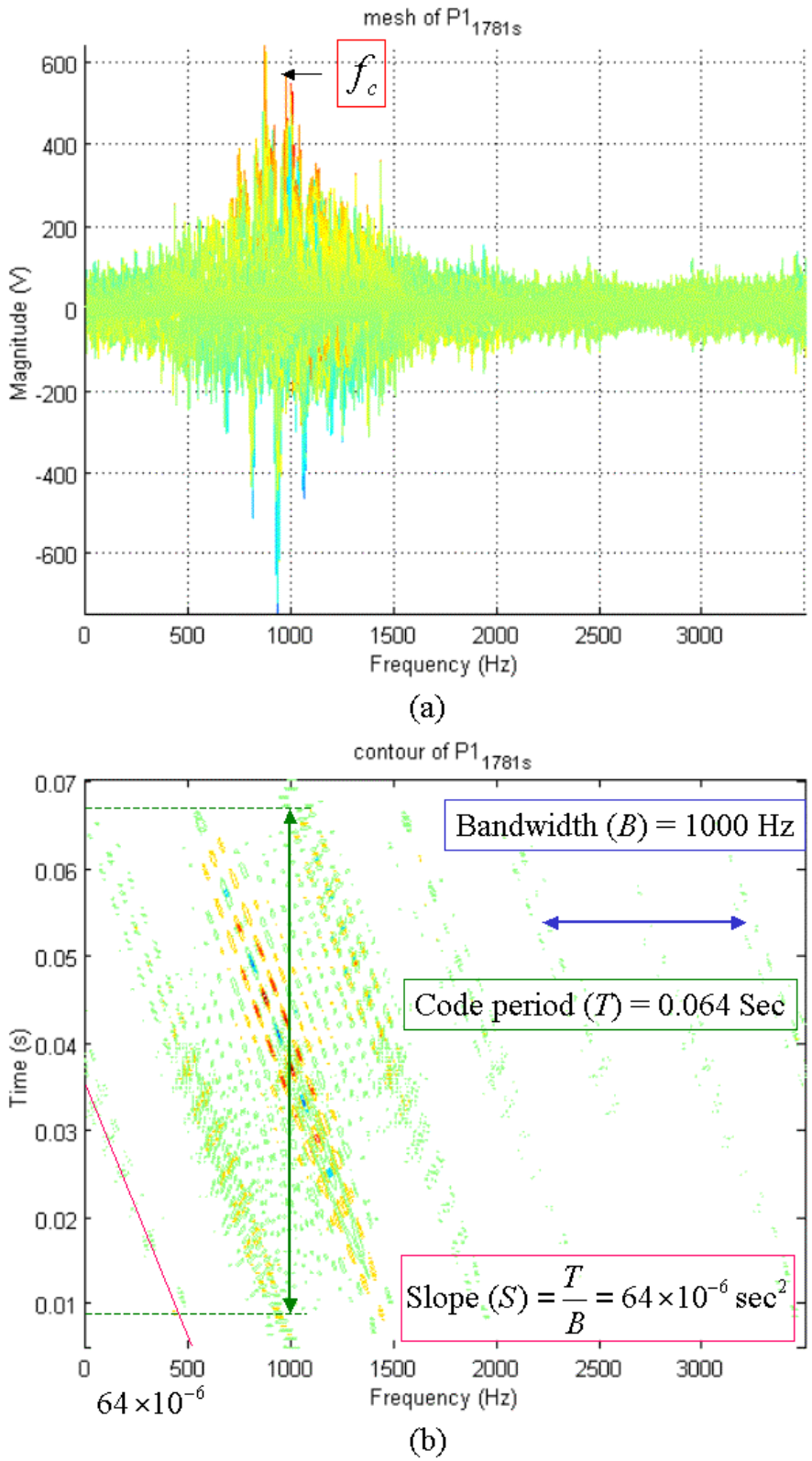

Figure 33. WD for P1 Code with Phase Length = 64, CPP = 1, Signal Only, (No.43) (a) 2D Mesh in Frequency Domain. (b) Contour.

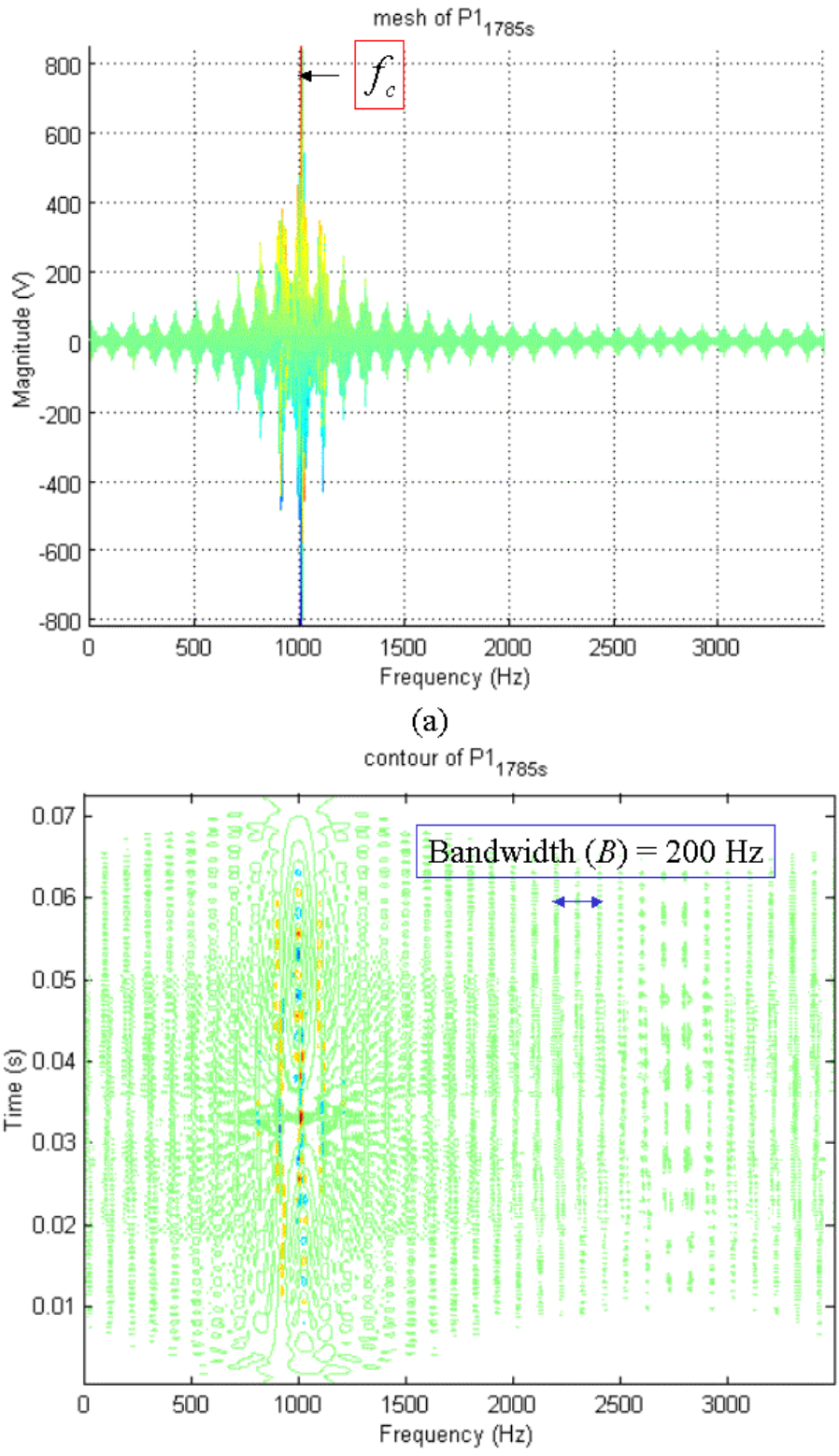

Figure 34. WD for P1 Code with Phase Length = 64, CPP = 5, Signal Only, (No.46) (a) 2D Mesh in Frequency Domain. (b) Contour.

2. Summary

Applying the Wigner Distribution, one can quickly know the carrier frequency (f_c) of the P1 codes. The carrier frequency is always the first parameter need to be identified. Once the carrier frequency is found, by the bandwidth can determine the *CPP* ; by the code period or the slope can determine the phase length(N^2).

In Figure 32(b) (N^2 =16, *CPP*=5) only bandwidth is obtained but not the code period. The reason is that the sample number (#*sample*) is not enough. From (5.7), the code period is $T = \frac{N^2}{B} = \frac{16}{200} = 0.080\,\text{sec}$, hence only when $\frac{\#sample}{f_s} \geq T$, the code period can be shown in the figure. In this chapter, the $\frac{\#sample}{f_s} = \frac{512}{7000} = 0.073 \leq 0.080$.

Table 9 below shows the detection effectiveness of the carrier frequency, 3dB bandwidth, code period and phase length from Figure 31 to 34. They are done by the visible inspection of the WD results.

P1				
No.	Carrier Frequency	Bandwidth	Code Period	Phase Length
37	120%	70%	100%	100%
38	110%	80%	100%	100%
39	0%	0%	0%	0%
40	100%	100%	0%	0%
41	100%	90%	0%	0%
42	0%	0%	0%	0%
43	90%	50%	100%	100%
44	90%	60%	100%	100%
45	0%	0%	0%	0%
46	100%	100%	0%	0%
47	100%	120%	0%	0%
48	0%	0%	0%	0%

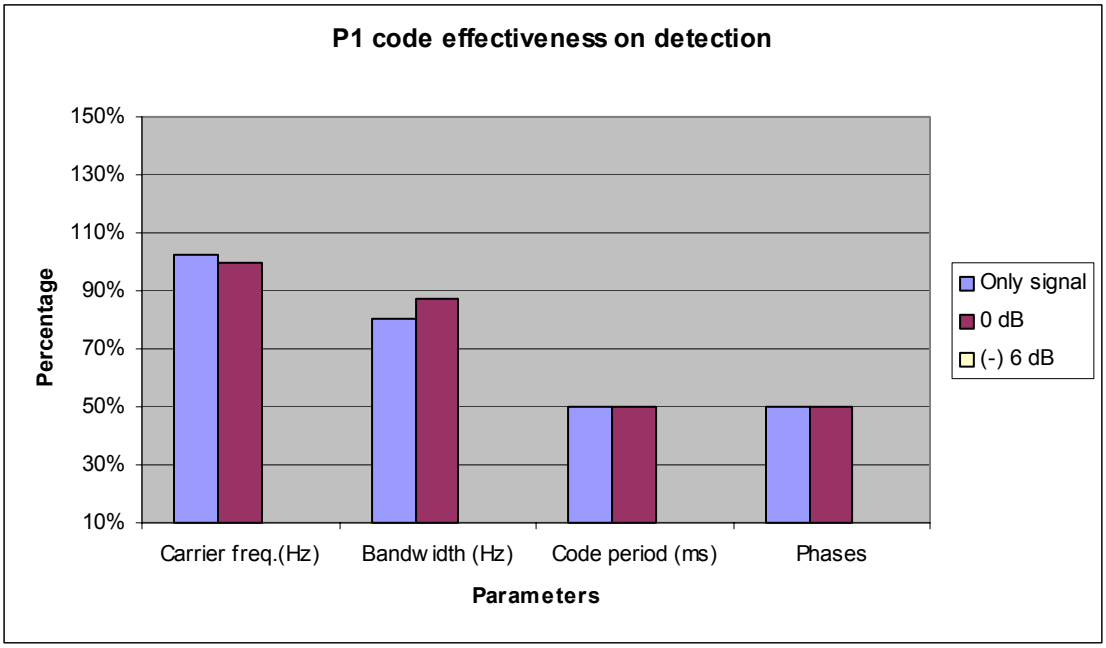

Table 9. WD Detection Effectiveness for P1 Code Signals.

D. P2 CODE

The P2 code also consists N^2 elements. If i is the number of the sample in a given frequency and j is the number of the frequency, the phase of the ith sample of jth frequency is [Ref. 20]

$$\phi_{i,j} = \frac{-\pi}{2N}(2i-1-N)(2j-1-N) \tag{5.9}$$

where $i = 1:N \quad and \quad j = 1:N$

Twelve P2 code signals are introduced in this chapter. They are numbered from 49 to 60 and listed in Table 10. Phase length N^2=16, 64 and *CPP*=1, 5 are used in this chapter. A 1kHz carrier frequency and 7kHz sampling frequency are used for these signals.

No.	P2	N (Phase)	Cycles/Phase	SNR
49	P2_1_7_4_1_s	4	1	Signal Only
50	P2_1_7_4_1_0	4	1	0 dB
51	P2_1_7_4_1_-6	4	1	-6 dB
52	P2_1_7_4_5_s	4	5	Signal Only
53	P2_1_7_4_5_0	4	5	0 dB
54	P2_1_7_4_5_-6	4	5	-6 dB
55	P2_1_7_8_1_s	8	1	Signal Only
56	P2_1_7_8_1_0	8	1	0 dB
57	P2_1_7_8_1_-6	8	1	-6 dB
58	P2_1_7_8_5_s	8	5	Signal Only
59	P2_1_7_8_5_0	8	5	0 dB
60	P2_1_7_8_5_-6	8	5	-6 dB

Table 10. P2 Code Signals.

1. Wigner Distribution for P2 Code

Consider the same twelve P2 code signals in Table 10 and use them as the inputs for Wigner Distribution (WD). The WD results of these twelve signals are showed in Figure 35 to 38. The mesh plots show the frequency domain of the P2 code signals after WD. The contour plots show both the frequency domain and time domain of the results.

Take Figure 35 as an example. First, the carrier frequency f_c can be clearly found by the location of the highest or lowest peak value in Figure 35(a). Secondly, in Figure 35(b), the 3dB bandwidth can be measured as 1000Hz. Since

$$B = \frac{1}{t_b} = \frac{f_c}{CPP} \tag{5.10}$$

so, the cycles per phase (*CPP*) can be computed by $CPP = \frac{f_c}{B} = \frac{1000}{1000} = 1$ For P2 code

$$T = N^2 t_b = \frac{N^2}{B} \tag{5.11}$$

since the code period (*T*) is measured as 0.016 in Figure 35(b), so the phase length (N^2) can be calculated from $N^2 = B \cdot T = 1000 \cdot 0.016 = 16$. The slope which measured in Figure 35(b) as 1.6×10^{-6} sec^2 can be also use to determine the N^2 and *CPP* by the following equation.

$$S = \frac{T}{B} = \frac{N^2}{B^2} = \frac{N^2 \cdot CPP^2}{f_c^2} \tag{5.12}$$

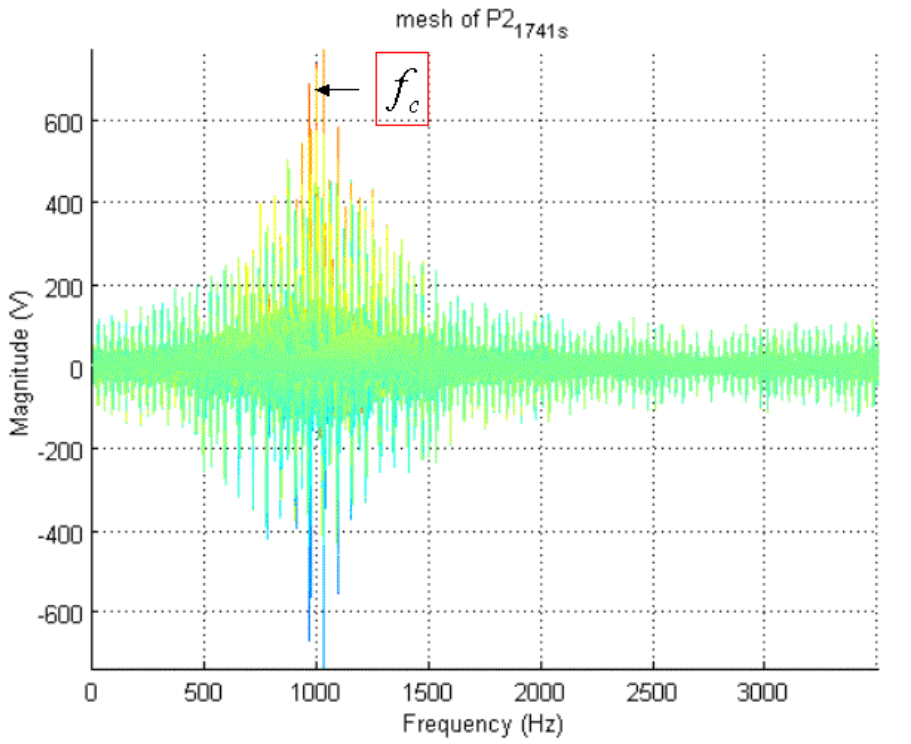

(a)

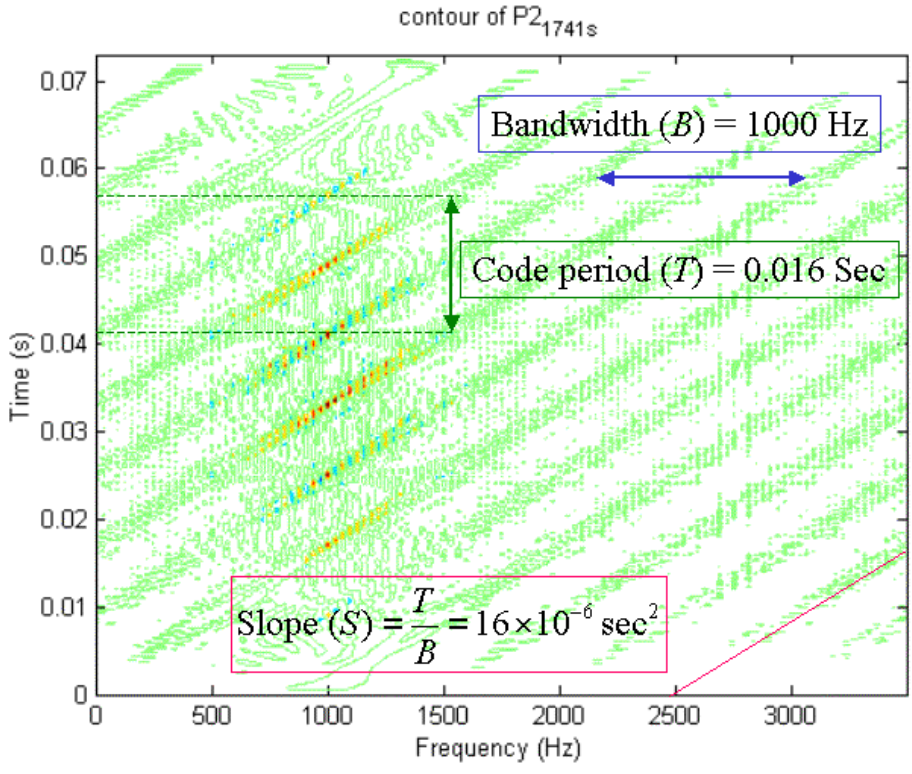

(b)

Figure 35. WD for P2 Code with Phase Length = 16, CPP = 1, Signal Only, (No.49) (a) 2D Mesh in Frequency Domain. (b) Contour.

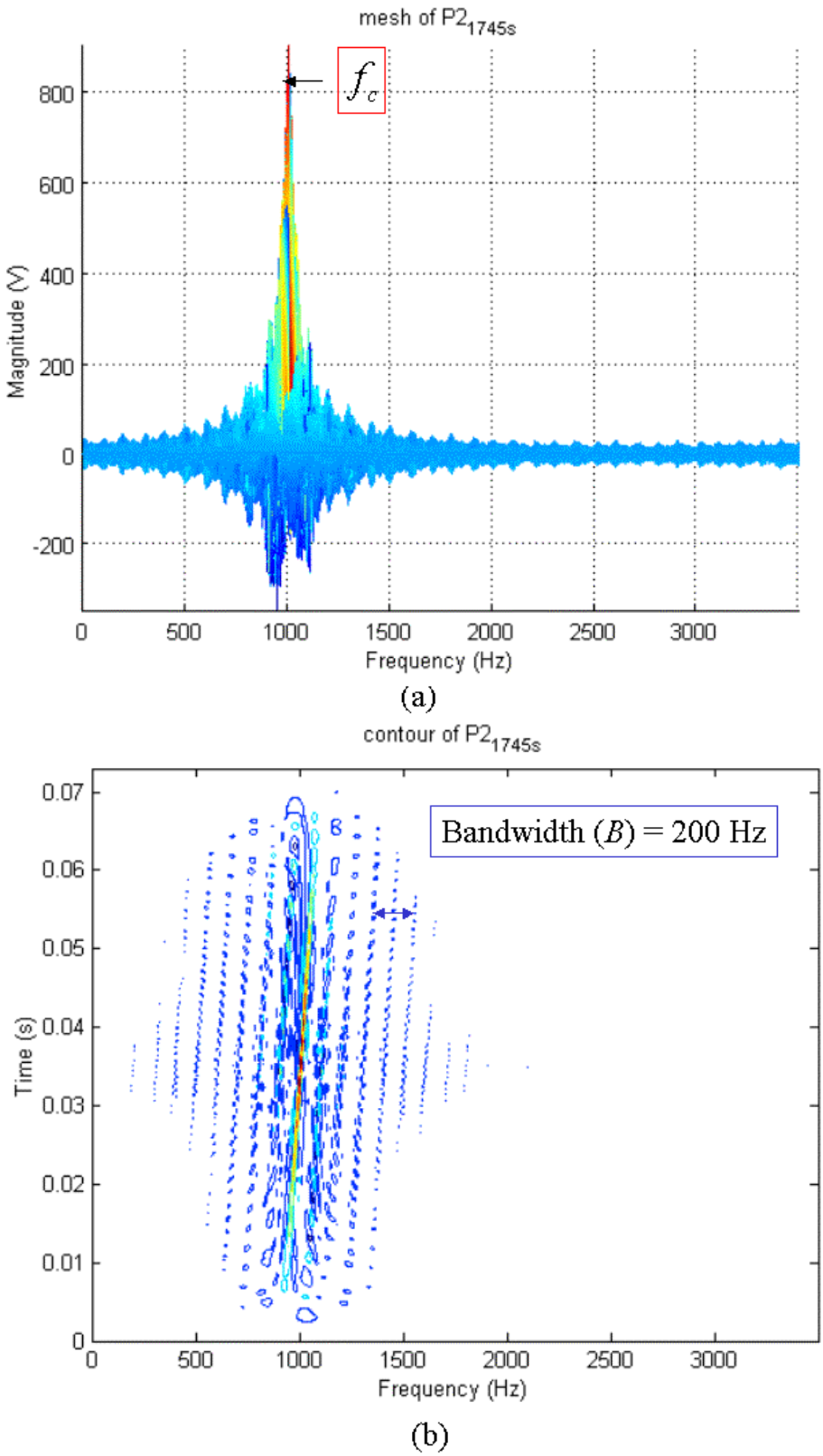

Figure 36. WD for P2 Code with Phase Length = 16, CPP = 5, Signal Only, (No.52) (a) 2D Mesh in Frequency Domain. (b) Contour.

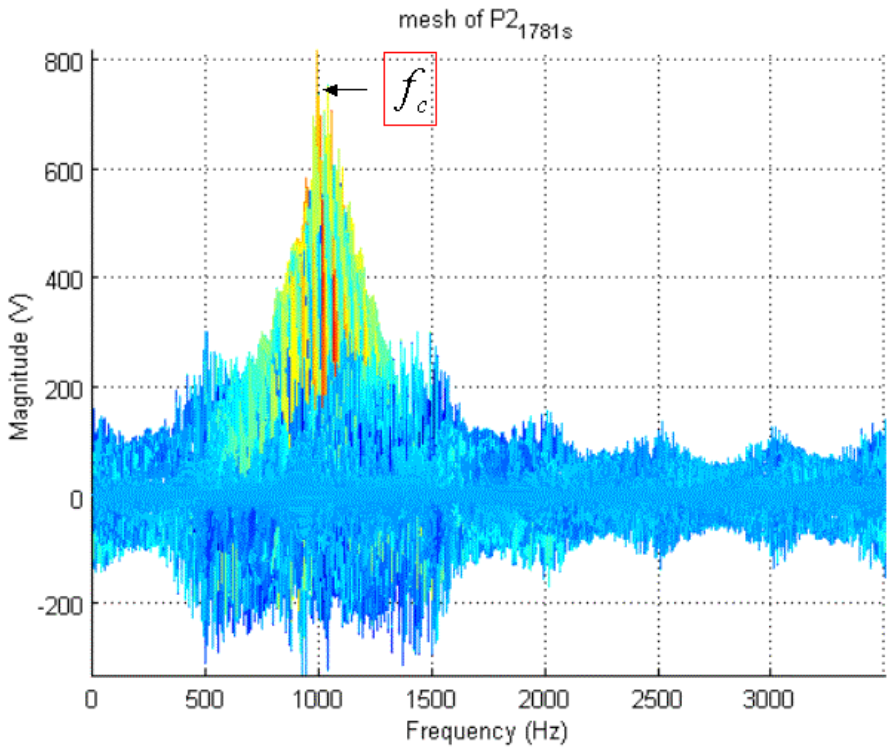

(a)

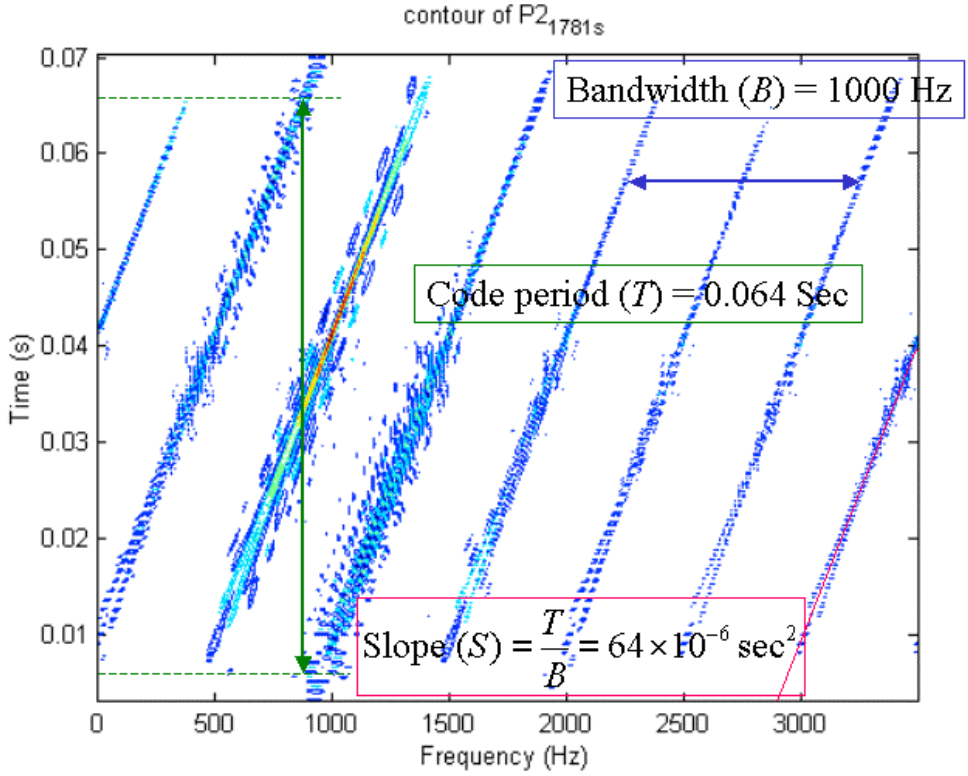

(b)

Figure 37. WD for P2 Code with Phase Length = 64, CPP = 1, Signal Only, (No.55) (a) 2D Mesh in Frequency Domain. (b) Contour.

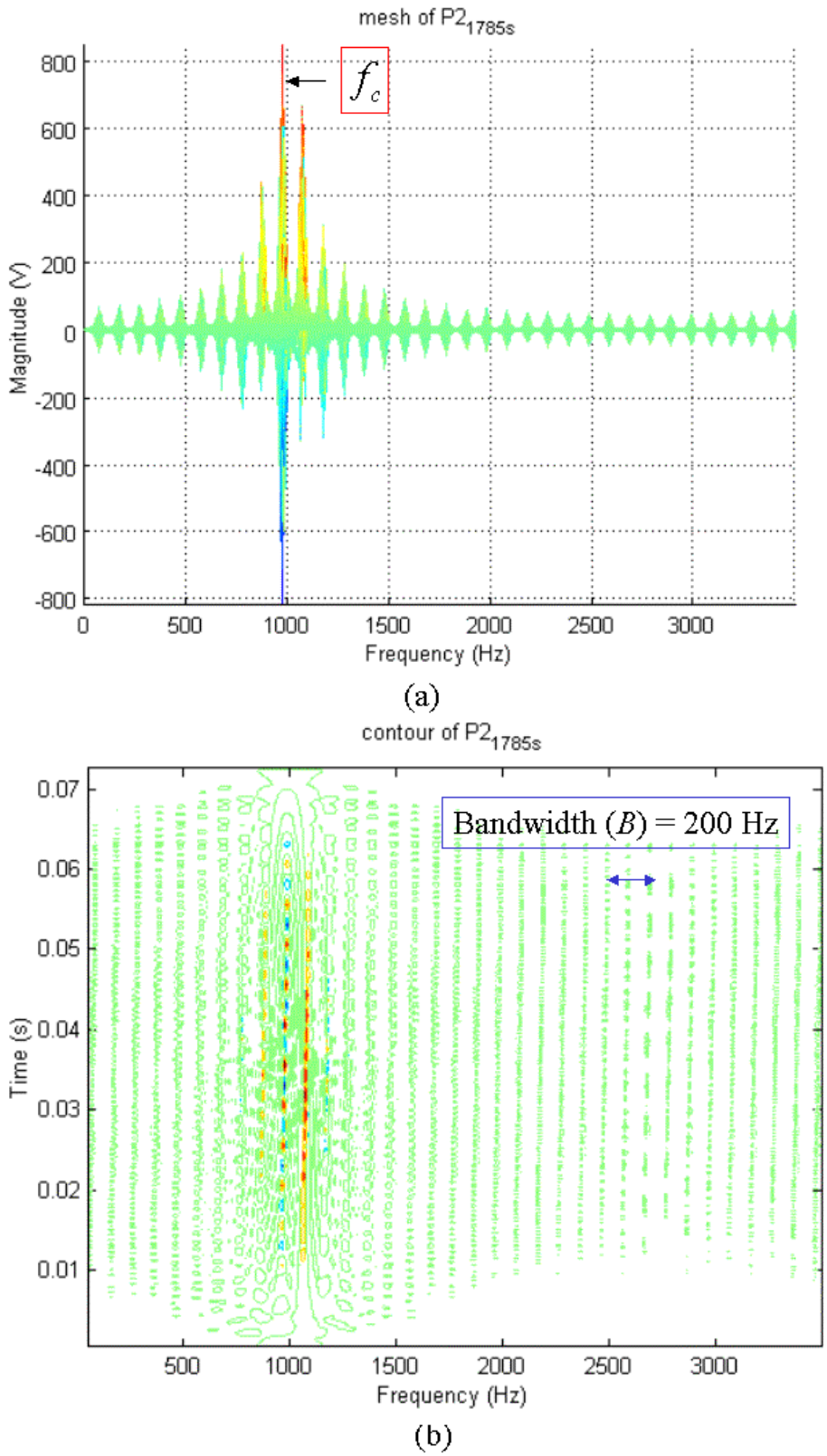

Figure 38. WD for P2 Code with Phase Length = 64, CPP = 5, Signal Only, (No.58) (a) 2D Mesh in Frequency Domain. (b) Contour.

2. Summary

Applying the Wigner Distribution, one can quickly know the carrier frequency (f_c) of the P2 codes. The carrier frequency is always the first parameter need to be identified. Once the carrier frequency is found, by the bandwidth can determine the *CPP* ; by the code period or the slope can determine the phase length(N^2).

In Figure 36(b) (N^2 =16, *CPP*=5) only bandwidth is obtained but not the code period. The reason is that the sample number (#*sample*) is not enough. From (5.11), the code period is $T = \frac{N^2}{B} = \frac{16}{200} = 0.080\,\text{sec}$, hence only when $\frac{\#sample}{f_s} \geq T$, the code period can be shown in the figure. In this chapter, the $\frac{\#sample}{f_s} = \frac{512}{7000} = 0.073 \leq 0.080$.

Table 11 below shows the detection effectiveness of the carrier frequency, 3dB bandwidth, code period and phase length from Figure 35 to 38. They are done by the visible inspection of the WD results.

P2				
No.	Carrier Frequency	Bandwidth	Code Period	Phase Length
49	100%	70%	100%	100%
50	110%	60%	90%	100%
51	0%	0%	0%	0%
52	100%	100%	0%	0%
53	100%	0%	0%	0%
54	95%	0%	0%	0%
55	100%	100%	100%	100%
56	100%	110%	110%	100%
57	0%	110%	110%	100%
58	100%	100%	0%	0%
59	100%	90%	0%	0%
60	120%	0%	0%	0%

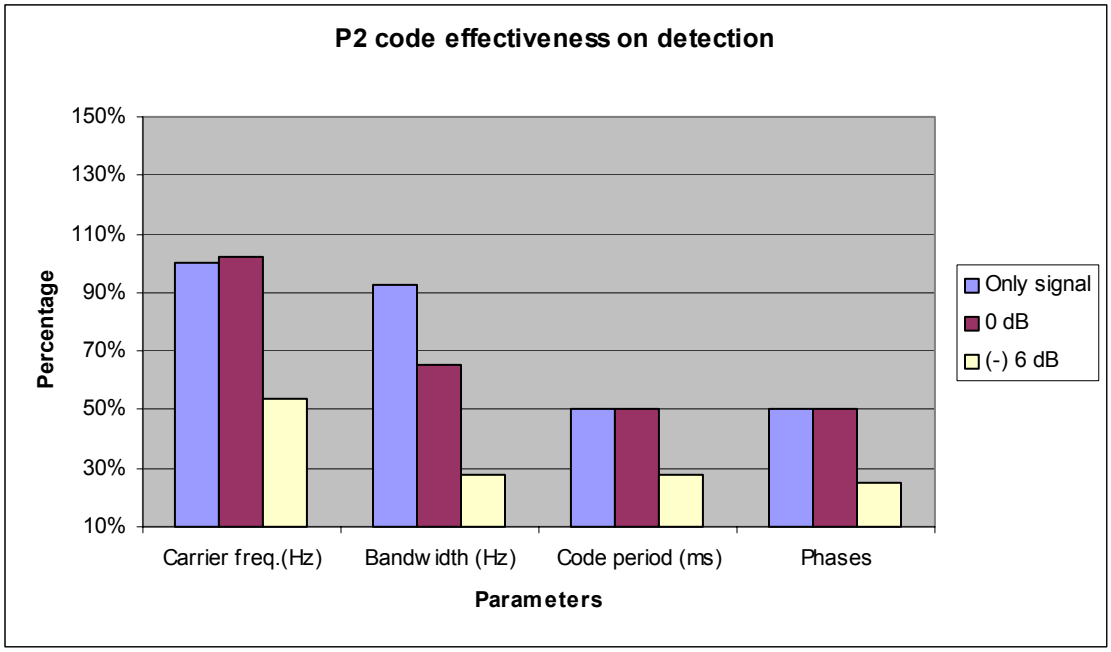

Table 11. WD Detection Effectiveness for P2 Code Signals.

E. P3 CODE

In the case of linear frequency modulation waveforms, the conceptual coherent detection using single sideband detection and sampling at the Nyquist rate yield a polyphase code call the P3. The phase of the *i*th sample of the P3 code is given by [Ref. 20]

$$\phi_i = \frac{\pi}{N}(i-1)(i-1) \tag{5.13}$$

where $i = 1:N$

Twelve P3 code signals are introduced in this chapter. They are numbered from 61 to 72 and listed in Table 12. In this chapter, the phase length N = 16 and 64 and cycles per phase (*CPP)* = 1 and 5 are used. A 1kHz carrier frequency and 7kHz sampling frequency are used for these signals.

No.	P3	N (Phase)	Cycles/Phase	SNR
61	P3_1_7_16_1_s	16	1	Signal Only
62	P3_1_7_16_1_0	16	1	0 dB
63	P3_1_7_16_1_-6	16	1	-6 dB
64	P3_1_7_16_5_s	16	5	Signal Only
65	P3_1_7_16_5_0	16	5	0 dB
66	P3_1_7_16_5_-6	16	5	-6 dB
67	P3_1_7_64_1_s	64	1	Signal Only
68	P3_1_7_64_1_0	64	1	0 dB
69	P3_1_7_64_1_-6	64	1	-6 dB
70	P3_1_7_64_5_s	64	5	Signal Only
71	P3_1_7_64_5_0	64	5	0 dB
72	P3_1_7_64_5_-6	64	5	-6 dB

Table 12. P3 Code Signals.

1. Wigner Distribution for P3 Code

Consider the same twelve P3 code signals in Table 12 and use them as the inputs for Wigner Distribution (WD). The WD results of these twelve signals are showed in Figure 39 to 42. The mesh plots show the frequency domain of the P3 code signals after WD. The contour plots show both the frequency domain and time domain of the results.

Take Figure 39 as an example. First, the carrier frequency f_c can be clearly found by the location of the highest or lowest peak value in Figure 39(a). Secondly, in Figure 39(b), the 3dB bandwidth can be measured as 1000Hz. Since

$$B = \frac{1}{t_b} = \frac{f_c}{CPP} \tag{5.14}$$

so, the cycles per phase (*CPP*) can be computed by $CPP = \frac{f_c}{B} = \frac{1000}{1000} = 1$ For P3 code

$$T = Nt_b = \frac{N}{B} \tag{5.15}$$

since the code period (*T*) is measured as 0.016 in Figure 39(b), so the phase length (N) can be calculated from $N = B \cdot T = 1000 \cdot 0.016 = 16$. The slope which measured in Figure 39(b) as 1.6×10^{-6} sec^2 can be also use to determine the N^2 and *CPP* by the following equation.

$$S = \frac{T}{B} = \frac{N}{B^2} = \frac{N \cdot CPP^2}{f_c^2} \tag{5.16}$$

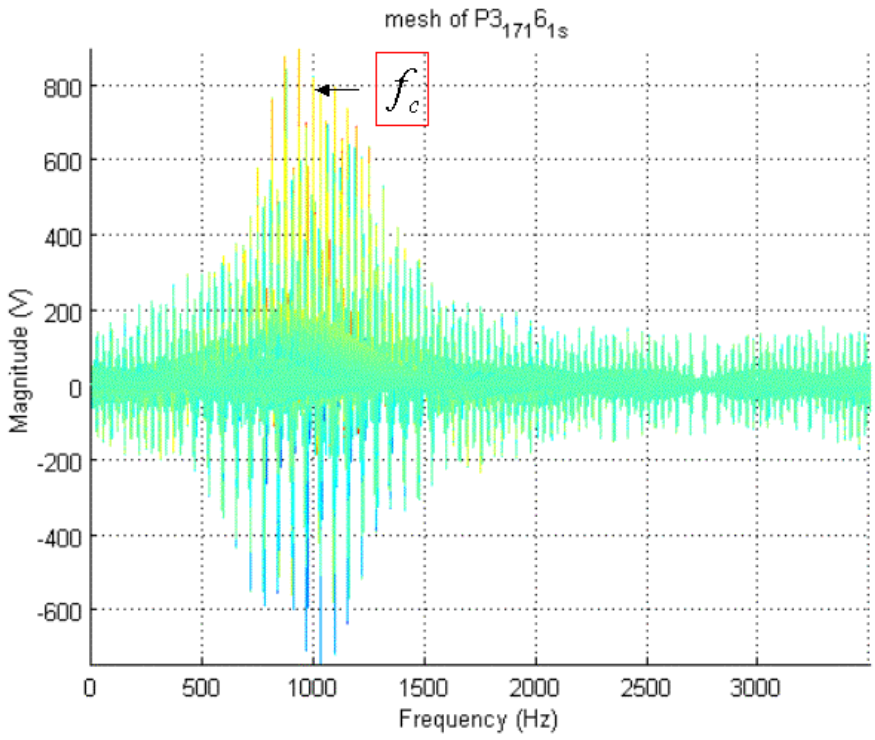

(a)

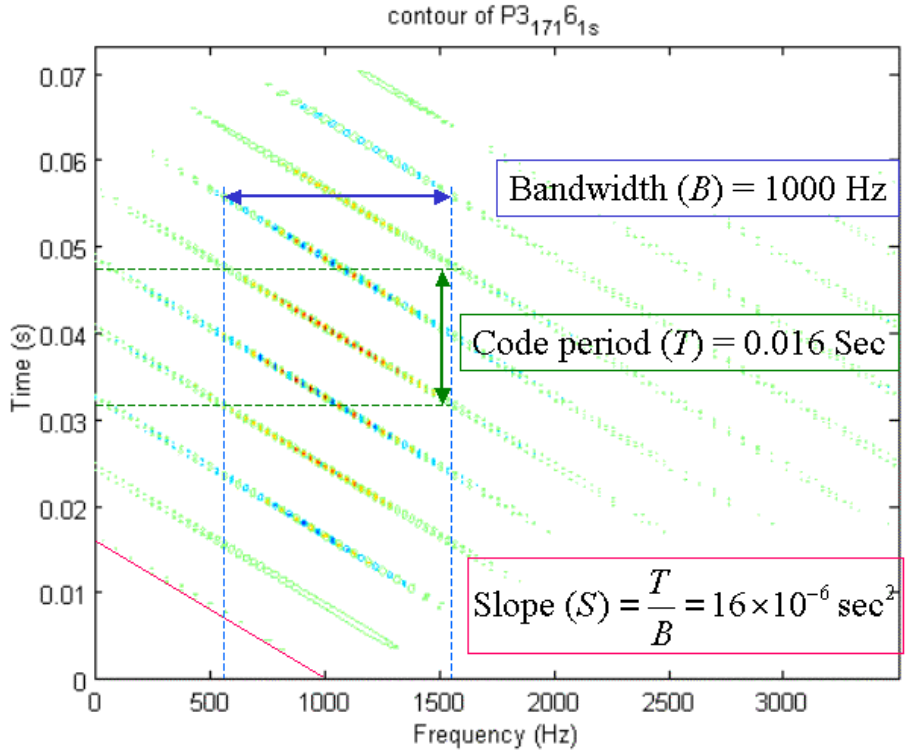

(b)

Figure 39. WD for P3 Code with Phase Length = 16, CPP = 1, Signal Only, (No.61) (a) 2D Mesh in Frequency Domain. (b) Contour.

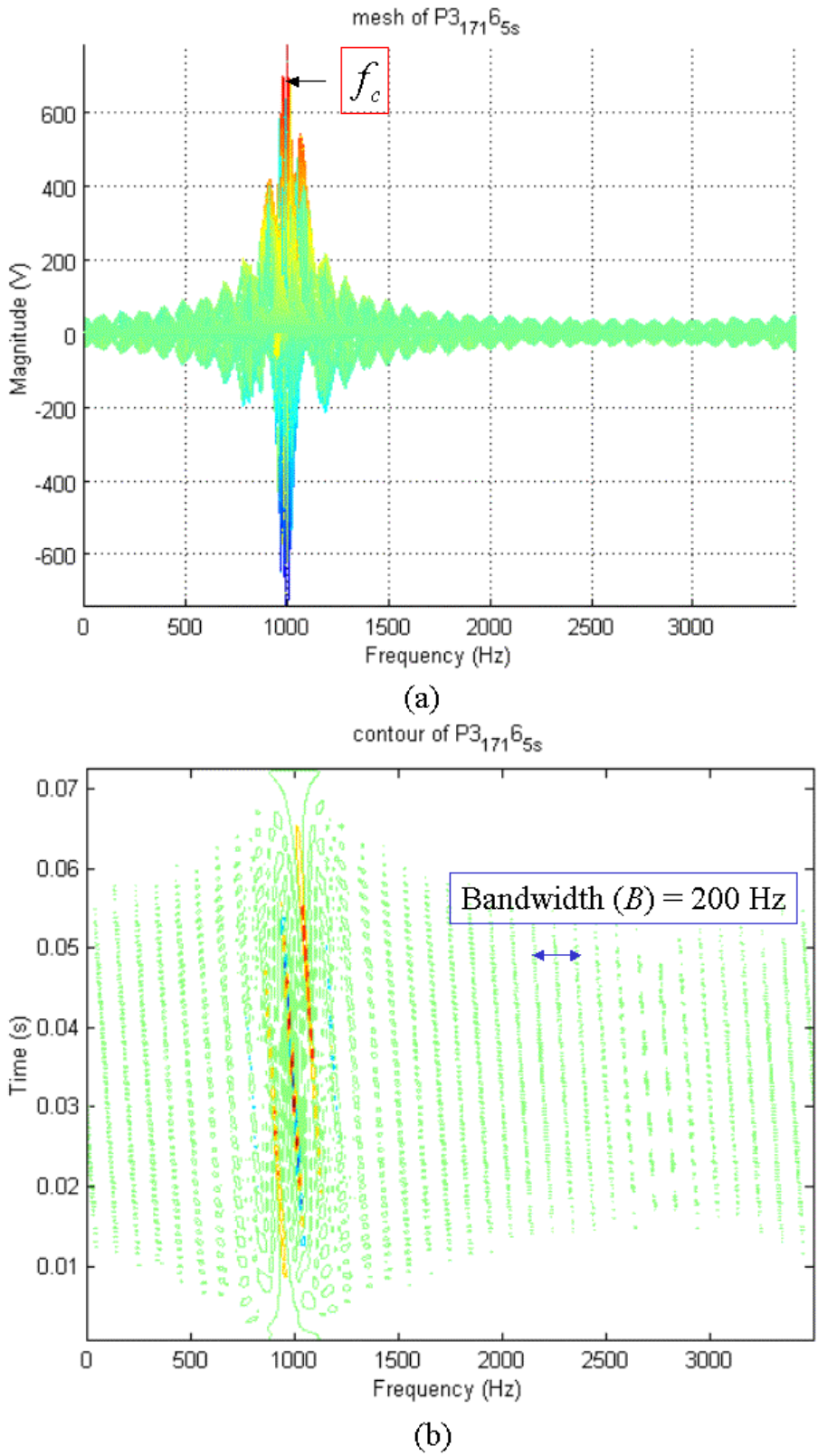

Figure 40. WD for P3 Code with Phase Length = 16, CPP = 5, Signal Only, (No.64) (a) 2D Mesh in Frequency Domain. (b) Contour.

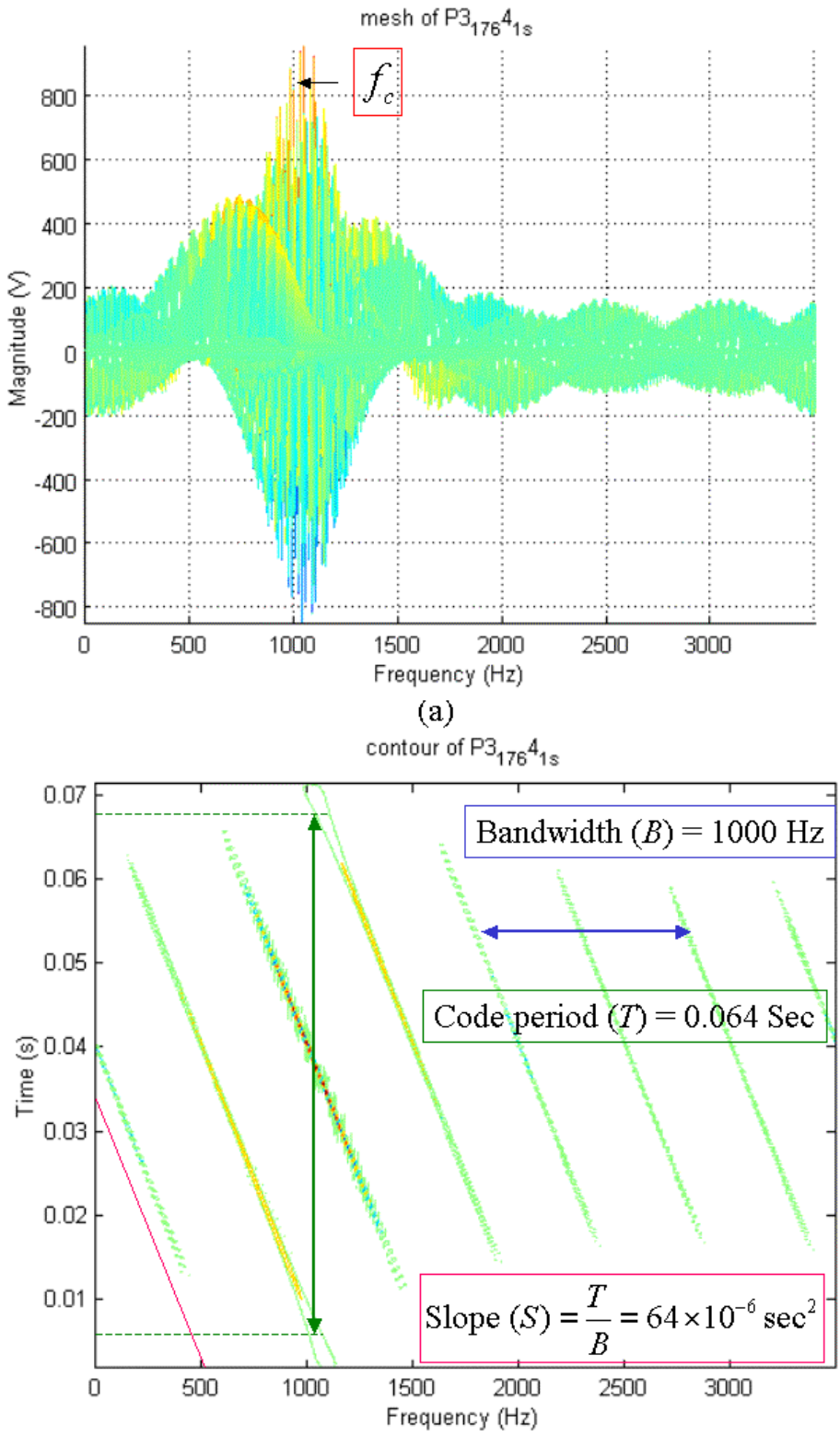

Figure 41. WD for P3 Code with Phase Length = 64, CPP = 1, Signal Only, (No.67) (a) 2D Mesh in Frequency Domain. (b) Contour.

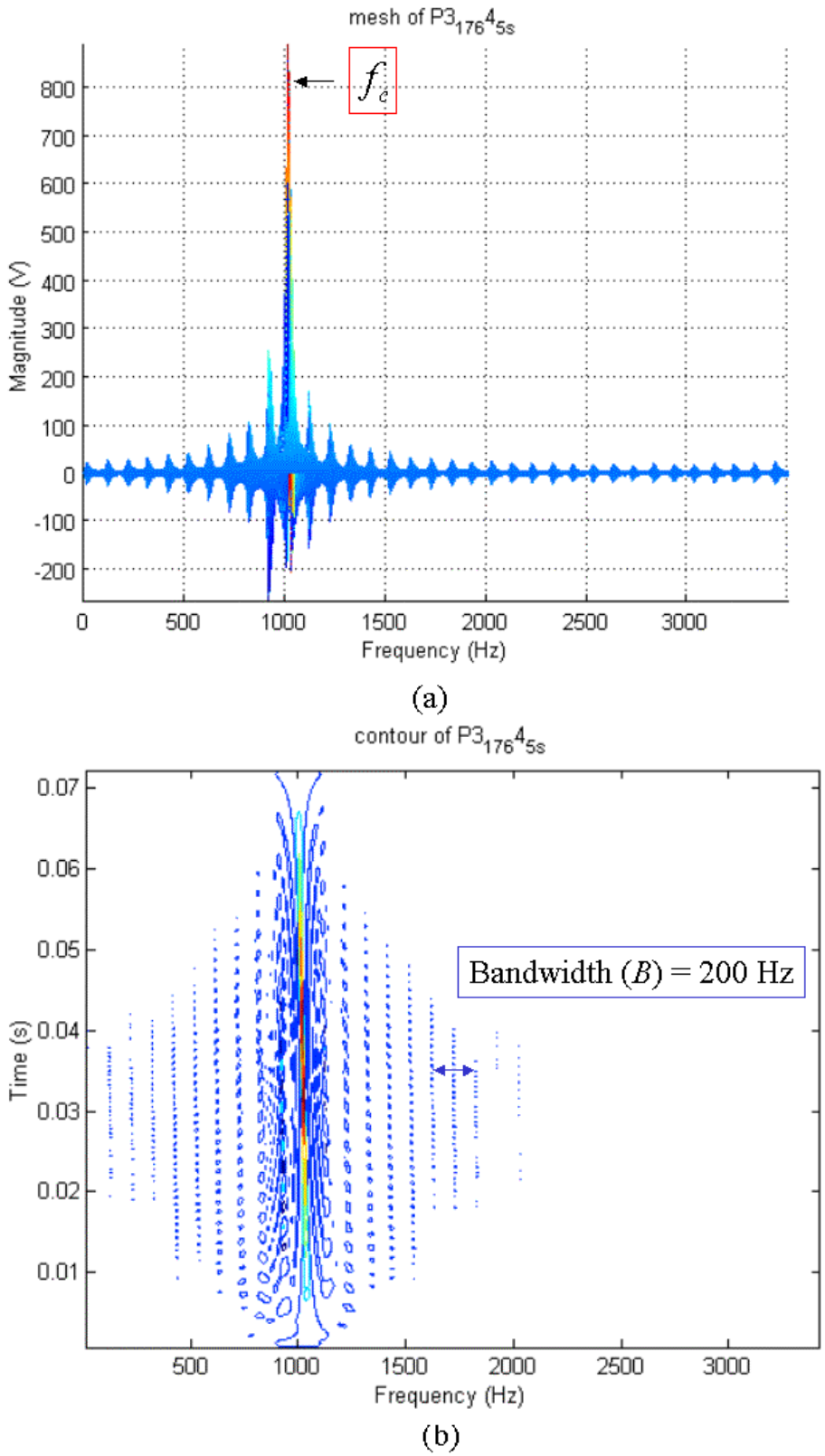

Figure 42. WD for P3 Code with Phase Length = 64, CPP = 5, Signal Only, (No.70) (a) 2D Mesh in Frequency Domain. (b) Contour.

2. Summary

Applying the Wigner Distribution, one can quickly know the carrier frequency (f_c) of the P3 codes. The carrier frequency is always the first parameter need to be identified. Once the carrier frequency is found, by the bandwidth can determine the *CPP* ; by the code period or the slope can determine the phase length(N).

In Figure 40(b) (N =16, *CPP*=5) only bandwidth is obtained but not the code period. The reason is that the sample number (#*sample*) is not enough. From (5.15), the code period is $T = \frac{N}{B} = \frac{16}{200} = 0.080\,\text{sec}$, hence only when $\frac{\#sample}{f_s} \geq T$, the code period can be shown in the figure. In this chapter, the $\frac{\#sample}{f_s} = \frac{512}{7000} = 0.073 \leq 0.080$.

Table 13 below shows the detection effectiveness of the carrier frequency, 3dB bandwidth, code period and phase length from Figure 39 to 42. They are done by the visible inspection of the WD results.

P3				
No.	Carrier Frequency	Bandwidth	Code Period	Phase Length
61	95%	100%	100%	100%
62	95%	110%	100%	100%
63	80%	110%	110%	100%
64	100%	100%	0%	0%
65	100%	120%	0%	0%
66	90%	0%	0%	0%
67	110%	100%	90%	100%
68	110%	100%	90%	100%
69	120%	110%	90%	100%
70	100%	100%	0%	0%
71	100%	0%	0%	0%
72	100%	0%	0%	0%

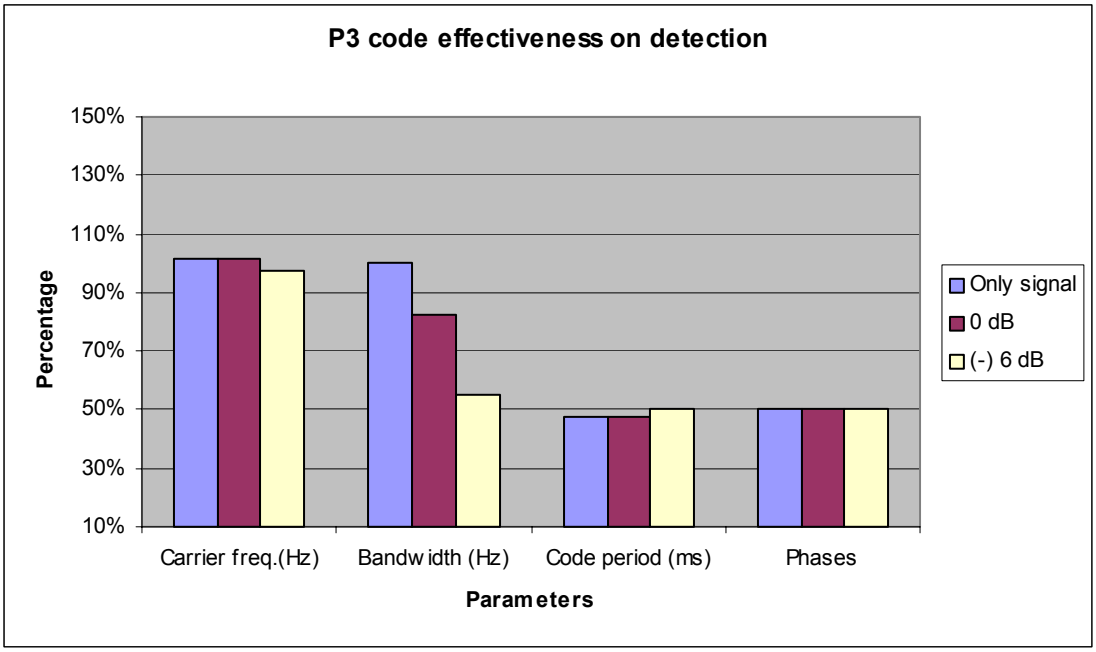

Table 13. WD Detection Effectiveness for P3 Code Signals.

F. P4 CODE

The P4 code consists of the discrete phase of the linear chirp waveform taken at specific time intervals and exhibits the same range Doppler coupling associated with the chirp waveform. The peak sidelobe levels are lower than those of the unweighted chirp waveform. The code element of the P4 code are given by [Ref. 20]

$$\phi_i = \pi \frac{(i-1)^2}{N} - \pi(i-1) \tag{5.17}$$

where $i = 1:N$

Twelve P4 code signals are introduced in this chapter. They are numbered from 73 to 84 and listed in Table 14. The phase length or phase elements *N* are also 16 or 64; *CPP* is 1 or 5 for P4 codes in this chapter. A 1kHz carrier frequency and 7kHz sampling frequency are used for these signals.

No.	P4	N (Phase)	Cycles/Phase	SNR
73	P4_1_7_16_1_s	16	1	Signal Only
74	P4_1_7_16_1_0	16	1	0 dB
75	P4_1_7_16_1_-6	16	1	-6 dB
76	P4_1_7_16_5_s	16	5	Signal Only
77	P4_1_7_16_5_0	16	5	0 dB
78	P4_1_7_16_5_-6	16	5	-6 dB
79	P4_1_7_64_1_s	64	1	Signal Only
80	P4_1_7_64_1_0	64	1	0 dB
81	P4_1_7_64_1_-6	64	1	-6 dB
82	P4_1_7_64_5_s	64	5	Signal Only
83	P4_1_7_64_5_0	64	5	0 dB
84	P4_1_7_64_5_-6	64	5	-6 dB

Table 14. P4 Code Signals.

1. Wigner Distribution for P4 Code

Consider the same twelve P4 code signals in Table 14 and use them as the inputs. The WD results of these twelve signals are showed in Figure 43 to 46. The mesh plots show the frequency domain of the P4 code signals after WD. The contour plots show both the frequency domain and time domain of the results.

Take Figure 43 as an example. First, the carrier frequency f_c can be clearly found by the location of the highest or lowest peak value in Figure 43(a). Secondly, in Figure 43 (b), the 3dB bandwidth can be measured as 1000Hz. Since

$$B = \frac{1}{t_b} = \frac{f_c}{CPP} \tag{5.18}$$

so, the cycles per phase (*CPP*) can be computed by $CPP = \frac{f_c}{B} = \frac{1000}{1000} = 1$ For P4 code

$$T = Nt_b = \frac{N}{B} \tag{5.19}$$

since the code period (*T*) is measured as 0.016 in Figure 43 (b), so the phase length (N) can be calculated from $N = B \cdot T = 1000 \cdot 0.016 = 16$. The slope which measured in Figure 43 (b) as 1.6×10^{-6} sec^2 can be also use to determine the N^2 and *CPP* by the following equation.

$$S = \frac{T}{B} = \frac{N}{B^2} = \frac{N \cdot CPP^2}{f_c^2} \tag{5.20}$$

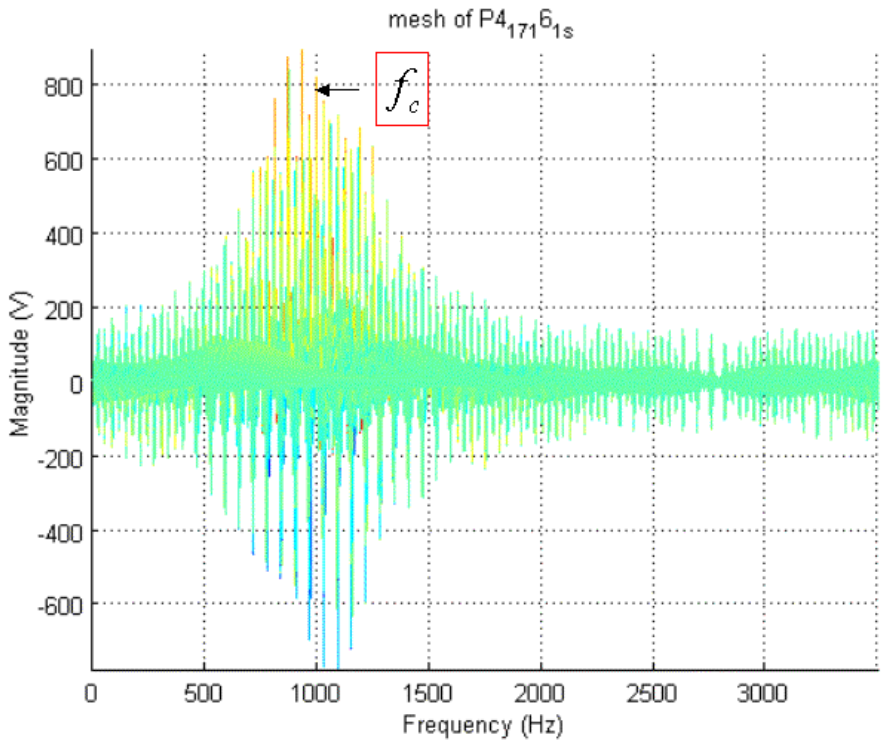

(a)

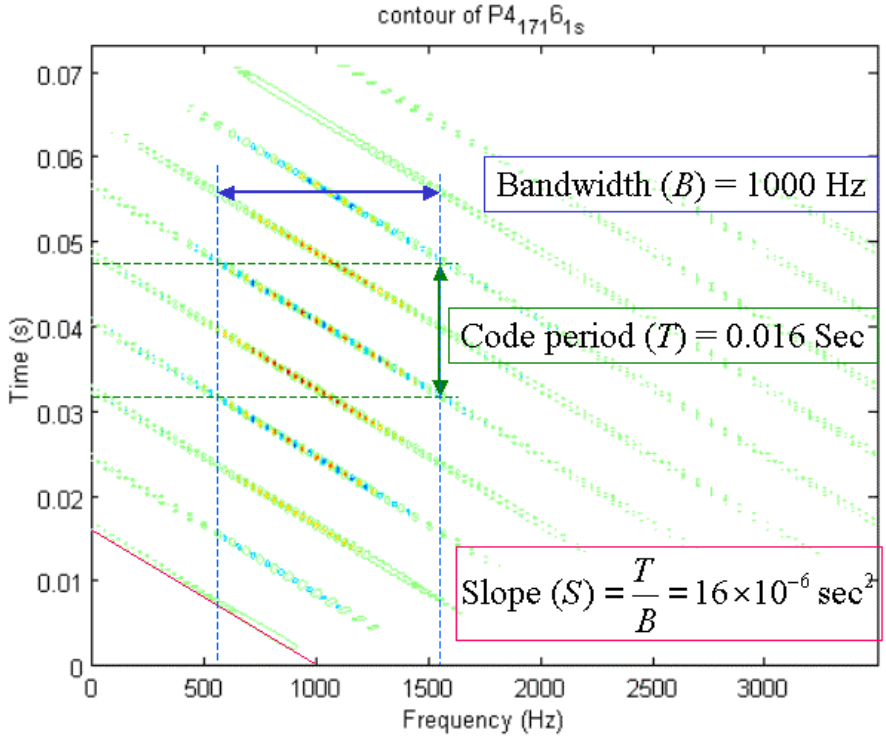

(b)

Figure 43. WD for P4 Code with Phase Length = 16, CPP = 1, Signal Only, (No.73) (a) 2D Mesh in Frequency Domain. (b) Contour.

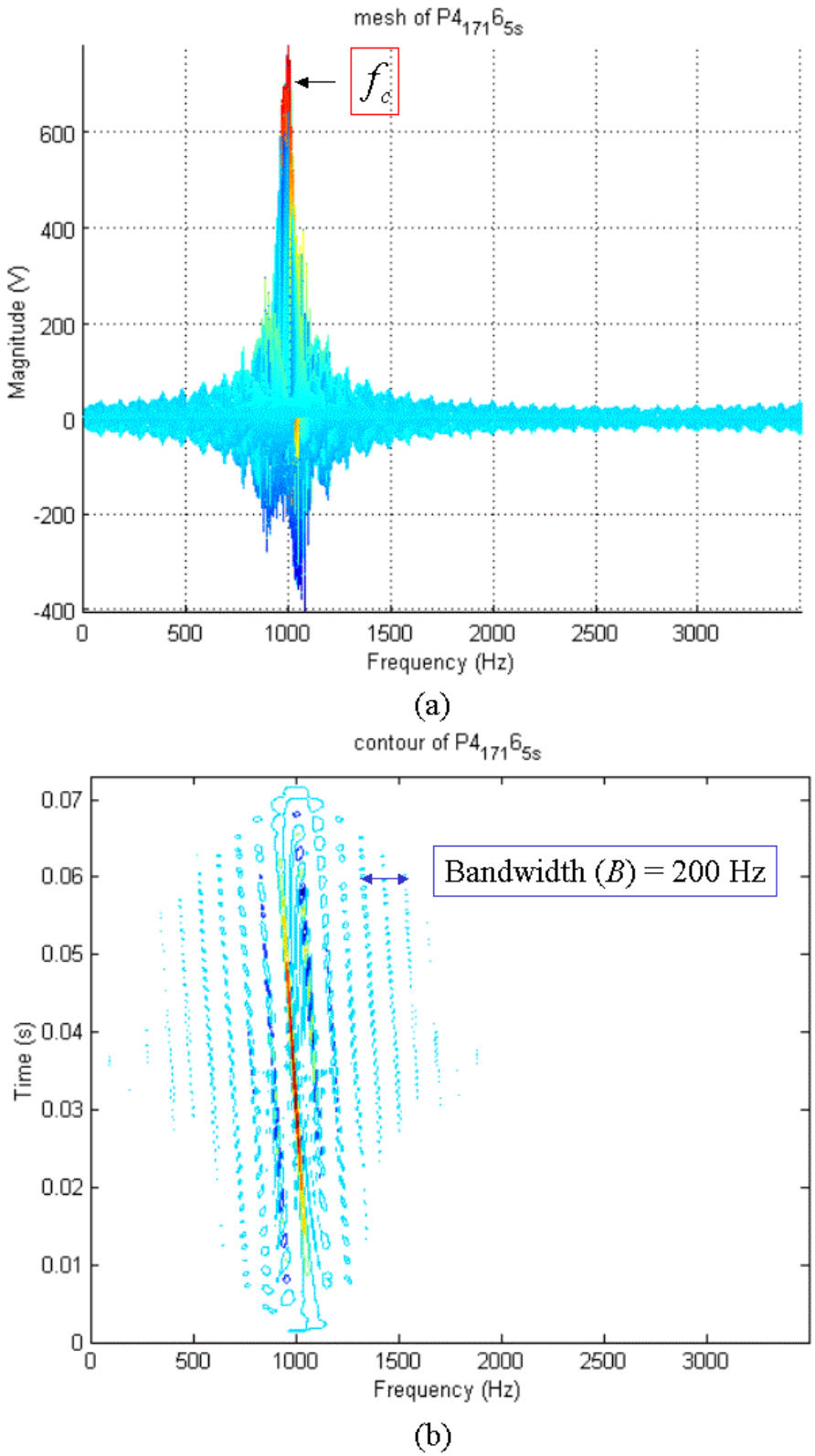

Figure 44. WD for P4 Code with Phase Length = 16, CPP = 5, Signal Only, (No.76) (a) 2D Mesh in Frequency Domain. (b) Contour.

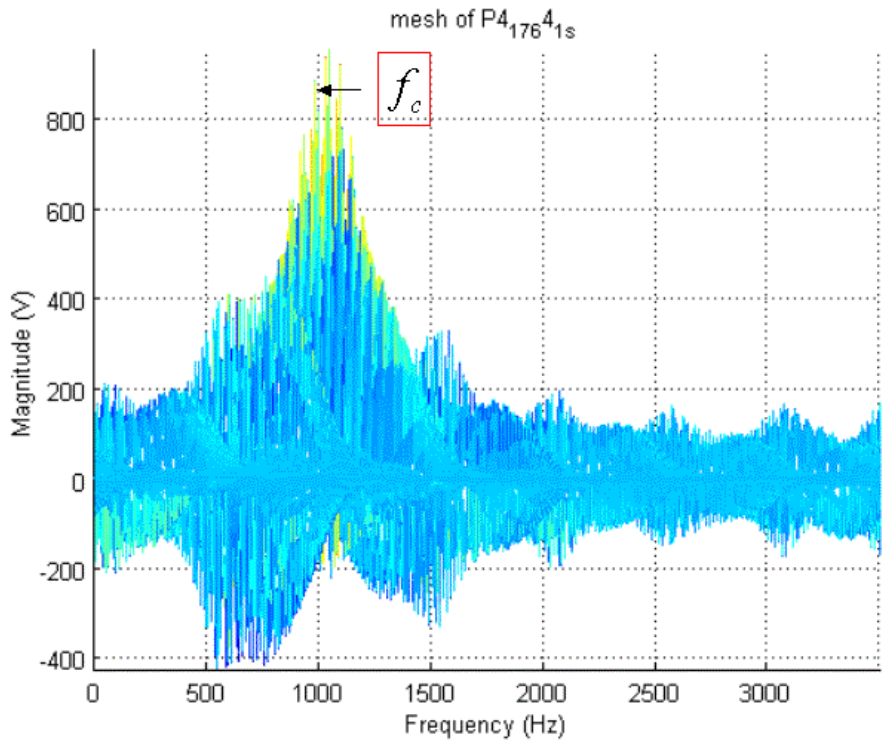

(a)

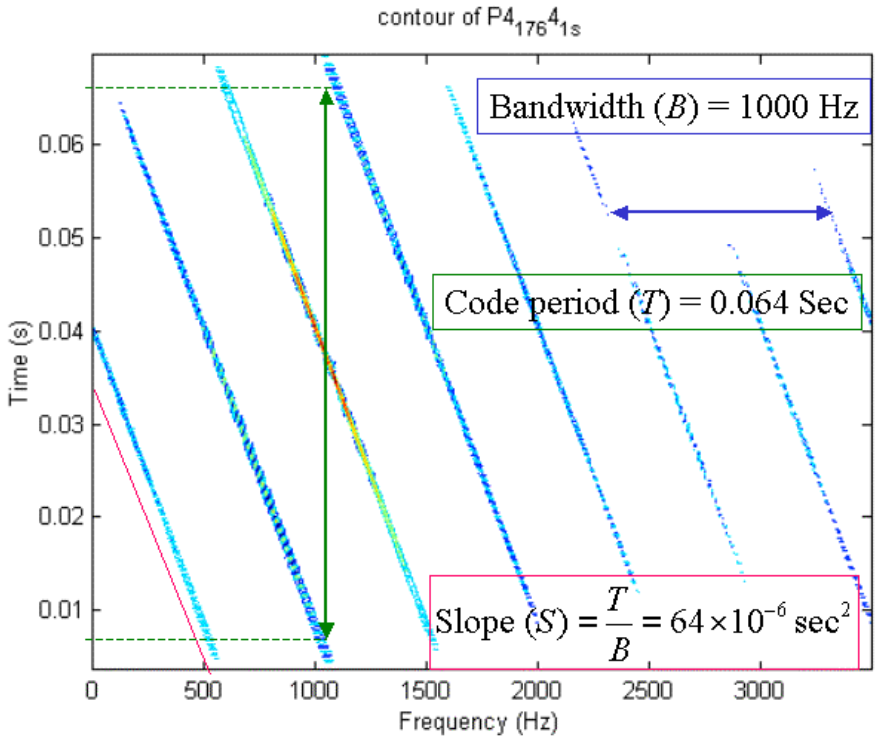

(b)

Figure 45. WD for P4 Code with Phase Length = 64, CPP = 1, Signal Only, (No.79) (a) 2D Mesh in Frequency Domain. (b) Contour.

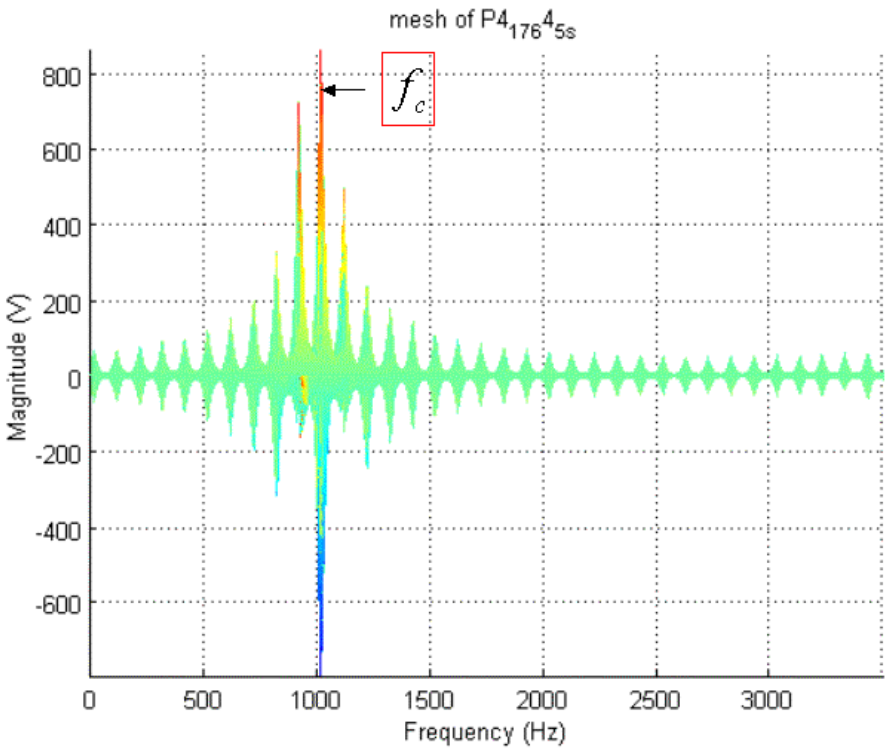

(a)

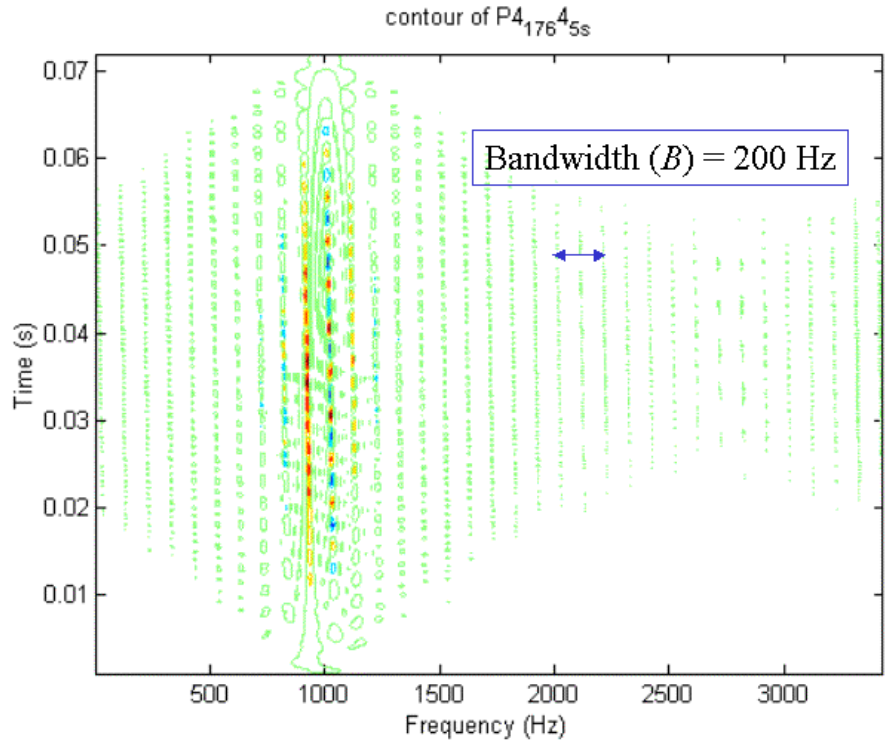

(b)

Figure 46. WD for P4 Code with Phase Length = 64, CPP = 5, Signal Only, (No.82) (a) 2D Mesh in Frequency Domain. (b) Contour.

2. Summary

Applying the Wigner Distribution, one can quickly know the carrier frequency (f_c) of the P4 codes. The carrier frequency is always the first parameter need to be identified. Once the carrier frequency is found, by the bandwidth can determine the *CPP* ; by the code period or the slope can determine the phase length(N).

In Figure 44(b) (N =16, *CPP*=5) only bandwidth is obtained but not the code period. The reason is that the sample number (#*sample*) is not enough. From (5.19), the code period is $T = \frac{N}{B} = \frac{16}{200} = 0.080\,\text{sec}$, hence only when $\frac{\#sample}{f_s} \geq T$, the code period can be shown in the figure. In this chapter, the $\frac{\#sample}{f_s} = \frac{512}{7000} = 0.073 \leq 0.080$.

Table 9 below shows the detection effectiveness of the carrier frequency, 3dB bandwidth, code period and phase length from Figure 43 to 46. They are done by the visible inspection of the WD results.

P4				
No.	Carrier Frequency	Bandwidth	Code Period	Phase Length
73	90%	100%	100%	100%
74	90%	95%	110%	100%
75	80%	90%	110%	100%
76	100%	100%	0%	0%
77	95%	0%	0%	0%
78	100%	0%	0%	0%
79	110%	100%	100%	100%
80	115%	105%	95%	100%
81	125%	110%	90%	100%
82	100%	100%	0%	0%
83	100%	110%	0%	0%
84	100%	120%	0%	0%

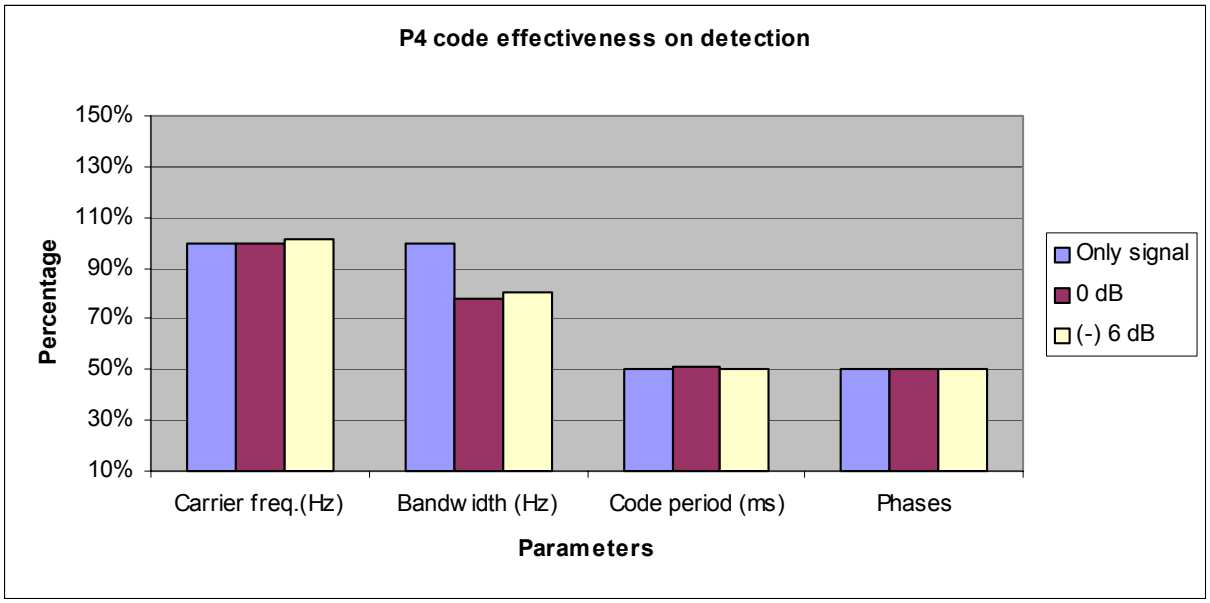

Table 15. WD Detection Effectiveness for P4 Code Signals.

G. COMPARISON OF POLYPHASE CODES

Table 16 shows the phases for all the different polyphase codes discussed in this thesis.

Frank Code	$\phi_{i,j} = \frac{2\pi}{N}(i-1)(j-1) \quad where \quad i = 1:N \quad and \quad j = 1:N$
P1 Code	$\phi_{i,j} = \frac{-\pi}{N}[N-(2j-1)][(j-1)N+(i-1)] \quad where \quad i = 1:N \quad and \quad j = 1:N$
P2 Code	$\phi_{i,j} = \frac{-\pi}{2N}(2i-1-N)(2j-1-N) \quad where \quad i = 1:N \quad and \quad j = 1:N$
P3 Code	$\phi_i = \frac{\pi}{N}(i-1)(i-1) \quad where \quad i = 1:N$
P4 Code	$\phi_i = \pi\frac{(i-1)^2}{N} - \pi(i-1) \quad where \quad i = 1:N$

Table 16. Phases of All the Polyphase Code.

Figure 47 compares the WD of all the polyphase codes with same *CPP* = 1 and phase length = 16. Figure 48 is the zoom in figure for Figure 47. Figure 49 compares the WD of all the polyphase codes with same *CPP* = 5 and phase length = 16. Figure 50 is the zoom in figure for Figure 49. Figure 51 compares the WD of all the polyphase codes with same *CPP* = 1 and phase length = 64. Figure 52 is the zoom in figure for Figure 51. Figure 53 compares the WD of all the polyphase codes with same *CPP* = 5 and phase length = 64. Figure 54 is the zoom in figure for Figure 53.

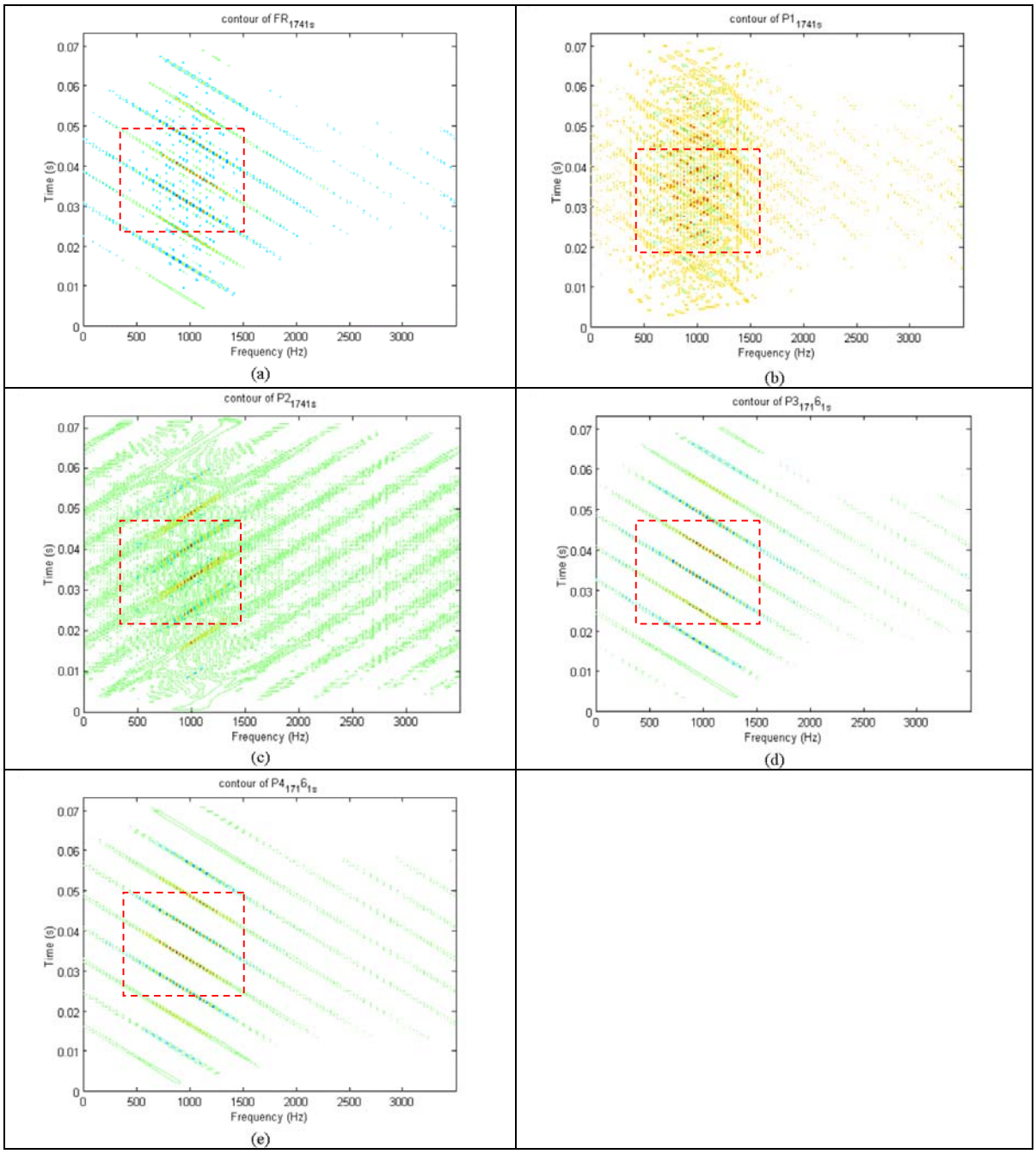

Figure 47. Wigner Distribution for Polyphase Codes with CPP = 1 and Phase Length = 16 (a) Frank Code. (b) P1 Code. (c) P2 Code. (d) P3 Code. (e) P4 Code.

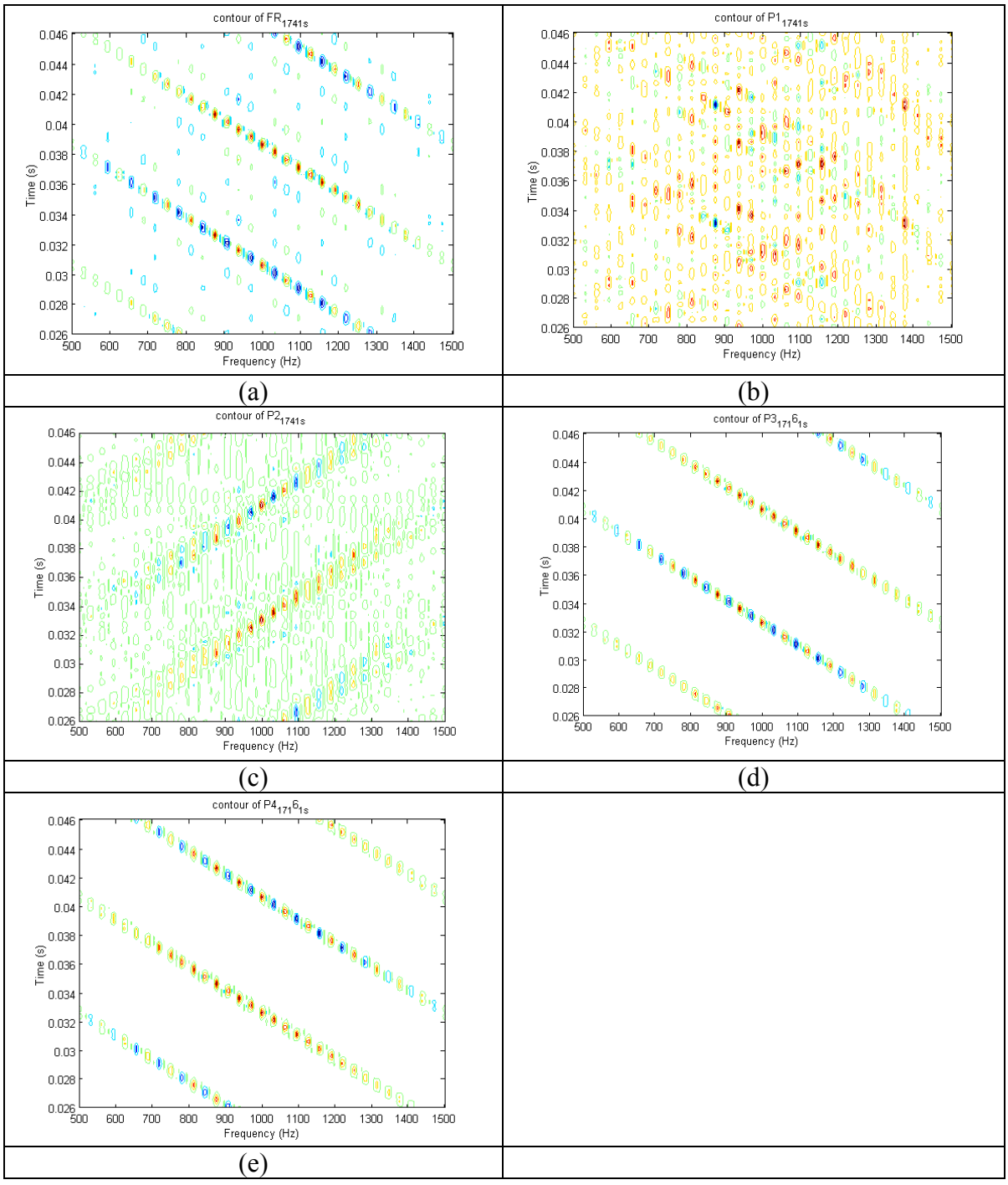

Figure 48. Zoom In for Figure 47 (a) Frank Code. (b) P1 Code. (c) P2 Code. (d) P3 Code. (e) P4 Code.

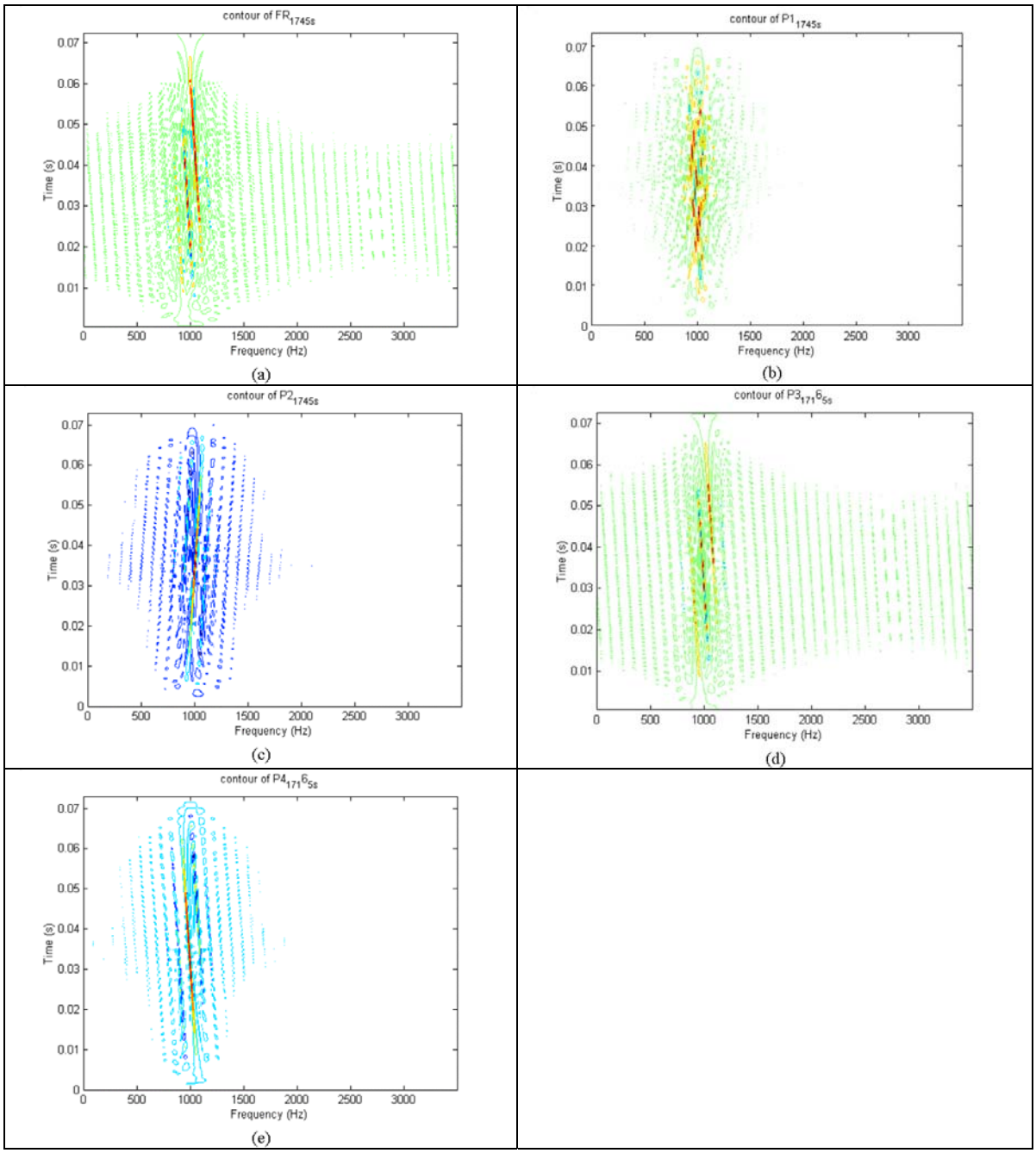

Figure 49. Wigner Distribution for Polyphase Codes with CPP = 5 and Phase Length = 16 (a) Frank Code. (b) P1 Code. (c) P2 Code. (d) P3 Code. (e) P4 Code.

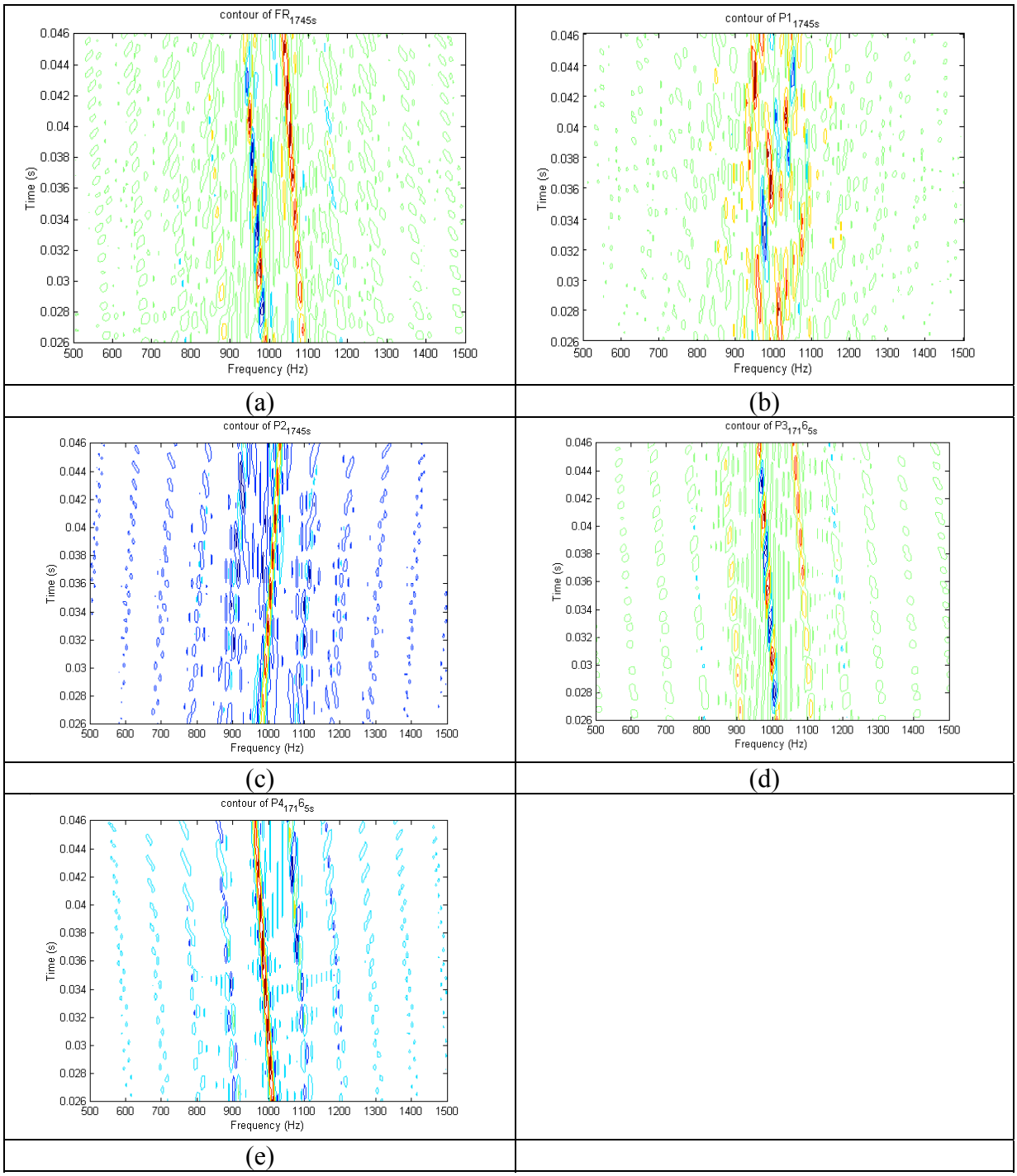

Figure 50. Zoom In for Figure 49 (a) Frank Code. (b) P1 Code. (c) P2 Code. (d) P3 Code. (e) P4 Code.

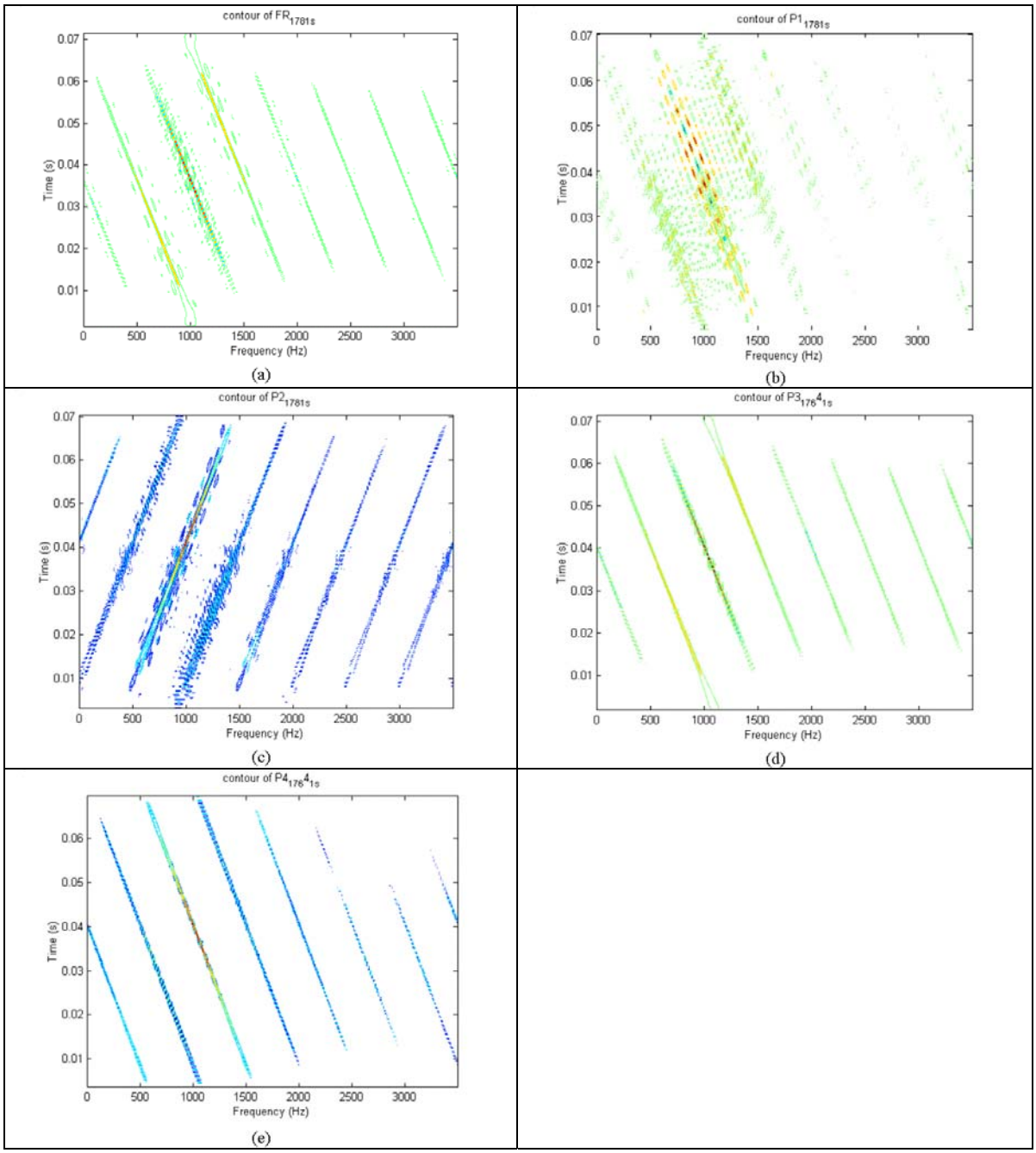

Figure 51. Wigner Distribution for Polyphase Codes with CPP = 1 and Phase Length = 64 (a) Frank Code. (b) P1 Code. (c) P2 Code. (d) P3 Code. (e) P4 Code.

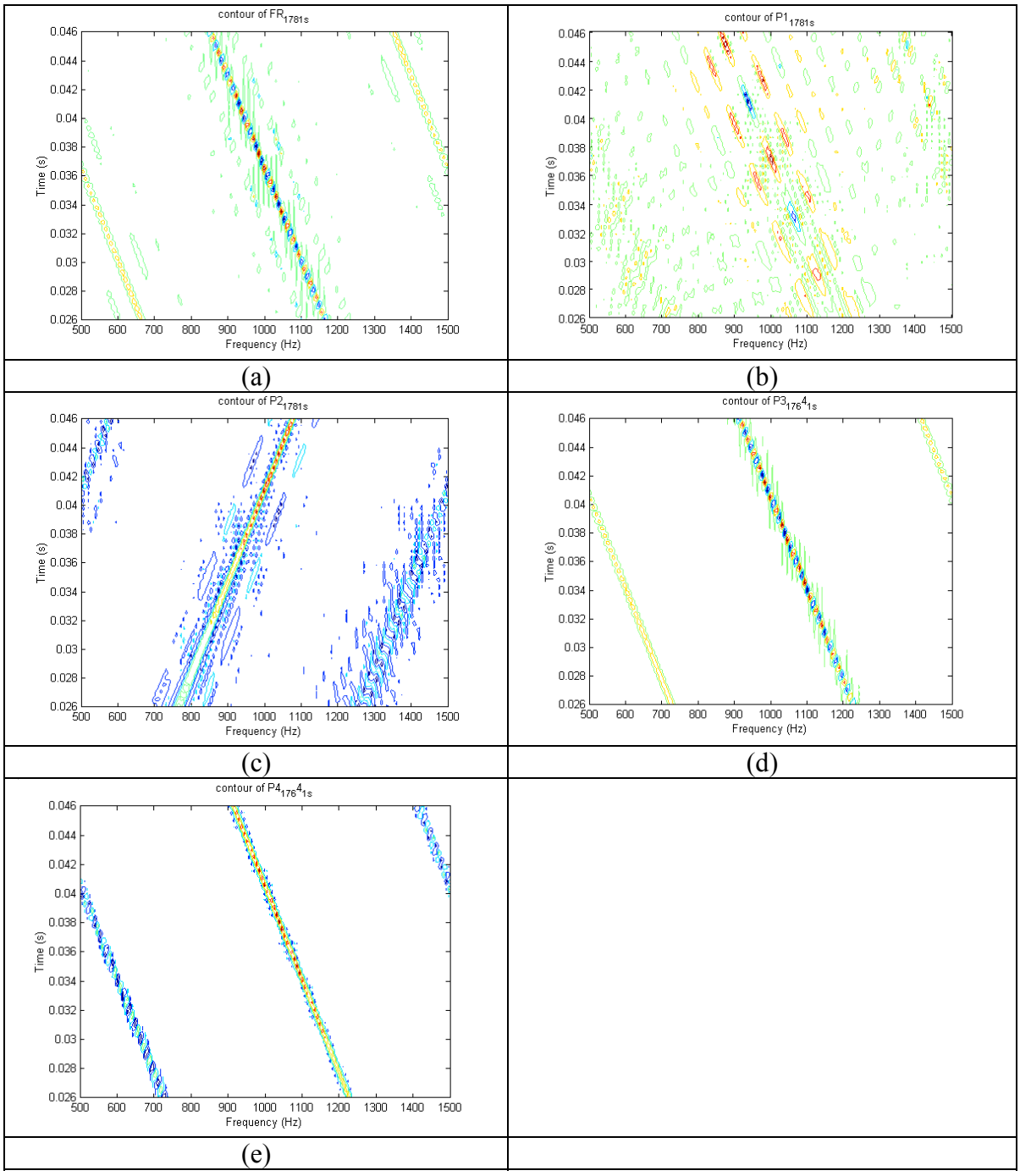

Figure 52. Zoom In for Figure 51 (a) Frank Code. (b) P1 Code. (c) P2 Code. (d) P3 Code. (e) P4 Code.

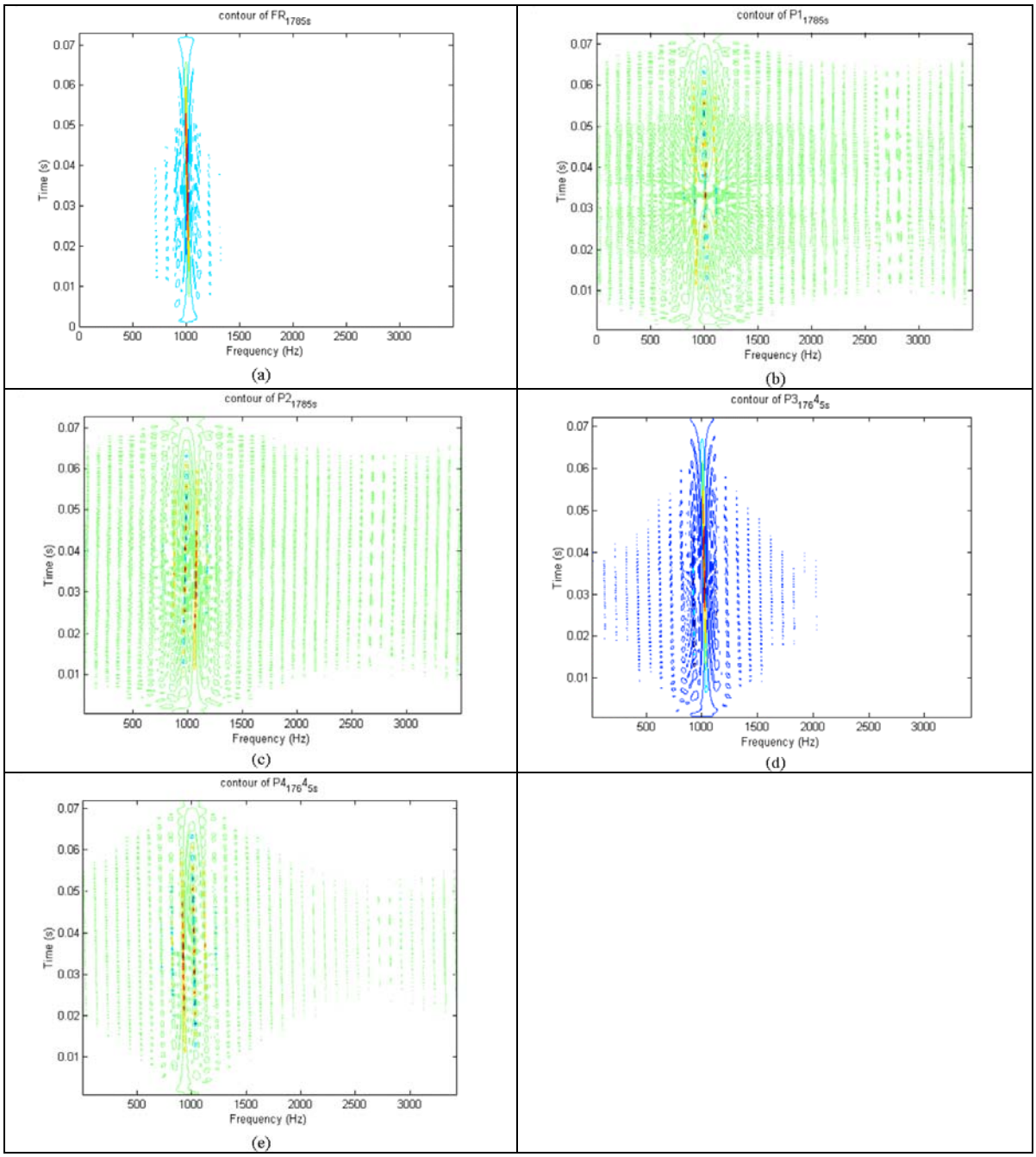

Figure 53. Wigner Distribution for Polyphase Codes with CPP = 5 and Phase Length = 64 (a) Frank Code. (b) P1 Code. (c) P2 Code. (d) P3 Code. (e) P4 Code.

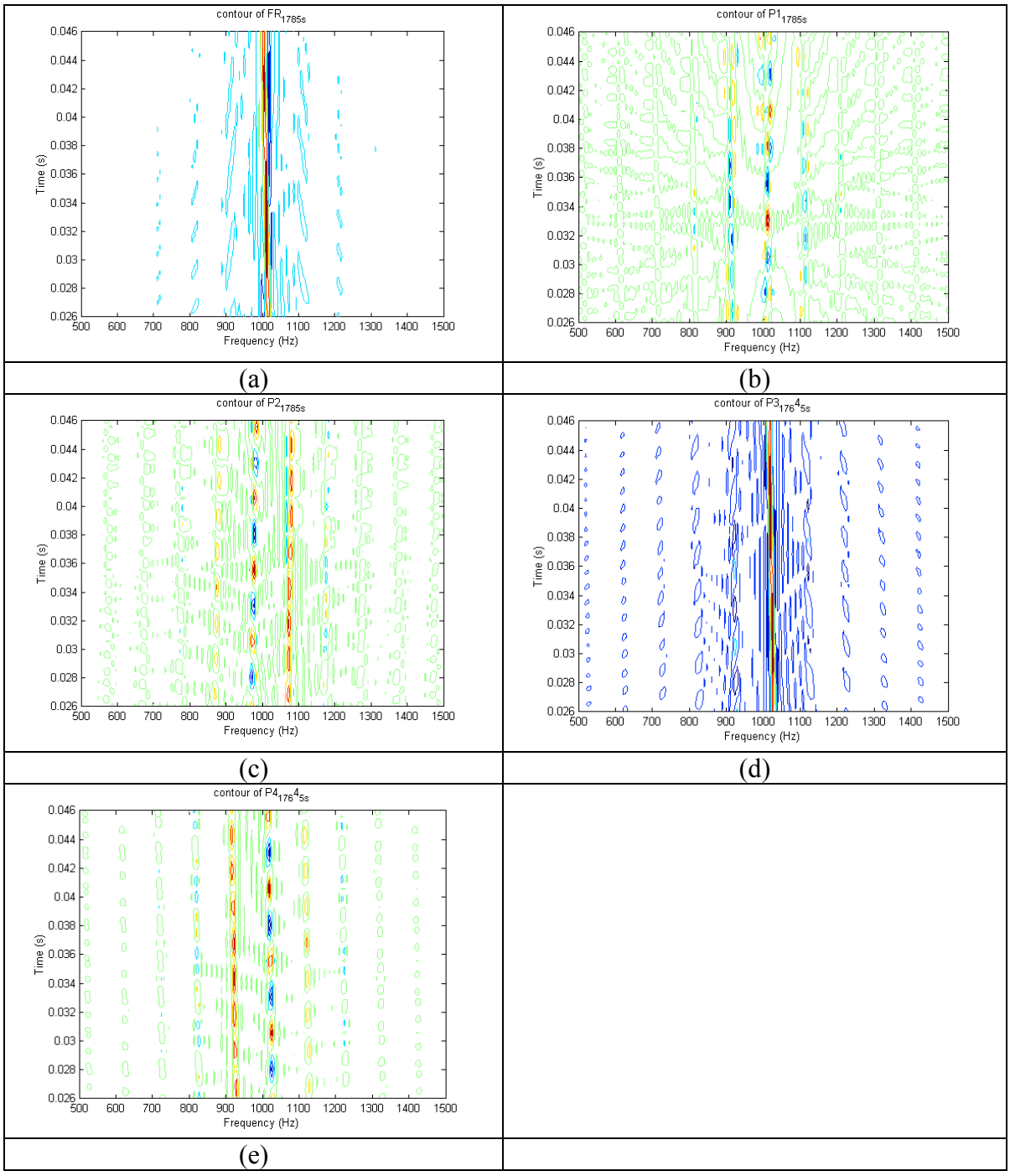

Figure 54. Zoom In for Figure 53 (a) Frank Code. (b) P1 Code. (c) P2 Code. (d) P3 Code. (e) P4 Code.

Some features are observed from the above eight figures. First, for all the polyphase signals with *CPP* =1 (Figures 47, 48, 51 and 52), the P2 codes have negative slope, which is different from other polyphase signals. Secondly, for the WD analysis, when *CPP* =1 (Figures 47, 48, 51 and 52), the P1 code is the most difficult to determine the 3 dB bandwidth as well as the code period. On the contrary, the P3 and P4 code can provide very clear parameters in Figure 48 and 52. Thirdly, when comparing with all the zoom in figures (Figures 48, 50, 52 and 54), the P3 code and the P4 code have the best parameter resolution among the five polyphase signals.

THIS PAGE INTENTIONALLY LEFT BLANK

VI. COSTAS FREQUENCY HOPPING

A. COSTAS

A Costas array is an $n \times n$ array of frequencies and times with exactly one frequency in each row and column, and with distinct vector differences between all pairs of frequencies. As a frequency-hopping pattern for radar or sonar, a Costas array has an optimum ambiguity function, since any translation of the array parallel to the coordinate axes produces at most one out of phase coincidence. [Ref. 21]

In a frequency hopping system, the signal consists of one or more frequencies being chosen from a set $\{f_1, f_2, ...f_m\}$ of available frequencies, for transmission at each of a set $\{t_1, t_2, ...t_n\}$ of consecutive time intervals. For modeling purposes, it is reasonable to consider the situation in which $m = n$, and a different one of n equally spaced frequencies $\{f_1, f_2, ...f_n\}$ is transmitted during each of the n equal duration time intervals $\{t_1, t_2, ...t_n\}$. Such a signal is represented by a $n \times n$ permutation matrix A, where the n rows correspond to the n frequencies, the n columns correspond to the n intervals, and the entry a_{ij} equals 1 means transmission and 0 otherwise.

For example if the coding sequence $\{a_j\}$ is {4,7,1,6,5,2,3,}, then the coding matrix, the difference matrix and the ambiguity sidelobe matrix of a Costas signal are shown as follows. [Ref. 22]

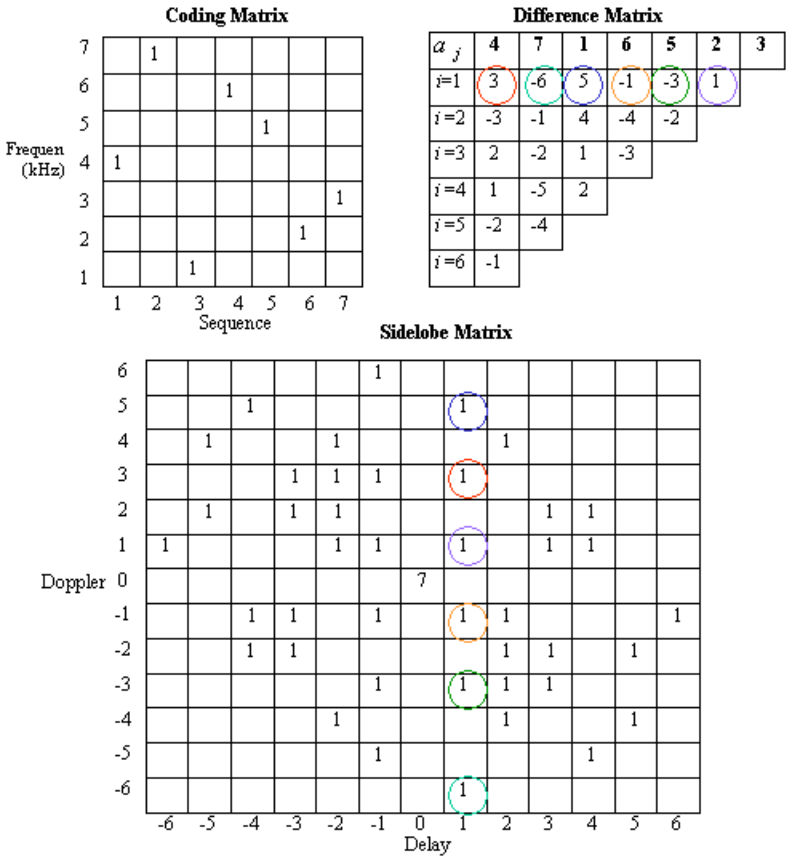

Figure 55. The Coding Matrix, Difference Matrix and Ambiguity Sidelobe Matrix of a Costas Signal.

The element of the difference matrix in row i and column j, is

$$D_{i,j} = a_{i+j} - a_j, \qquad i + j \le N \tag{6.1}$$

with blanks at the remaining locations. Thus the first row is formed by taking differences between adjacent terms in the sequence, the second row by taking differences between next adjacent terms, and so on. The corresponding values in the difference matrix and sidelobe matrix were marker with different color circles. [Ref. 22]

The difference matrix not only determines whether a sequence is Costas or not, but it also identifies the major sidelobe locations in the positive delay slots of the

ambiguity function. The sidelobes in the negative delay slots are obtained by applying the rule of symmetry with respect with the origin. [Ref. 22]

Twelve Costas signals are introduced in this chapter. They are numbered from 85 to 96 and listed in Table 17. The "Sequence" means the frequency hopping sequence. There are two different sequences used in this table. They are the carrier frequency in order of the number in the sequence. The unit of these carrier frequencies is kHz. The "Cycles/ Frequency" means the number of cycles per frequency, the number 10 and 20 are used here. The sampling frequency for these Costas signals is 15kHz for sequence 4716523 and 17kHz for sequence 2638751.

No.	COSTAS	Sequence	Cycles/Frequency	SNR
85	C_1_15_10_s	4716523	10	Signal Only
86	C_1_15_10_0	4716523	10	0 dB
87	C_1_15_10_-6	4716523	10	-6 dB
88	C_1_15_20_s	4716523	20	Signal Only
89	C_1_15_20_0	4716523	20	0 dB
90	C_1_15_20_-6	4716523	20	-6 dB
91	C_2_17_10_s	2638751	10	Signal Only
92	C_2_17_10_0	2638751	10	0 dB
93	C_2_17_10_-6	2638751	10	-6 dB
94	C_2_17_20_s	2638751	20	Signal Only
95	C_2_17_20_0	2638751	20	0 dB
96	C_2_17_20_-6	2638751	20	-6 dB

Table 17. COSTAS Signals.

B. WIGNER DISTRIBUTION FOR COSTAS

Consider the same twelve Costas frequency-hopping signals in Table 17 and use them as the inputs for Wigner Distribution (WD). The WD results of signals number 85, 88, 91, 94 are showed in Figures 56 to 59. The mesh plots show the frequency domain of the Costas frequency-hopping signals after WD. The contour plots show both the frequency domain and time domain of the results.

First, the seven carrier frequencies and the entire cross terms are shown in every figure. Since the carrier frequencies are 1kHz, 2kHz, 3kHz, 4kHz, 5kHz, 6kHz and 7kHz, the cross terms will be

$$\frac{1}{2}\{(1+2),(1+3),(1+4),(1+5),(1+6),(1+7)$$
$$,(2+3),(2+4),(2+5),(2+6),(2+7)$$
$$,(3+4),(3+5),(3+6),(3+7)$$
$$,(4+5),(4+6),(4+7)$$
$$,(5+6),(5+7)$$
$$,(6+7)\} \text{ kHz}$$

From the above calculation, the cross terms appear at 1.5 kHz one time, 2 kHz one time, 2.5 kHz two times, 3 kHz two times, 3.5 kHz three times, 4 kHz three times, 4.5 kHz three times, 5 kHz two times, 5.5 kHz two times, 6 kHz one time, 6.5 kHz one time. In Figure 349 to 360, only the 1kHz and 7kHz are real carrier frequencies, all the others are possibly carrier frequencies or cross terms.

Secondly, in Figure 56(b) to 59(b) there marked with the blue arrows, which indicate the frequency sequence from the top to the bottom. Take Figure 56(b) as an example, the carrier frequency sequence is, as the blue arrows shown from the top to the bottom, $4kHz \to 7kHz \to 1kHz \to 6kHz \to 5kHz \to 2kHz \to 3kHz$.

As can be seen, the colors of carrier frequencies and cross terms in Figure 57(b) are different. The color of the cross terms is red line enclosed by yellow, but the real carrier frequencies display different color and shapes. They are yellow circles with green curves on the right and left hand sides. According to Figure 10, the frequency of the cross terms is half of the two real carrier frequencies. The time period of the cross terms is also half of the time period sum of the two real carrier frequencies.

Taking a look of the 4kHz in Figure 57(b), there are four 4kHz bars on this plot. From the top to the bottom, the first yellow bar is the real carrier frequency. The second red bar is a cross term caused by 7kHz and 1kHz, the appearing time period is right on the center of those of in 7kHz and 1kHz. The third red bar is a cross term caused by 6kHz and 2kHz, and with time period in the center of those in 6kHz and 2kHz. The forth red bar is a cross term caused by 5kHz and 3kHz with time period in the center of those in 5kHz and 3kHz. Note there are two 3kHz red bars in Figure 57(b). The first is caused by 4kHz and 2kHz carrier frequencies, the second one is caused by 1kHz and 5kHz carrier frequencies. Another 3kHz yellow bar is a real carrier frequency. Figure 58 and Figure 59 show another sequence, the carrier frequencies are also examined in the figures.

In these figures the time scale depends on the sampling frequency and the number of sample points. The total time is $\frac{\#sample}{f_s}$, which can be used to determine the time in each frequency. Since the total sample number is too big to use the WD, in this chapter WD processes 350 points for Cycles/Frequency = 10 and 700 points for Cycles/Frequency = 20.

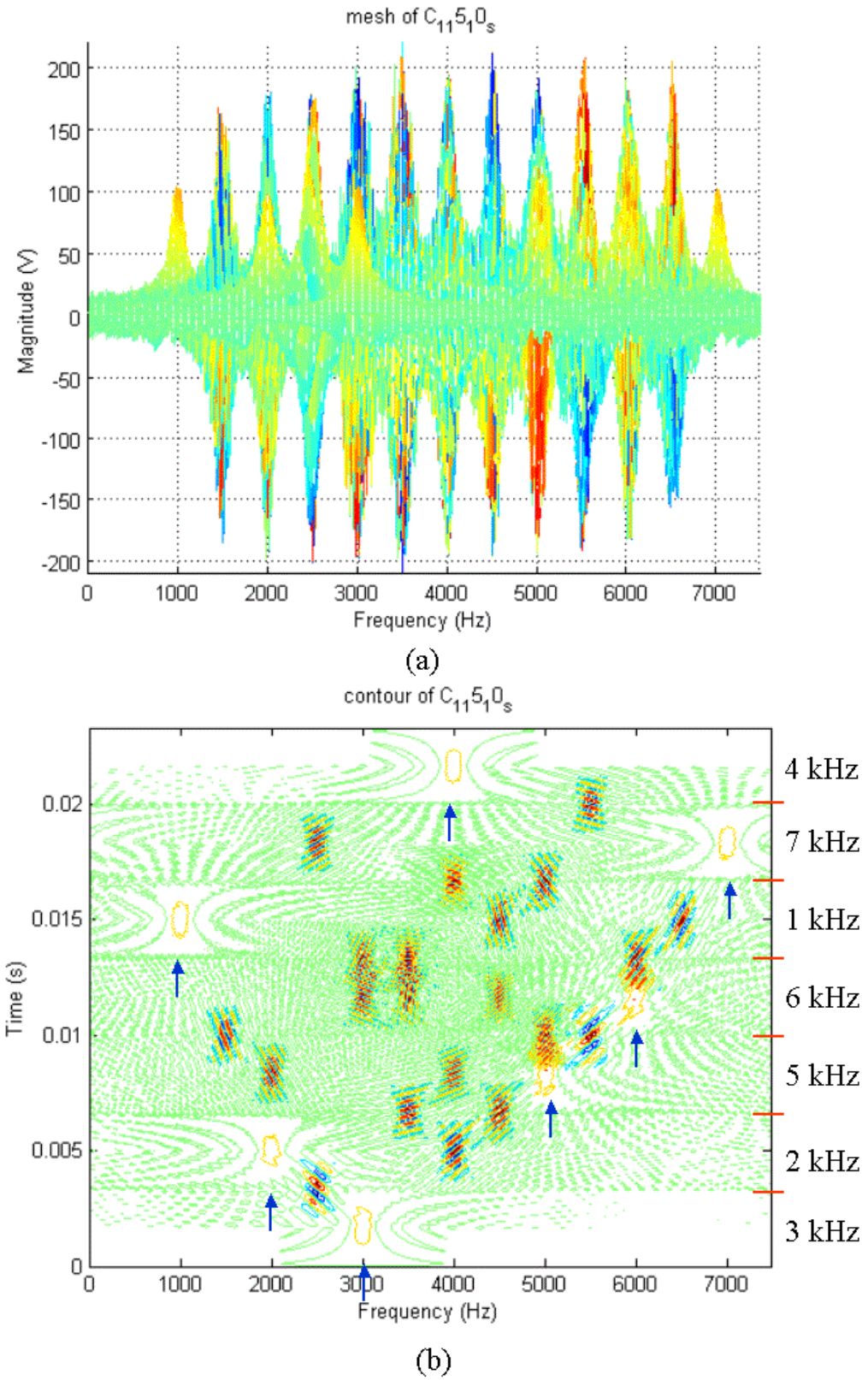

Figure 56. WD for COSTAS Frequency Hopping, Signal Only, (No.85) (a) 2D Mesh in Frequency Domain. (b) Contour.

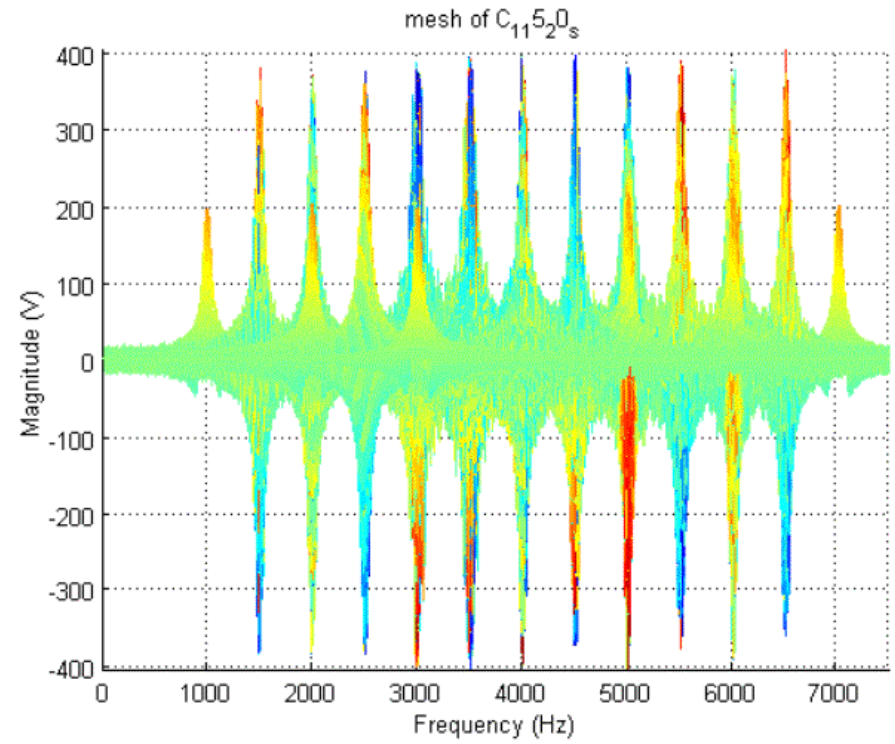

(a)

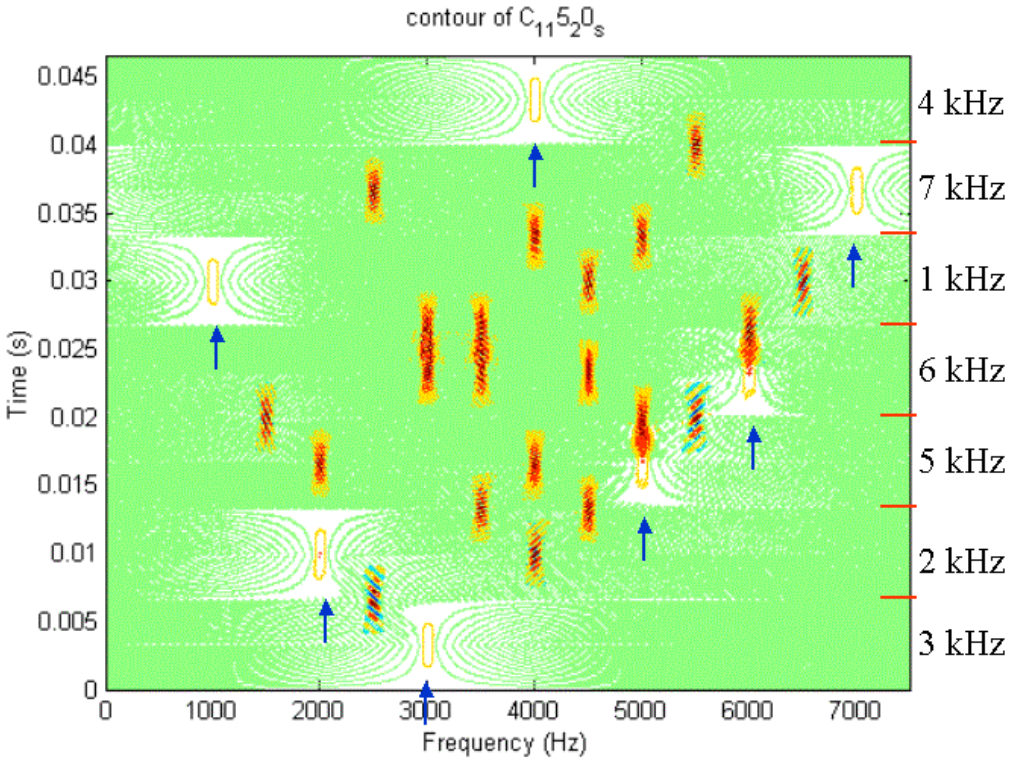

(b)

Figure 57. WD for COSTAS Frequency Hopping, Signal Only, (No.88) (a) 2D Mesh in Frequency Domain. (b) Contour.

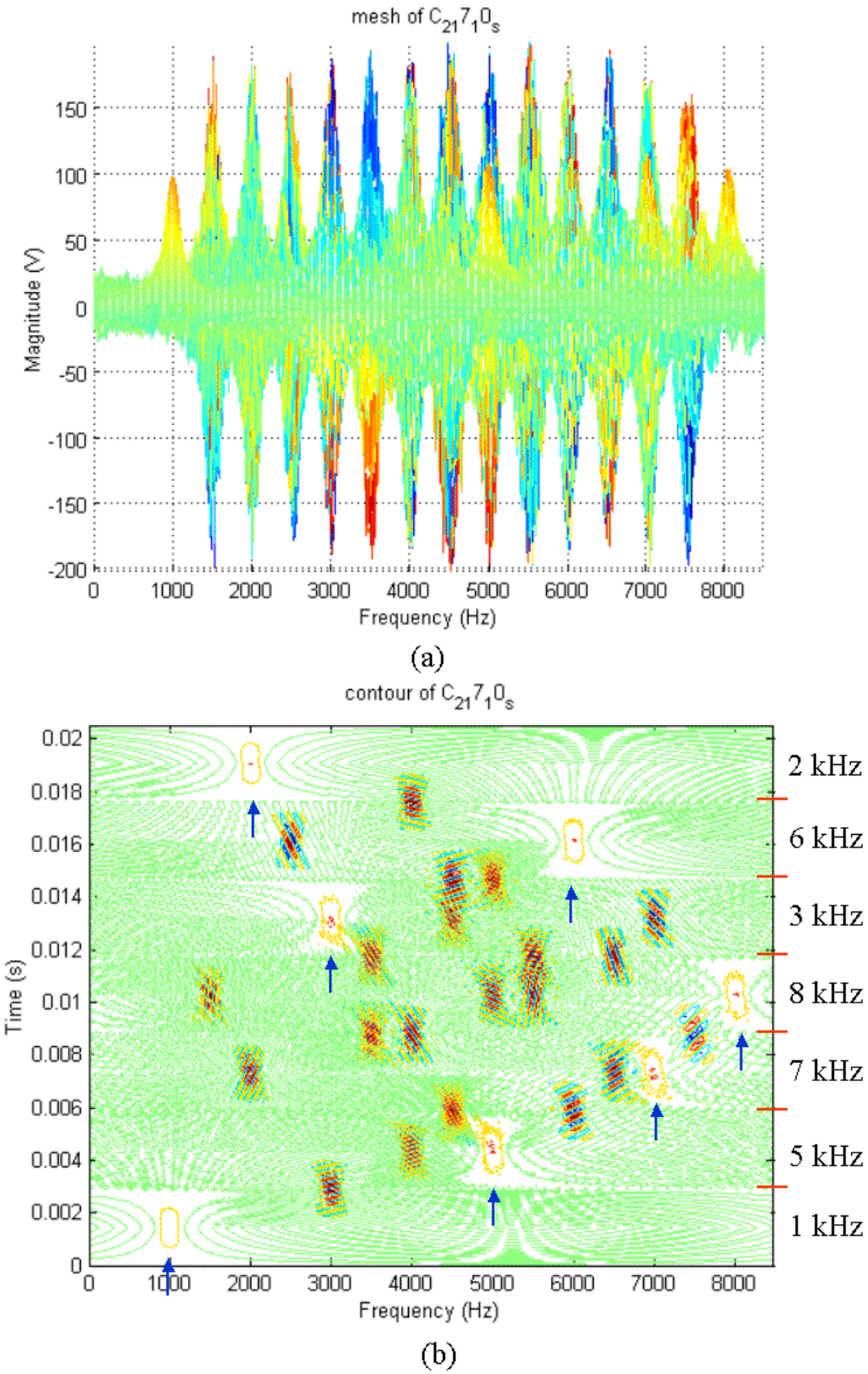

Figure 58. WD for COSTAS Frequency Hopping, Signal Only, (No.91) (a) 2D Mesh in Frequency Domain. (b) Contour.

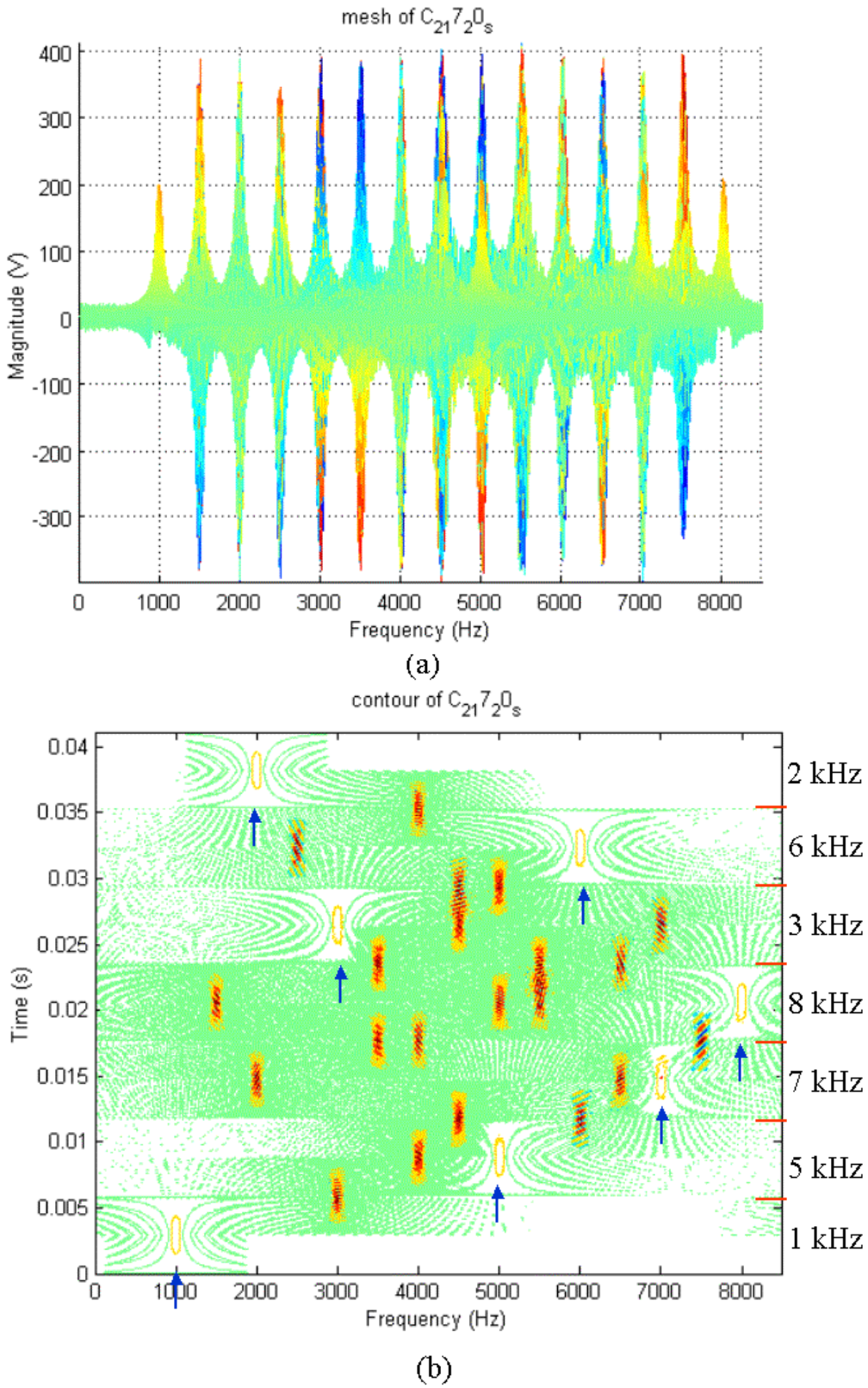

Figure 59. WD for COSTAS Frequency Hopping, Signal Only, (No.94) (a) 2D Mesh in Frequency Domain. (b) Contour.

C. SUMMARY

To analyze a signal using Wigner distribution, the cross terms are unavoidable for multi-frequencies as well as frequency-hopping signals, like Costas. The cross terms have the same magnitude as the real carrier frequencies. The frequency of any cross term is half of the sum of any two real carrier frequencies. For example, if f_{c1} and f_{c2} are real carrier frequencies, then the cross term generated by these two frequencies is $\frac{f_{c1}+f_{c2}}{2}$.

Both real carrier frequencies and cross term exist in the mesh plots and contour plots. Fortunately, the contour plots still can see the sequence of the Costas frequency hopping signals. As long as the carrier frequencies and their sequence have been found, then the COSTAS frequency hopping signals can be recovered.

Table 18 below shows the detection effectiveness of the carrier frequency sequence, the time in each sequence and the code period from Figure 56 to 59. They are done by the visible inspection of the WD results.

COSTAS			
No.	Sequence	Time in Each Frequency	Code Period
85	100%	100%	100%
86	80%	50%	50%
87	0%	0%	0%
88	100%	100%	100%
89	80%	70%	70%
90	0%	0%	0%
91	100%	100%	100%
92	80%	50%	50%
93	0%	0%	0%
94	100%	100%	100%
95	80%	70%	70%
96	0%	0%	0%

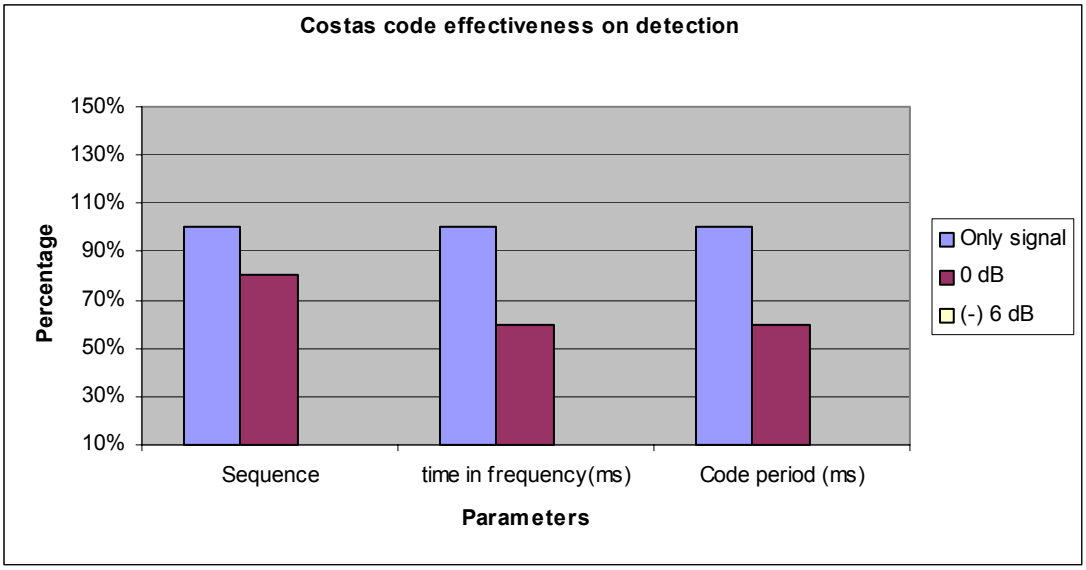

Table 18. WD Detection Effectiveness for COSTAS Code Signals.

THIS PAGE INTENTIONALLY LEFT BLANK

VII. PHASE SHIFT KEYING/FREQUENCY SHIFT KEYING (PSK/FSK)

A. PSK/FSK USING A COSTAS-BASED FREQUENCY-HOPPING TECHNIQUE

The PSK/FSK using Costas modulation technique is the result of a combination of frequency-shift keying based on a Costas frequency-hopping matrix and phase-shift keying using Barker sequences with different lengths. Here will briefly describe the phase encoding applied to a Costas signal, generating the FSK/PSK combined waveform.

Consider a Costas frequency-hopped signal, the firing order defines which frequencies will appear and with which duration. For CW radars, the usual terminology does not apply to this case. Instead of a "burst" of pulses, frequencies have being continuously emitted during a defined period of time. This period may be divided into sub-periods, labeled T_F for each frequency. The length of each sub-period depends on the sampling interval. During each sub-period, as the signal stays in one of the frequencies, a binary phase modulation occurs according to a Barker sequence of length five (+ + + - +), seven (+ + + - - + -), eleven (+ + + - - - + - - + -) or thirteen (+ + + + + + - - + + - + - +). [Ref. 23]

For example, the FSK/PSK signal defined by: S = {1^+, 1^+, 1^+, 1^-, 1^+, 2^+, 2^+, 2^+, 2^-, 2^+, 3^+, 3^+, 3^+, 3^-, 3^+, 4^+, 4^+, 4^+, 4^-, 4^+, 5^+, 5^+, 5^+, 5^-, 5^+ } represents a waveform comprised of five different frequencies, which are each subdivided into five phase slots, labeled T_P, according to the Barker sequence of length five (+ + + - +).

The final waveform may be seen as a binary phase-shifting modulation within each frequency hop, resulting in 25 phase slots equally distributed in each frequency.

If consider N_F as the number of frequency hops and N_P as the number of phase slots of duration T_P in each frequency sub-period T_F, the total number of phase slots in the FSK/PSK waveform is given by: $N = N_F \cdot N_P$. [Ref. 23]

The Barker sequence is generated and the frequency-hopping signal is then phase-modulated accordingly. For example, if the first Costas sequence is selected, after a phase modulation using a Barker sequence of length 5, the final waveform becomes:

S = 4^+, 4^+, 4^+, 4^-, 4^+, 7^+, 7^+, 7^+, 7^-, 7^+, 1^+, 1^+, 1^+, 1^-, 1^+, 6^+, 6^+, 6^+, 6^-, 6^+, 5^+, 5^+, 5^+, 5^-, 5^+, 2^+, 2^+, 2^+, 2^-, 2^+, 3^+, 3^+, 3^+, 3^-, 3^+ [Ref. 23]

B. FSK/ PSK COMBINED USING A TARGET-MATCHED FREQUENCY HOPPING

Instead of spreading the energy of the signal equally over a broad bandwidth, this type of technique concentrates the signal energy in specific spectral locations of most importance for the radar and its typical targets, within the broad-spectrum bandwidth. The produced signals have a pulse compression characteristic, and therefore they can achieve a low probability of intercept.

The implementation starts with a simulated-target time-radar response. This data is the Fourier transformed, the frequency components, their correspondent magnitudes, and their initial phases. A random selection process chooses each frequency with a probability distribution function defined by the spectral characteristics of the target of interest obtained from the Fast Fourier Transform so that frequencies at the spectral peaks

of the target (highest magnitudes) are transmitted more often. Each "frequency hop," transmitted during a specific period of time, is also modulated in phase, having its initial phase value modified by a pseudo-random spreading-phase sequence code of values equally likely to be zero or π radians.

The matched FSK/PSK radar will then use a correlation receiver with a phase mismatched reference signal instead of a perfectly phase matched reference. This allows the radar to generate signals that can match a target's spectral response in both magnitude and phase.

This simulation serves the purpose of testing the performance of a new digital cyclostationary receiver against these kinds of signals. A better implementation would require an iterative solution since the response of a target is not always known beforehand. [Ref. 23]

C. PSK/FSK AND TEST SIGNALS PAF AND PSD ANALYSIS

Eight PSK/FSK COSTAS, eight PSK/FSK target and two single carrier frequency signals are introduced in this chapter. They are numbered from 97 to 114 and listed in Table 19. The "Sequence" means the frequency hopping sequence. The numbers in the sequence are the order of the carrier frequencies. The unit of these carrier frequencies is kHz. The "Cycles/ Phase" means the number of cycles per phase, the number 1, 5 and 10 are used here. The sampling frequency is 15kHz for these PSK/FSK signals, 7kHz for the two test signals.

No.	FSK/PSK COSTAS	Sequence	Barker Code Length	Cycles/ Phase	SNR
97	FSK_PSK_C_1_15_5_5_s	4716523	5	5	Signal Only
98	FSK_PSK_C_1_15_5_5_0	4716523	5	5	0 dB
99	FSK_PSK_C_1_15_5_1_s	4716523	5	1	Signal Only
100	FSK_PSK_C_1_15_5_1_0	4716523	5	1	0 dB
101	FSK_PSK_C_1_15_11_5_s	4716523	11	5	Signal Only
102	FSK_PSK_C_1_15_11_5_0	4716523	11	5	0 dB
103	FSK_PSK_C_1_15_11_1_s	4716523	11	1	Signal Only
104	FSK_PSK_C_1_15_11_1_0	4716523	11	1	0 dB

No.	FSK/PSK Target	Sequence	Random Hops	Cycles/ Phase	SNR
105	FSK_PSK_T_15_128_5_s	1	128	5	Signal Only
106	FSK_PSK_T_15_128_5_0	1	128	5	0 dB
107	FSK_PSK_T_15_256_5_s	1	256	5	Signal Only
108	FSK_PSK_T_15_256_5_0	1	256	5	0 dB
109	FSK_PSK_T_15_128_10_s	2	128	10	Signal Only
110	FSK_PSK_T_15_128_10_0	2	128	10	0 dB
111	FSK_PSK_T_15_256_10_s	2	256	10	Signal Only
112	FSK_PSK_T_15_256_10_0	2	256	10	0 dB

No.	Test Signal	f_c (kHz)	f_s (kHz)	SNR
113	T_1_7_1_s	1	7	Signal Only
114	T_2_7_1_s	1 and 2	7	Signal Only

Table 19. FSK/PSK and Test Signals.

D. WIGNER DISTRIBUTION FOR PSK/FSK AND TEST SIGNALS

Consider the same eight PSK/FSK COSTAS, eight PSK/FSK target and two single carrier frequency signals introduced in Table 19 and use them as the inputs for Wigner Distribution (WD). The WD results of these twelve signals are showed in Figure 60 to 67. The mesh plots show the frequency domain of these signals after WD. The contour plots show both the frequency domain and time domain of the results.

The following figures for the PSK/FSK COSTAS signals are very similar to the figures of COSTAS signals. Comparing with Figure 60(b) and Figure 56(b) and 57(b),

the Wigner distribution analysis gets very similar results for the PSK/FSK COSTAS signals and COSTAS signals. The carrier frequencies sequence, 4716523, can be seen as yellow circles and the frequency cross terms can be seen as red bars in Figure 60(b). As a matter of fact, no matter whether the 5 bits or 11 bits Barker code length, the time-frequency relationships are the same for the PSK/FSK COSTAS signals.

In Figure 61(b) and 63(b), the *CPP* is one, so the shape of the carrier frequencies are different from those with five cycles per phase in Figure 60(b) and 62(b). One can still distinguish the real carrier frequencies by the lighter colors.

Since the phase changes are by random, for the PSK/FSK target signals neither the carrier frequencies nor the cross terms can be examined on the mesh plots and contour plots. Figure 68 shows the one carrier frequency test signal. Figure 69 shows the two carrier frequencies and frequency cross term as described in Chapter II.

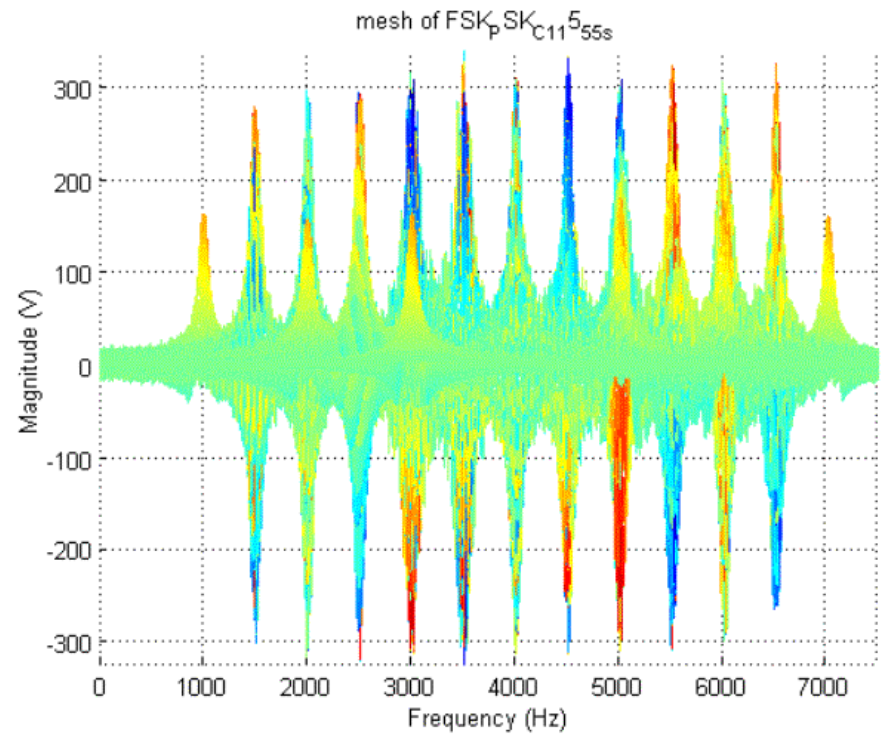

(a)

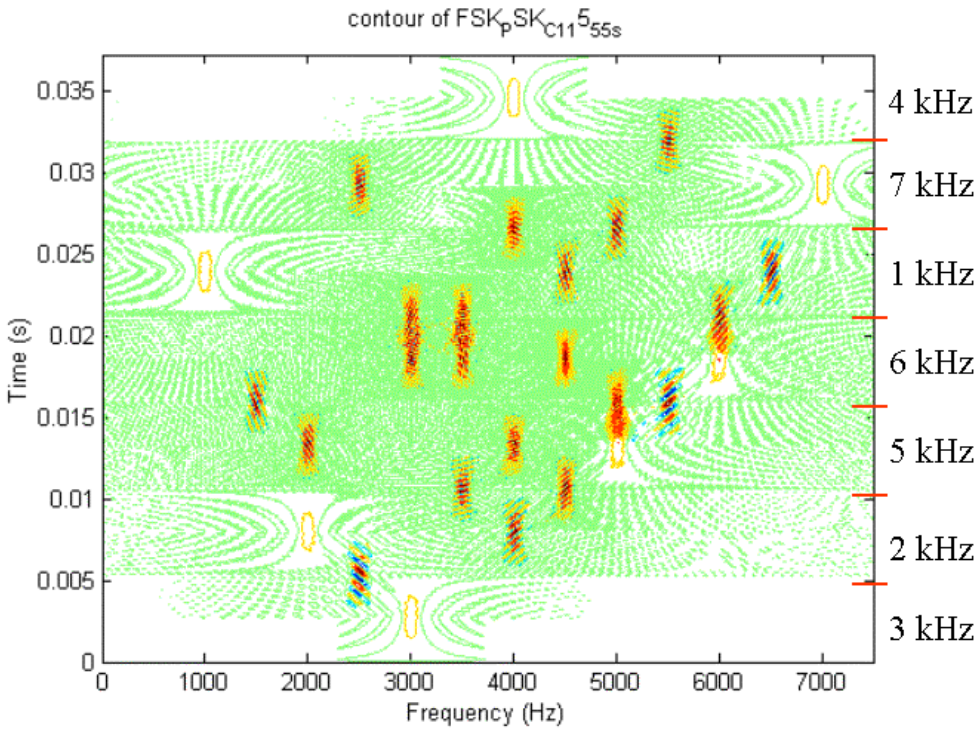

(b)

Figure 60. WD for FSK/PSK COSTAS with 5 bit Barker Code, CPP = 5, Signal Only, (No.97) (a) 2D Mesh in Frequency Domain. (b) Contour.

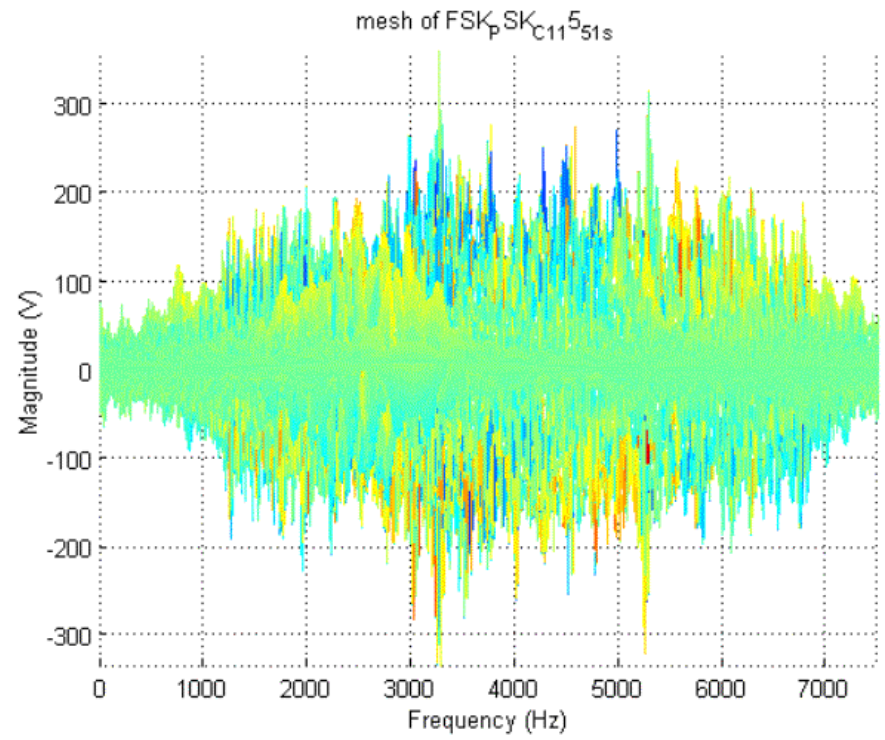

(a)

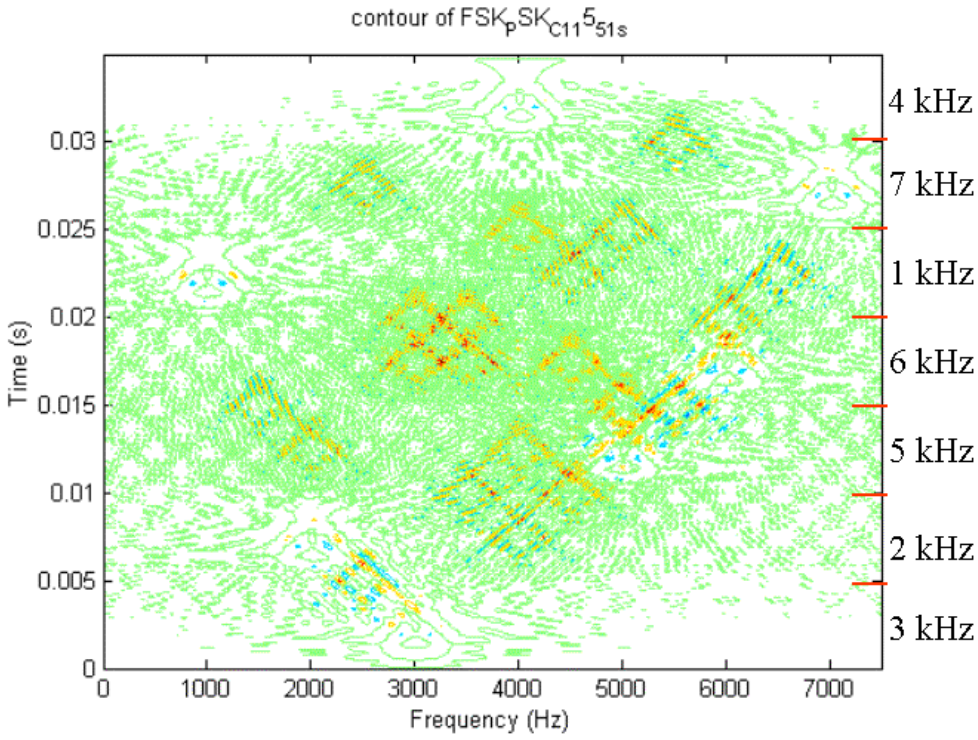

(b)

Figure 61. WD for FSK/PSK COSTAS with 5 bit Barker Code, CPP = 1, Signal Only, (No.99) (a) 2D Mesh in Frequency Domain. (b) Contour.

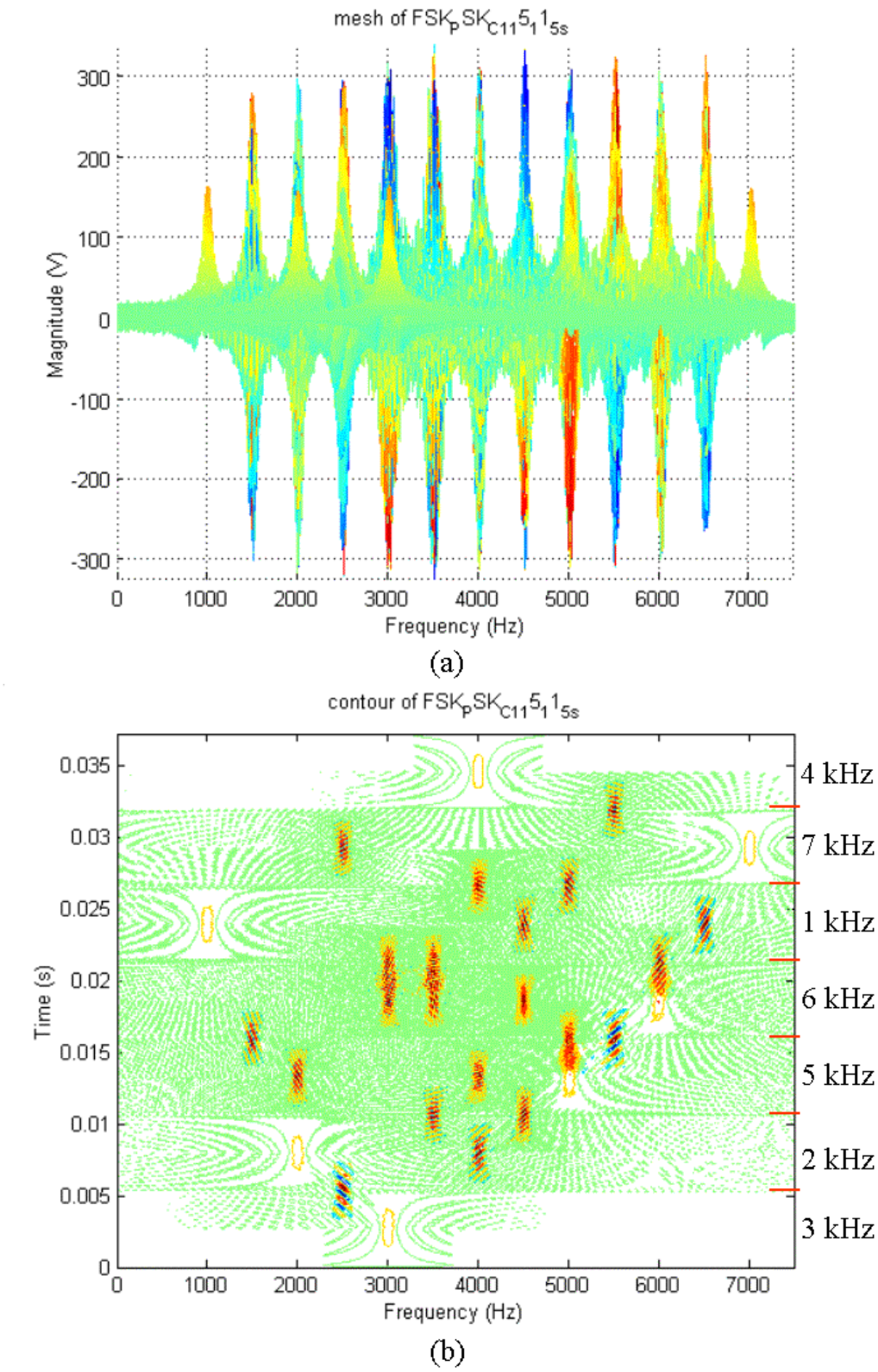

Figure 62. WD for FSK/PSK COSTAS with 11 bit Barker Code, CPP = 5, Signal Only, (No.101) (a) 2D Mesh in Frequency Domain. (b) Contour.

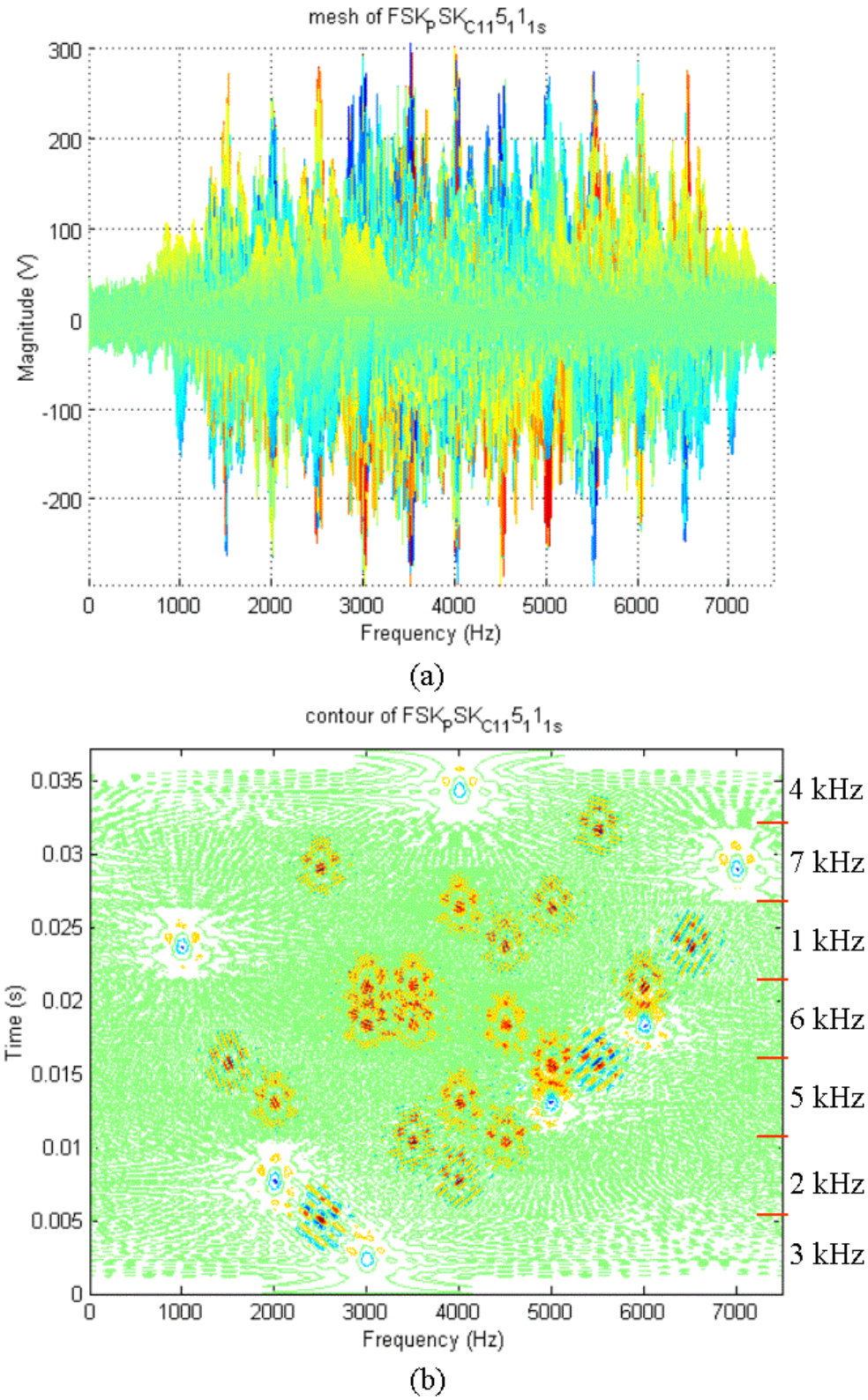

Figure 63. WD for FSK/PSK COSTAS with 11 bit Barker Code, CPP = 1, Signal Only, (No.103) (a) 2D Mesh in Frequency Domain. (b) Contour.

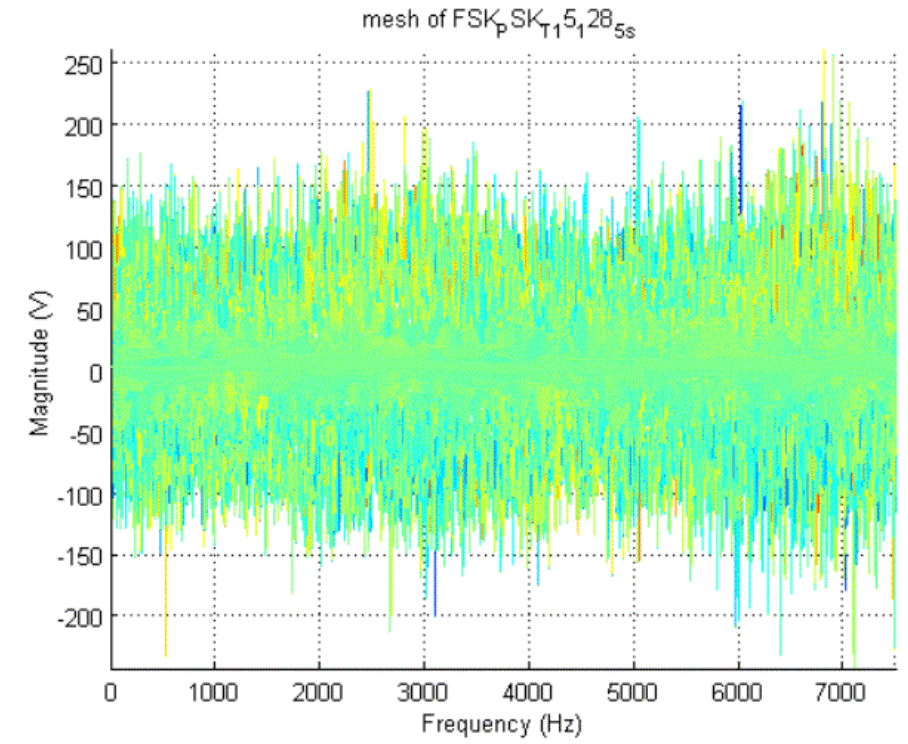

(a)

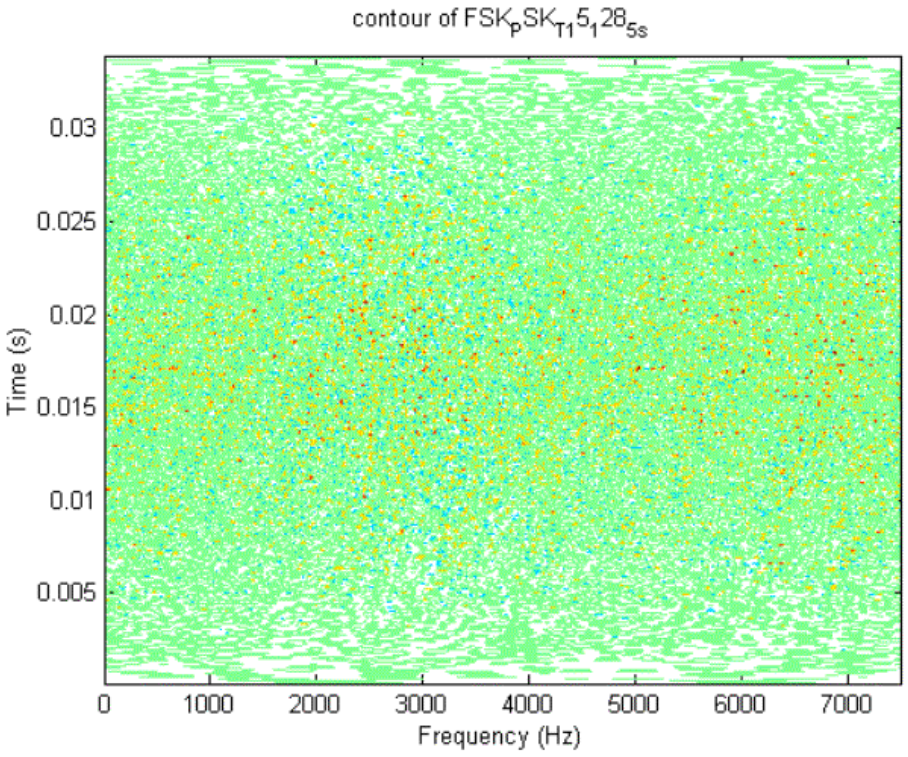

(b)

Figure 64. WD for FSK/PSK Target with 128 Random Hops, CPP = 5, Signal Only, (No.105) (a) 2D Mesh in Frequency Domain. (b) Contour.

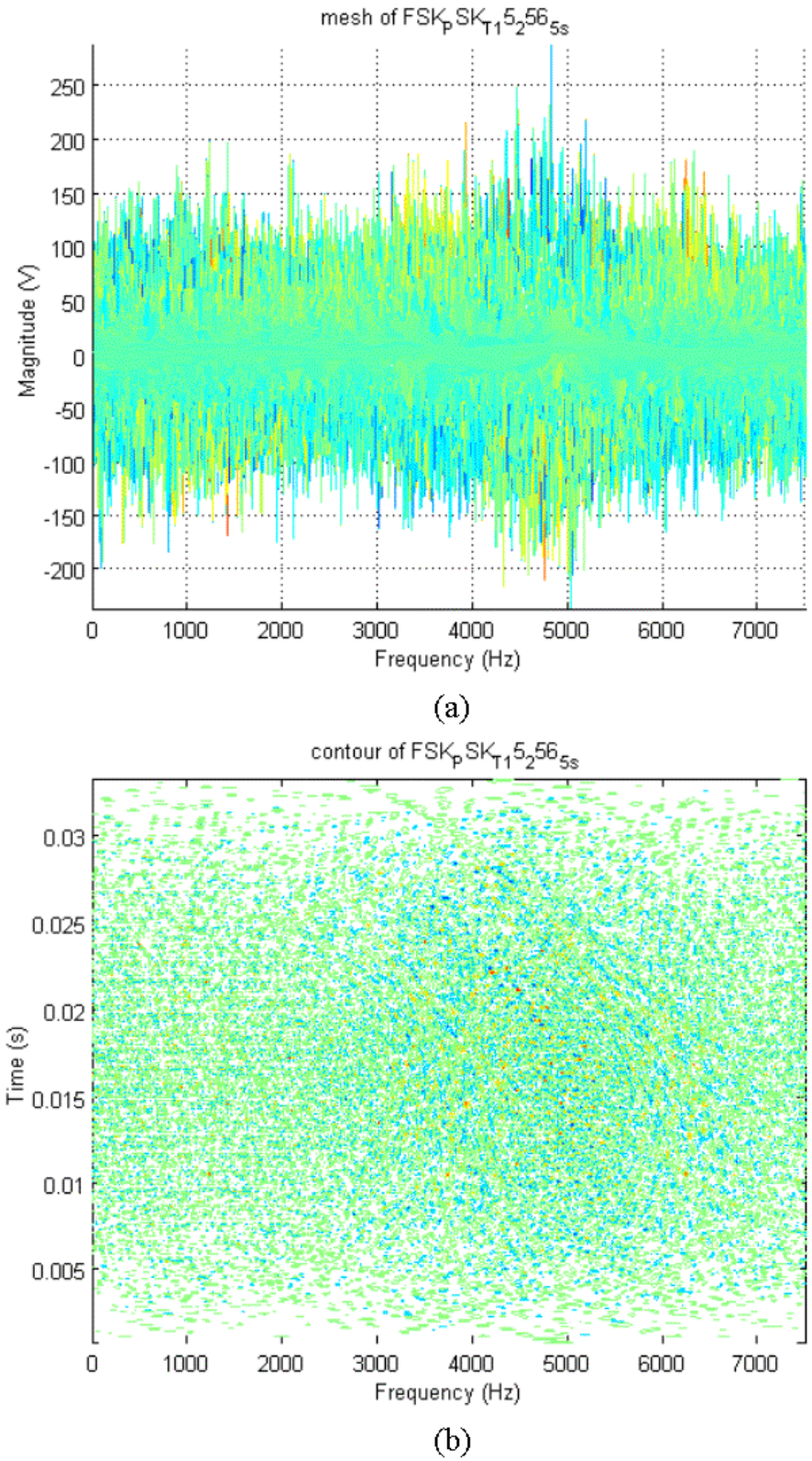

Figure 65. WD for FSK/PSK Target with 256 Random Hops, CPP = 5, Signal Only, (No.107) (a) 2D Mesh in Frequency Domain. (b) Contour.

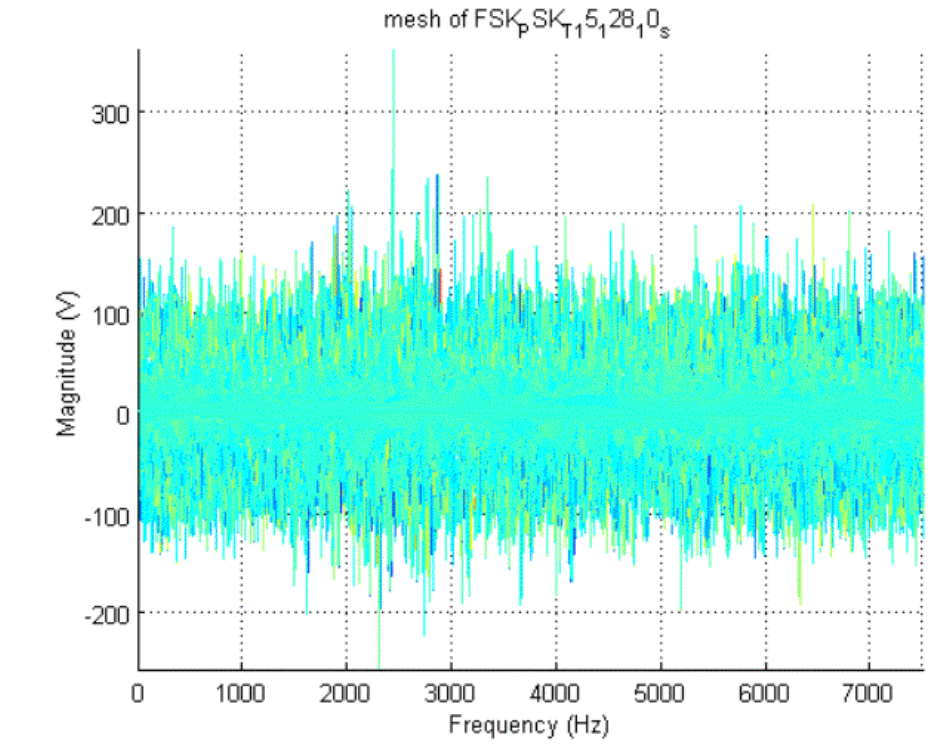

(a)

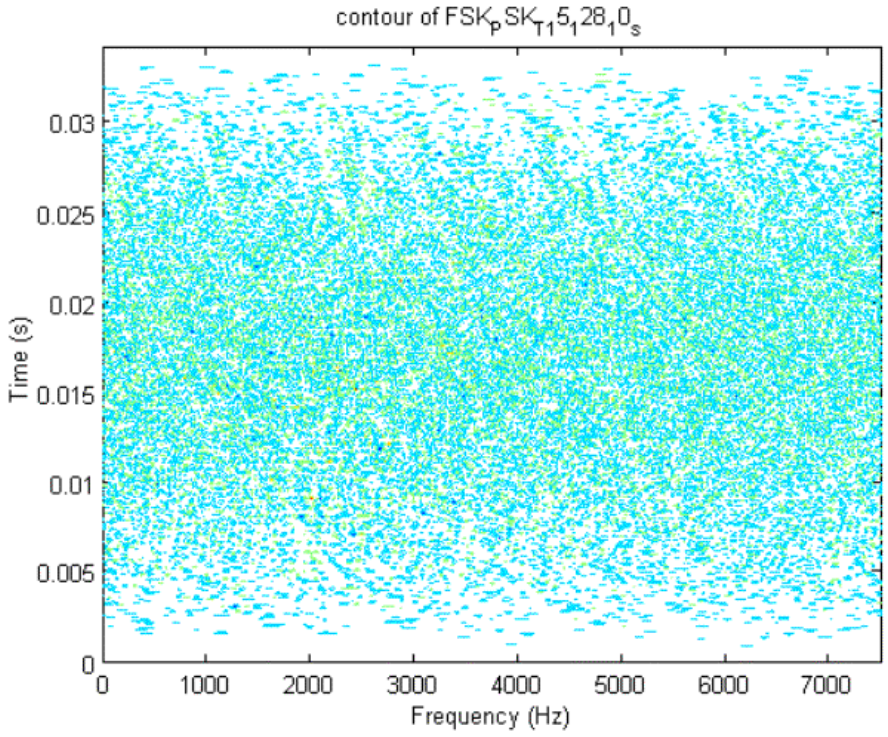

(b)

Figure 66. WD for FSK/PSK Target with 128 Random Hops, CPP = 10, Signal Only, (No.109) (a) 2D Mesh in Frequency Domain. (b) Contour.

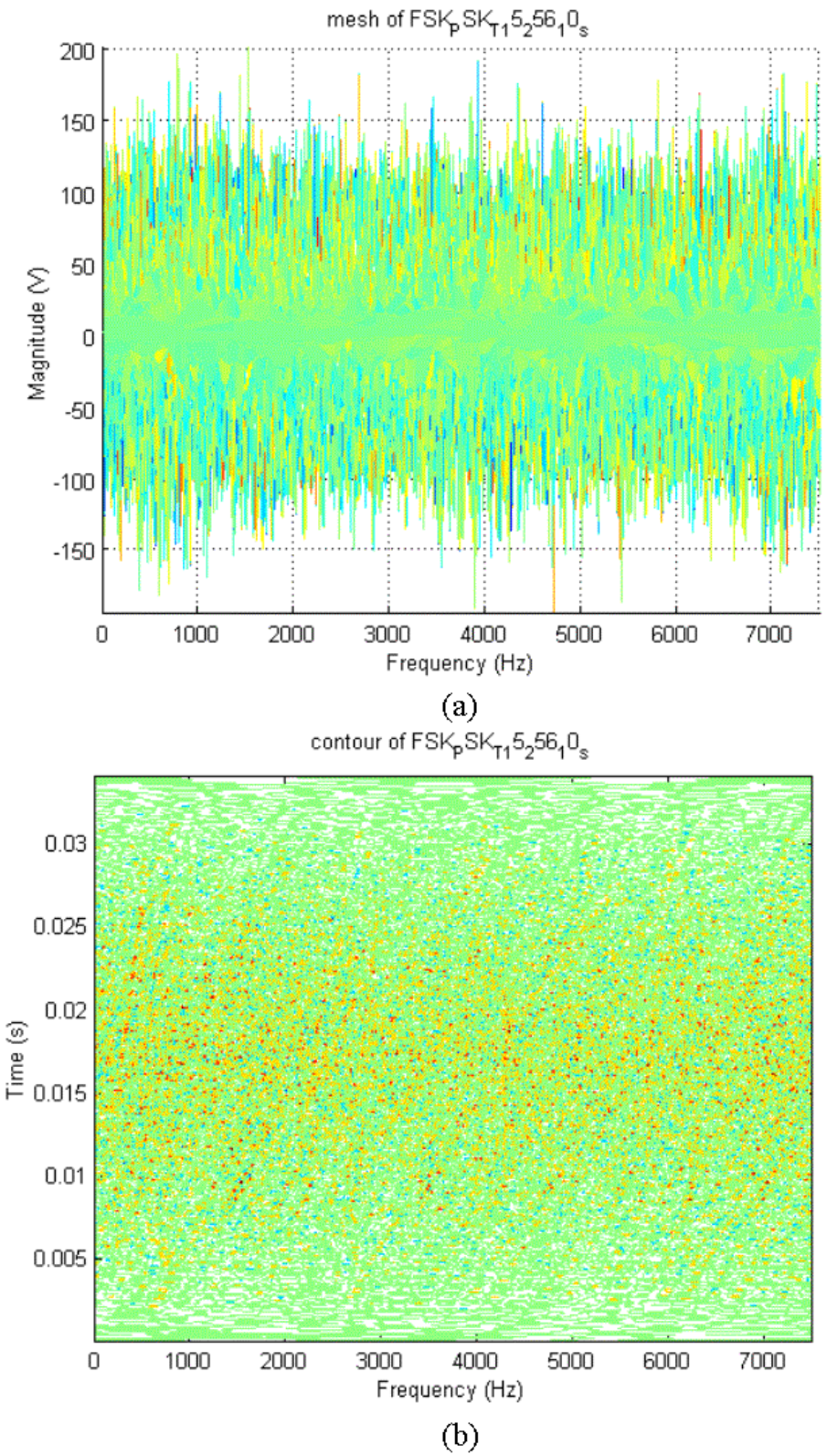

Figure 67. WD for FSK/PSK Target with 256 Random Hops, CPP = 10, Signal Only, (No.111) (a) 2D Mesh in Frequency Domain. (b) Contour.

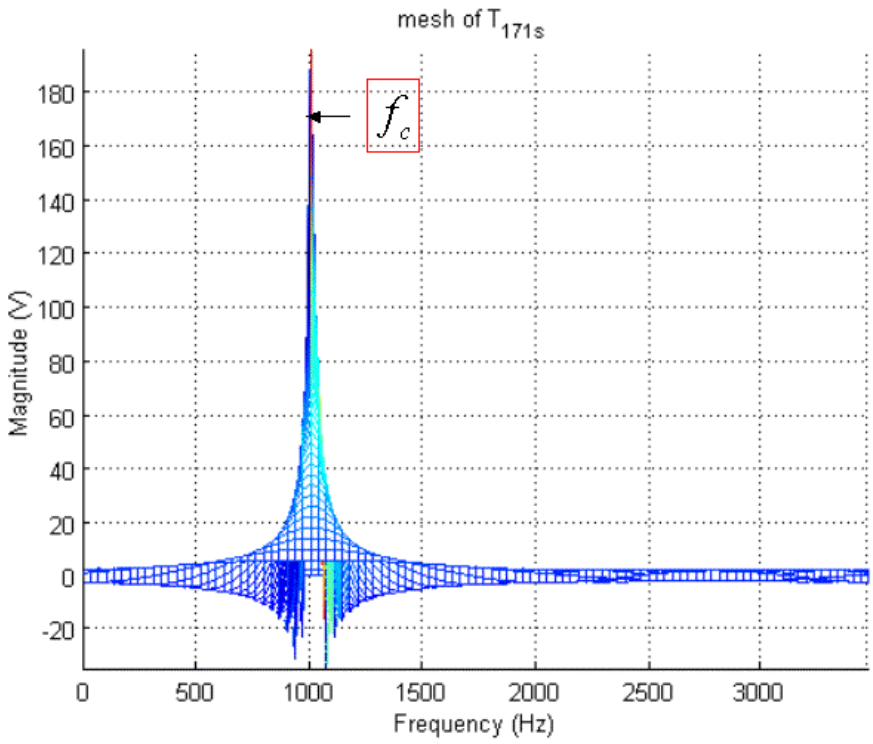

(a)

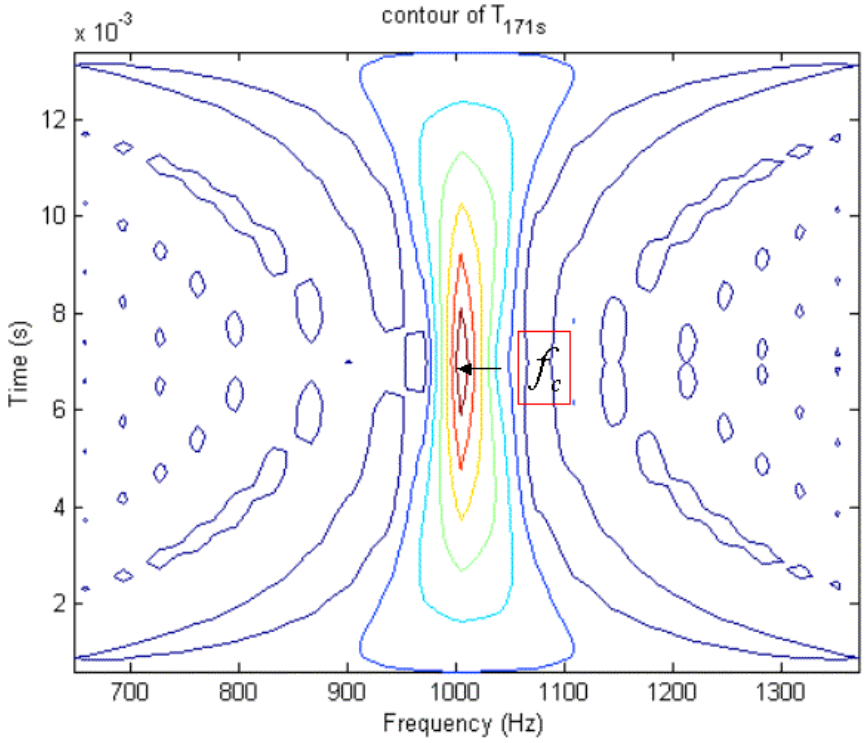

(b)

Figure 68. WD for 1 kHz Carrier Frequency Test Signal, (No.113) (a) 2D Mesh in Frequency Domain. (b) Contour.

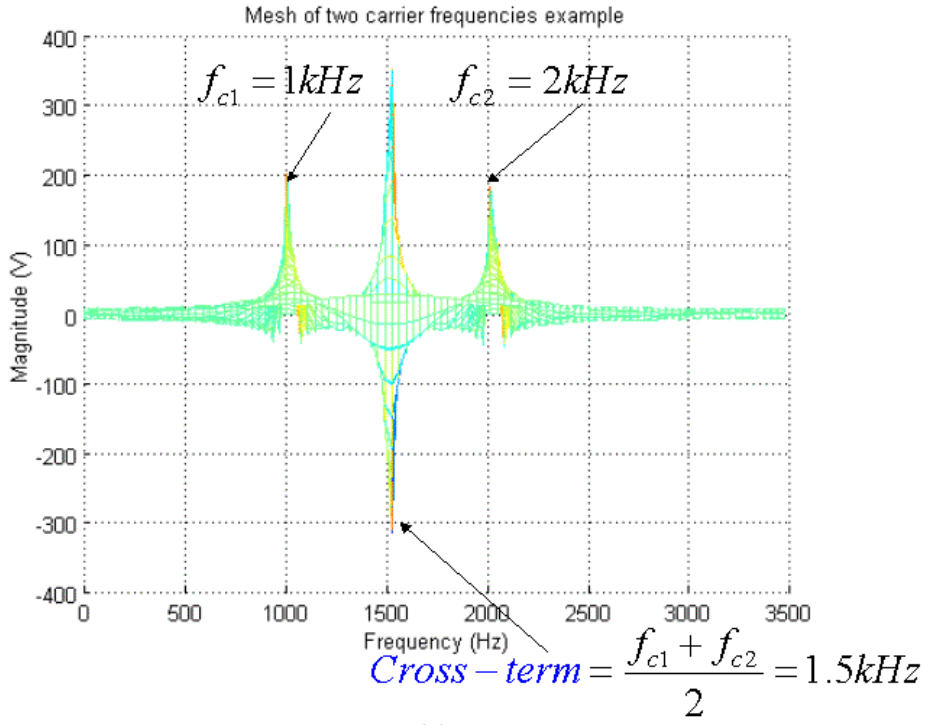

(a)

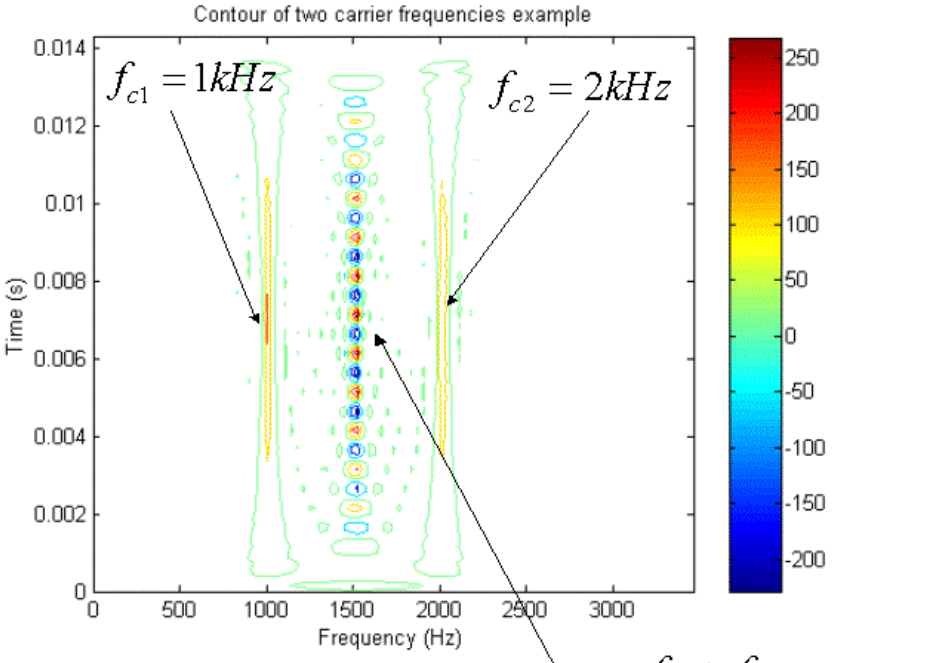

(b)

Figure 69. WD for 1kHz and 2 kHz Carrier Frequency Test Signal, (No.114) (a) 2D Mesh in Frequency Domain. (b) Contour.

E. SUMMARY

From the above Figures, only the PSK/FSK COSTAS signals and the last two test signals show the carrier frequencies or their sequence. Wigner Distribution cannot analyze the PSK/FSK target frequency hopping signals.

Table 20 below shows the detection effectiveness of the sequence, bandwidth, code period and phase from Figure 60 to 67.

FSK/PSK_COSTAS			
No.	Sequence	Bandwidth	Code Period
97	100%	100%	100%
98	50%	50%	50%
99	100%	100%	100%
100	50%	50%	50%
101	100%	100%	100%
102	50%	50%	50%
103	100%	100%	100%
104	50%	50%	50%
FSK/PSK_TARGET			
No.	Sequence	Bandwidth	Phase
105	0%	0%	0%
106	0%	0%	0%
107	0%	0%	0%
108	0%	0%	0%
109	0%	0%	0%
110	0%	0%	0%
111	0%	0%	0%
112	0%	0%	0%

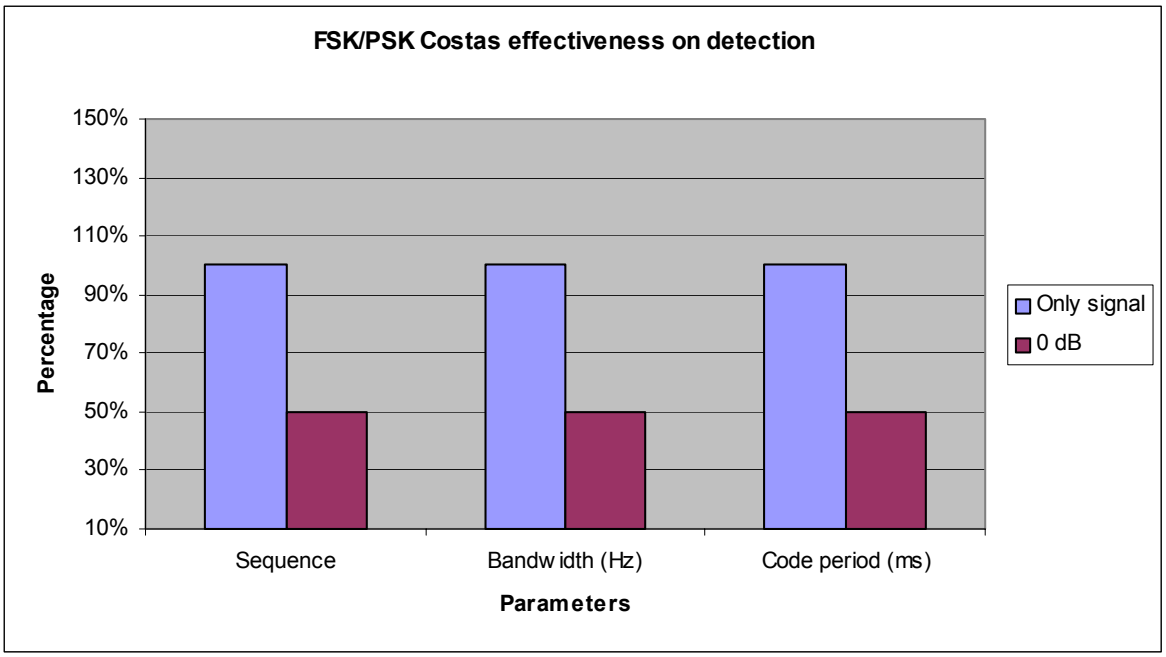

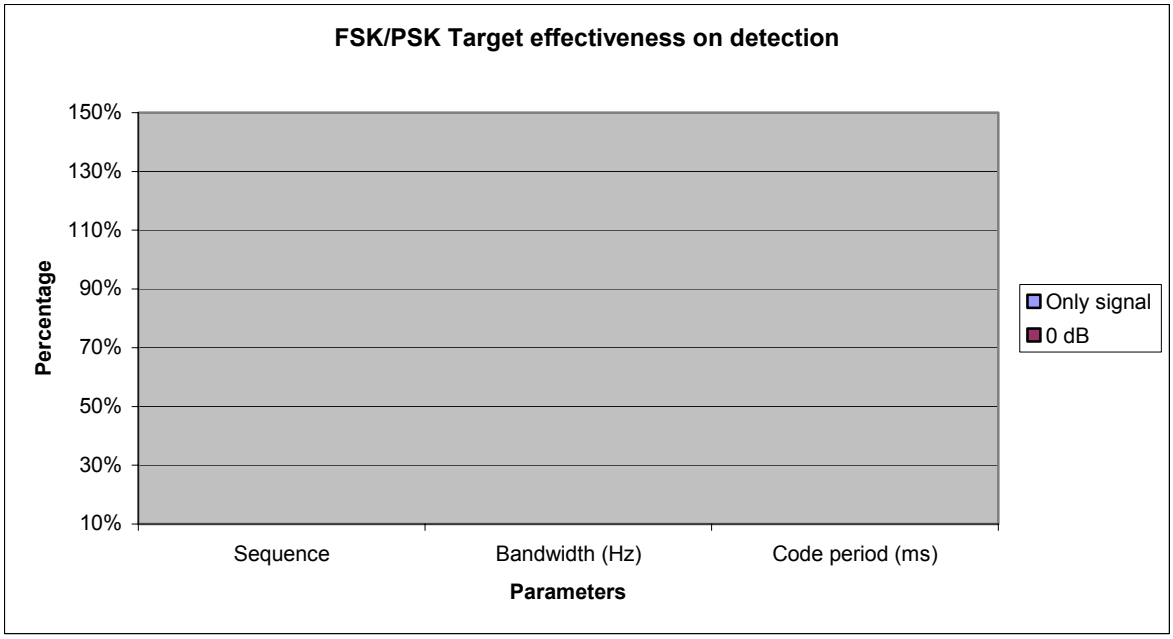

Table 20. WD Detection Effectiveness for FSK/PSK Signals.

THIS PAGE INTENTIONALLY LEFT BLANK

VIII. CONCLUSIONS AND RECOMMENDATIONS

A. CONCLUSIONS

Nine types of Low Probability of Intercept (LPI) signals were considered in this thesis. They are Binary Phase Shift Keying (BPSK), Frequency Modulation Continuous Wave (FMCW), Frank code, P1 code, P2 code, P3 code, P4 code, COSTAS frequency hopping and Phase Shift Keying/Frequency Shift Keying (PSK/FSK) signals. There are 114 signals were generated for Wigner distribution analysis in this thesis. The detail parameters of these 114 test signals are listed in Appendix B.

The Wigner distribution is a two-dimension function describing the frequency content of a signal as a function of time. The Wigner distribution has been noted as one of the more useful time-frequency analysis techniques for signal processing. Using the Wigner distribution one can identify the frequency and time changes in most of the LPI signals. This thesis successfully examined the nine types of LPI signals mentioned above. All the signal parameters excluding the PSK/FSK signals can be represented by Wigner distribution. For those detectable signals, some of them can show the parameters at both SNR = 0dB and -6 dB, some of them cannot be detected at SNR = -6dB. That is to say the signal to noise ratio is a main concern to the analysis of the LPI signals. Please see the technical report. [Ref. 7]

Other than the signal to noise ratio, there are some other important characteristics that need to be emphasized. For BPSK signals, the number of Barker bits can be displayed clearly only when the number of cycles per barker bit is one (*NPBB* = 1). For FMCW signals, the parameters can be displayed meaningfully when the modulation

period less than or equal to half of the sample points divided by sampling frequency ($t_m \le \frac{\#\text{sample}}{2f_s}$) and when the modulation bandwidth less than or equal to 2 times of carrier frequency ($\Delta F \le 2f_c$) or ($\Delta F \le 2(f_s/2 - f_c)$). For the poly phase signals including Frank codes, P1 codes, P2 codes, P3 codes and P4 codes, the phase length (*N* or N^2) can be obtained precisely when the number of cycles per phase is one (*CPP* = 1). The higher the *CPP*, the harder it is to get the right phase length.

Last, the frequency cross terms are irremovable for COSTAS frequency hopping signals or any other multi-carrier-frequency signal. The cross terms have the same amplitude as real carrier frequencies and their frequencies are the average of any two real carrier frequencies ($\frac{f_{c1} + f_{c2}}{2}$).

B. RECOMMENDATIONS

The Choi-Williams Distribution (CWD) is a time frequency analysis technique that evolved from Wigner Distribution (WD). The most important advantage of using the Choi-Williams distribution is that it has the ability to eliminate the frequency cross terms. The definition equation of the Choi-Williams Distribution was introduced in chapter I, but no experiments were examined in this thesis. The CWD is deserving of further study.

The output of the Wigner distribution is a real two-dimensional matrix with the size of length (*I*) times length (*Q*), where *I* and *Q* are the in-phase and the quadrature component of the input signal. The input signal in this thesis was defined as $x = I + j*Q$. If the length of *I* or *Q* is 10k points, then the size of the output matrix will be 100M points. In other words, the output matrix will occupy 800MB memory.

Thus, the bigger the input signal size, the better and more information will be shown in the mesh and contour plots. But the size of the output matrix is too great for MATLAB® processing on the computer used in this study; MATLAB® ran out of memory.

The specifications of the computer used to run the Wigner distribution MATLAB® program is Intel Pentium© 4 CPU with 2.0 GHz clock speed and 1 GB RAM. It is representative of the best in the personal computer market. Future Wigner distribution analysis obviously requires more capable computers.

THIS PAGE INTENTIONALLY LEFT BLANK

APPENDIX A. MATLAB CODE

A. WIGNERM.M

```
function [W] = wigner_fft(x)
% Design a variable W as the Wigner distribution function for
input signal x

% Paul Milne
% EC4700 Project in Naval Postgraduate School
% May 2001
%
% Modified by Jen-Yu, Gau
% Jan. 2002

N = length(x)/2;                    % Set 2N as the length of the
input signal x
odd = 0;                           % Initial the signal length as
even

if mod(2*N,2) ~= 0                % If the signal has odd length

  disp('WARNING: Input Sequence Odd:');
  disp('         A zero will be appended for calculations.');
  % Display warning messages

  x = [0 x];     % Add a zero at the beginning to make even length
  N = length(x)/2;       % Re-compute length 2N
  odd = 1;         % Mark the original input signal has odd length

end

M = 2*N-1             % Set M = 2N-1
a = -N;                 % Set a as integration down limit
b = N-1;                % Set b as integration up limit
y = x;                     % Set y as another name for the input
signal

for n = a:b             % Set index n from -N to N-1

  x = shiftz(y,n);      % Call function shiftz.m to shift the
 initial input signal x
  x1 = [x(1,N: M) 0 x(1,1:N-1)];
  x2 = [fliplr(x(1,1:N)) 0 fliplr(x(1,N+1: M))];

  % Compute the shifted signal x1 and x2 in order to get the
    kernel
 kern = x1.*conj(x2);     % Compute the kernel as in Eq(2.5)

  W(n-a+1,:) = fft(kern);

 % Apply the fast Fourier transform (FFT) algorithm of Matlab
command
end

W=2*real(W)     %Wigner distribution results are always real
 % The final result of the Wigner distribution as in Eq(2.13)

if odd        % If the original input signal has odd length
```

```
  % Then remove extra output created by the adding zero
  W = W(2:2*N,1:2*N-1);  % The final result becomes

end
```

B. SHIFTZ.M

```
function [y] = shift(x,n)
% The function is used to shift input signal x with n zeros to the
right and left
% in order to get the kernel as in Eq(2.5)
% When x length 2N, then n is from –N to N-1

% Paul Milne
% EC4700 Naval Postgraduate School
% May 2001
%
% Modified by Jen-Yu, Gau
% Jan. 2002

N = length(x)/2;      % Set 2N as the length of the input signal x

if n >= 0           % First shift the up half part of x
  y = [zeros(1,n) x(1:2*N-n)];    % Shift x to the right with n
zeros
else               % Then shift the down half part of x
  n = abs(n);
  y = [x(1+n:2*N) zeros(1,n)];
  % Shift x to the left with n zeros
end
```

APPENDIX B. TEST MATRIX

No.	BPSK	Barker Code Length	NPBB	SNR
1	B_1_7_7_1_s	7	1	Signal Only
2	B_1_7_7_1_0	7	1	0 dB
3	B_1_7_7_1_-6	7	1	-6 dB
4	B_1_7_11_1_s	11	1	Signal Only
5	B_1_7_11_1_0	11	1	0 dB
6	B_1_7_11_1_-6	11	1	-6 dB
7	B_1_7_7_5_s	7	5	Signal Only
8	B_1_7_7_5_0	7	5	0 dB
9	B_1_7_7_5_-6	7	5	-6 dB
10	B_1_7_11_5_s	11	5	Signal Only
11	B_1_7_11_5_0	11	5	0 dB
12	B_1_7_11_5_-6	11	5	-6 dB
	FMCW	**Mod. BW (Hz)**	**Mod. Period (ms)**	**SNR**
13	F_1_7_250_20_s	250	20	Signal Only
14	F_1_7_250_20_0	250	20	0 dB
15	F_1_7_250_20_-6	250	20	-6 dB
16	F_1_7_250_30_s	250	30	Signal Only
17	F_1_7_250_30_0	250	30	0 dB
18	F_1_7_250_30_-6	250	30	-6 dB
19	F_1_7_500_20_s	500	20	Signal Only
20	F_1_7_500_20_0	500	20	0 dB
21	F_1_7_500_20_-6	500	20	-6 dB
22	F_1_7_500_30_s	500	30	Signal Only
23	F_1_7_500_30_0	500	30	0 dB
24	F_1_7_500_30_-6	500	30	-6 dB
	FRANK	**N (Phase)**	**Cycles/Phase**	**SNR**
25	FR_1_7_4_1_s	4	1	Signal Only
26	FR_1_7_4_1_0	4	1	0 dB
27	FR_1_7_4_1_-6	4	1	-6 dB
28	FR_1_7_4_5_s	4	5	Signal Only
29	FR_1_7_4_5_0	4	5	0 dB
30	FR_1_7_4_5_-6	4	5	-6 dB
31	FR_1_7_8_1_s	8	1	Signal Only
32	FR_1_7_8_1_0	8	1	0 dB
33	FR_1_7_8_1_-6	8	1	-6 dB
34	FR_1_7_8_5_s	8	5	Signal Only
35	FR_1_7_8_5_0	8	5	0 dB
36	FR_1_7_8_5_-6	8	5	-6 dB
	P1	**N (Phase)**	**Cycles/Phase**	**SNR**

37	P1_1_7_4_1_s	4	1	Signal Only
38	P1_1_7_4_1_0	4	1	0 dB
39	P1_1_7_4_1_-6	4	1	-6 dB
40	P1_1_7_4_5_s	4	5	Signal Only
41	P1_1_7_4_5_0	4	5	0 dB
42	P1_1_7_4_5_-6	4	5	-6 dB
43	P1_1_7_8_1_s	8	1	Signal Only
44	P1_1_7_8_1_0	8	1	0 dB
45	P1_1_7_8_1_-6	8	1	-6 dB
46	P1_1_7_8_5_s	8	5	Signal Only
47	P1_1_7_8_5_0	8	5	0 dB
48	P1_1_7_8_5_-6	8	5	-6 dB
	P2	**N (Phase)**	**Cycles/Phase**	**SNR**
49	P2_1_7_4_1_s	4	1	Signal Only
50	P2_1_7_4_1_0	4	1	0 dB
51	P2_1_7_4_1_-6	4	1	-6 dB
52	P2_1_7_4_5_s	4	5	Signal Only
53	P2_1_7_4_5_0	4	5	0 dB
54	P2_1_7_4_5_-6	4	5	-6 dB
55	P2_1_7_8_1_s	8	1	Signal Only
56	P2_1_7_8_1_0	8	1	0 dB
57	P2_1_7_8_1_-6	8	1	-6 dB
58	P2_1_7_8_5_s	8	5	Signal Only
59	P2_1_7_8_5_0	8	5	0 dB
60	P2_1_7_8_5_-6	8	5	-6 dB
	P3	**N (Phase)**	**Cycles/Phase**	**SNR**
61	P3_1_7_16_1_s	16	1	Signal Only
62	P3_1_7_16_1_0	16	1	0 dB
63	P3_1_7_16_1_-6	16	1	-6 dB
64	P3_1_7_16_5_s	16	5	Signal Only
65	P3_1_7_16_5_0	16	5	0 dB
66	P3_1_7_16_5_-6	16	5	-6 dB
67	P3_1_7_64_1_s	64	1	Signal Only
68	P3_1_7_64_1_0	64	1	0 dB
69	P3_1_7_64_1_-6	64	1	-6 dB
70	P3_1_7_64_5_s	64	5	Signal Only
71	P3_1_7_64_5_0	64	5	0 dB
72	P3_1_7_64_5_-6	64	5	-6 dB
	P4	**N (Phase)**	**Cycles/Phase**	**SNR**
73	P4_1_7_16_1_s	16	1	Signal Only
74	P4_1_7_16_1_0	16	1	0 dB
75	P4_1_7_16_1_-6	16	1	-6 dB
76	P4_1_7_16_5_s	16	5	Signal Only
77	P4_1_7_16_5_0	16	5	0 dB
78	P4_1_7_16_5_-6	16	5	-6 dB

79	P4_1_7_64_1_s	64		1	Signal Only
80	P4_1_7_64_1_0	64		1	0 dB
81	P4_1_7_64_1_-6	64		1	-6 dB
82	P4_1_7_64_5_s	64		5	Signal Only
83	P4_1_7_64_5_0	64		5	0 dB
84	P4_1_7_64_5_-6	64		5	-6 dB
	COSTAS	**Sequence**		**Cycles/Freq.**	**SNR**
85	C_1_15_10_s	4716523		10	Signal Only
86	C_1_15_10_0	4716523		10	0 dB
87	C_1_15_10_-6	4716523		10	-6 dB
88	C_1_15_20_s	4716523		20	Signal Only
89	C_1_15_20_0	4716523		20	0 dB
90	C_1_15_20_-6	4716523		20	-6 dB
91	C_2_17_10_s	2638751		10	Signal Only
92	C_2_17_10_0	2638751		10	0 dB
93	C_2_17_10_-6	2638751		10	-6 dB
94	C_2_17_20_s	2638751		20	Signal Only
95	C_2_17_20_0	2638751		20	0 dB
96	C_2_17_20_-6	2638751		20	-6 dB
	FSK/PSK COSTAS	**Sequence**	**Barker Code Length**	**Cycles/ Phase**	**SNR**
97	FSK_PSK_C_1_15_5_5_s	4716523	5	5	Signal Only
98	FSK_PSK_C_1_15_5_5_0	4716523	5	5	0 dB
99	FSK_PSK_C_1_15_5_1_s	4716523	5	1	Signal Only
100	FSK_PSK_C_1_15_5_1_0	4716523	5	1	0 dB
101	FSK_PSK_C_1_15_11_5_s	4716523	11	5	Signal Only
102	FSK_PSK_C_1_15_11_5_0	4716523	11	5	0 dB
103	FSK_PSK_C_1_15_11_1_s	4716523	11	1	Signal Only
104	FSK_PSK_C_1_15_11_1_0	4716523	11	1	0 dB
	FSK/PSK Target	**Sequence**	**Random Hops**	**Cycles/ Phase**	**SNR**
105	FSK_PSK_T_15_128_5_s	1	128	5	Signal Only
106	FSK_PSK_T_15_128_5_0	1	128	5	0 dB
107	FSK_PSK_T_15_256_5_s	1	256	5	Signal Only
108	FSK_PSK_T_15_256_5_0	1	256	5	0 dB
109	FSK_PSK_T_15_128_10_s	2	128	10	Signal Only
110	FSK_PSK_T_15_128_10_0	2	128	10	0 dB
111	FSK_PSK_T_15_256_10_s	2	256	10	Signal Only
112	FSK_PSK_T_15_256_10_0	2	256	10	0 dB
	Test Signal	**f_c (kHz)**	**f_s (kHz)**		**SNR**
113	T_1_7_1_s	1	7		Signal Only
114	T_2_7_1_s	1 and 2	7		Signal Only

THIS PAGE INTENTIONALLY LEFT BLANK

LIST OF REFERENCES

1 GuoSui Liu, Hong Gu, WeiMin Su, HongBO Sun, "The Analysis and Design of Modern Low Probability of Intercept Radar", *2001 CIE International Conference*, Page(s): 120-124, 2001.

2 Phillip E. Pace, "Introduction to LPI Radars", EC4690 Class Notes, Naval Postgraduate School, Monterey, April 2002.

3 Filippo Neri, "Introduction to Electronic Defense Systems", Second Edition, Artech House Publishers, 2001.

4 Merrill I. Skolnik, "Introduction to Radar Systems', Third Edition, McGraw-Hill Higher Education, 2001.

5 Simon Haykin, Tarun Bhattacharya, " Wigner-Ville Distribution: An Important Functional Block for Radar Target Detection in Clutter", *Systems and Computers, 1994. 1994 Conference Record of the Twenty-Eighth Asilomar Conference on*, Volume: 1 , Page(s): 68 -72, 1994

6 R. H. Clayton, A. Murray, "Comparison of Techniques for Time-Frequency Analysis of the ECG during Human Ventricular Fibrillation", *Proc.-Sci. Meas. Technol. IEEE*, Volume: 145, no.6, Page(s): 301-306, Nov. 1998

7 MATLAB®, The Language of Technical Computing, Version 6.1, Release 12.1, The MathWorks, Inc.

8 MinGui Sun, Ching Chung Li, Laligam N. Sekhar, Robert J. Sclabassi, "A Wigner Spectral Analyzer for Nonstationary Signals", *Instrumentation and Measurement, IEEE Transactions*, Volume: 38 Issue: 5, Page(s): 961-966, Oct. 1989.

9 D. Chester, F.J. Taylor, and M. Doyle, "On Wigner Distribution", *Proc. IEEE ICASSP, Boston*, Page(s): 491-493, 1986

10 D. Chester, "Discrete Wigner Implementations", *Proc. Inc. Symp. Circuit Systems, San Jose*, Page(s): 38-41, 1986

11 Wayne Tomasi, "Electronic Communications Systems", Forth Edition, Prentice Hall, Inc., 2001.

12 Bassem R. Mahafza, "Radar System Analysis and Design Using MATLAB", Chapman & Hall/CRC, 2001.

13 Stephen S. Schwarz, "BPSK", *EC4700 Principles of Digital Receiver Design for Information Operations*, May 2001.

14 A.G. Stove, "Linear FMCW Radar Techniques," *IEE Proceedings F – Radar and Signal Processing*, Volume: 139 Issue: 5, Page(s): 343-350, Oct 1992.

15 Joe J. Johnson, "Triangular FMCW Systems: Analysis and Signal Generation", *EC4700 Principles of Digital Receiver Design for Information Operations*, May 2001.

16 Jen-Yu Gau, " Analysis of Low Probability of Intercept Radar Signals Using Wigner Distribution", Technical Report, Naval Postgraduate School, Monterey, September 2001. (To Be Published)

17 Bernard L. Lewis, "Range-Time-Sidelobe Reduction Technique for FM- Derived Polyphase PC Codes", *Aerospace and Electronic Systems, IEEE Transactions on*, Volume: 29, Issue: 3, Page(s): 834 –840, , July 1993

18 Frank F. Kretschmer, Jr., Karl R. Gerlach, "Low Sidelobe Pulse Compression Waveform", *Systems and Computers, 1988. Twenty-Second Asilomar Conference on* , Volume: 2 , Page(s): 663 –667, 1988

19 Eric J. Carlson, "Low Probability of Intercept (LPI) Techniques and Implementations for Radar Systems", *Proceedings of the 1988 IEEE National Radar Conference*, Page(s): 56-60, 1988.

20 Phillip E. Pace, "LPI Phase Coding Radar Technique", EC4690 Laboratory Exercise, Naval Postgraduate School, Monterey, April 2002.

21 Solomon W. Golomb, Herbert Taylor, "Constructions and Properties of Costas Arrays", *Proc*. *IEEE*, Volume: 72, no.9, Page(s): 1143-1163, Sep. 1984

22 Fernando L Taboada, Venezuela Army, " Detection And Classification of Low Probability of Intercept Radar Signals Using Parallel Filter Arrays And Higher Order Statistics", Master's Thesis, Naval Postgraduate School, Monterey, September 2001.

23 Antonio Lima, Brazil Air force" Analysis And Classification of Low Probability of Intercept Radar Signals Using Cyclostationary Processing", Master's Thesis, Naval Postgraduate School, Monterey, September 2001.

INITIAL DISTRIBUTION LIST

1. Defense Technical Information Center
   Ft. Belvoir, VA

2. Dudley Knox Library
   Naval Postgraduate School
   Monterey, CA

3. Chairman
   Department of Information Sciences
   Naval Postgraduate School
   Monterey, CA

4. Dr. Herschel H. Loomis Jr.
   Department of Electrical and Computer Engineering
   Naval Postgraduate School
   Monterey, CA

5. Dr. Phillip E. Pace
   Department of Electrical and Computer Engineering
   Naval Postgraduate School
   Monterey, CA

6. Jen-Yu Gau
   Taiwan Army
   Taoyuan, Taiwan, R.O.C.